# Elucidation of the Molecular Mechanisms Underlying the Ability of *C. Elegans* Pharynx to Recognize as Toxicant the Soluble, Pre-Fibrillar Assemblies of the Amyloidogenic Proteins

## Thesis

# Elucidation of the Molecular Mechanisms Underlying the Ability of *C. elegans* Pharynx to Recognize as Toxicant the Soluble, Pre-Fibrillar Assemblies of the Amyloidogenic Proteins

**Margherita Romeo**

Degree of Doctor of Philosophy

The Open University

Discipline of Health and Chemical Sciences

Affiliated Research Centre:

Istituto di Ricerche Farmacologiche Mario Negri IRCCS

Milan, Italy

September 2018

# Abstract

Immunoglobulin light chain amyloidosis (AL) is the most common form of systemic amyloidosis in which a plasma-cell dyscrasia results in the overproduction of amyloidogenic immunoglobulin light chains (LC). Although LC organize in extracellular deposits in different target organs, approximately 75% of patients manifest heart involvement at presentation, with a median survival of only 6 months if chemotherapy fails to stop LC production. Although an active role of radical oxygen species (ROS) has already been envisaged, the actual mechanisms behind their generation remain elusive.

In this study, it was observed that amyloidogenic LC purified from patients with cardiac involvement intrinsically generated high levels of ROS and, when administered to *C. elegans* resulted in ROS production. These species can directly target the pharyngeal cells, causing remarkable damage particularly at the mitochondrial level, similar to that observed in amyloid-affected hearts from AL patients. Tetracycline counteracted all these ROS-mediated effects and, when added to standard chemotherapy, they reduced early deaths in patients with cardiac AL. To limit and repair the stress-induced damage, different intracellular signalling events are activated. In particular, the nuclear translocation of the FOXO/DAF-16 transcription factor triggers the transcription of stress-responsive genes, including heat-shock protein (*hsp)-16.2* and manganese superoxide dismutase (*sod)-3*, and controlling stress resistance and survival.

All these effects were entirely dependent on the presence of metal ions, particularly copper. Metal chelators or metal-binding compounds, particularly the new drug PBT2, block ROS production and interrupt the vicious cycle of oxidative stress. In *C. elegans*, low doses of PBT2 in combination with tetracycline result in a synergistic beneficial effect, highlighting the potential application of this pharmacological strategy for AL patients. These findings indicate that metal-induced oxidative stress, already reported to be linked with some neurological disorders, is also a key element in cardiac AL amyloidosis.

***For YOU***

"*Be the best of whatever you are*"

Martin Luther King

# Acknowledgements

I would like to thank all people that with their motivation, enthusiasm and encouragement helped me to complete this work successfully.

Firstly, I would like to express my deep gratitude to my director of studies, Dr.Luisa Diomede, who patiently and steadily guided me every day during all these years.

I would like to give my sincere thanks to my supervisors Dr.Clive Bate and Dr.Mario Salmona, for providing me their continuous support and precious suggestions throughout my project.
Thanks to all the old and new members of my lab and in particular Monica, for her considerable patience and assistance, especially in molecular biology experiments.

Thanks are due to every member in the Department of Biochemistry and Molecular Pharmacology, without whose help and support I would not have been able to complete this project. Moreover, this work was not possible without the collaboration with the Amyloid Research and Treatment Centre, Foundation IRCCS Policlinico San Matteo (Pavia, Italy), and particularly Dr.Paola Rognoni. Special thanks are to Dr. Fabio Fiordaliso, from the department of Cardiovascular Research for his help in electron microscopy experiments.

Thanks to my friends here in Milan, Emma, Marco, Nikos, Alessandro, Ersilia, Piotti, Giovanni F., Giorgina, Valentina, Martina, Carmen N., Mariagrazia, Giovanni N. and to my “forever friends” Maria Grazia and Carmen. Without you, all these years would not have been the same. Thank you for all the moments that we have enjoyed together and for all those that that we will have next.

Lastly, but not least, a special thanks is to my parents and my sister Gresy, that with their wholehearted supported me when the lab lights were off and helped me to complete this extraordinary experience.

Thank you all.

# Preface

The work described in this thesis was performed at the Istituto di Ricerche Farmacologiche Mario Negri IRCSS in Milan, from 2014 to 2018.

The work was performed under the supervision of the Dr. Luisa Diomede (director of studies), Dr. Clive Bate (external supervisor) and Dr. Mario Salmona (internal supervisor).

# Declaration

This thesis has not been submitted in whole or in part for a degree or diploma or other qualifications to any other university.

I performed by myself the experimental work described herein. Collaborations to perform specific parts of the project are indicated in the “Material and Methods” chapter.

# Table of contents

# List of figures

# List of tables

# List of publications

**Candidate's publications on topics associated with the work described in this thesis:**

- L. Diomede, **M. Romeo**, P. Rognoni, C. Foray, E. Ghibaudi, G. Palladini, R.A. Cherny, L. Verga, G.L. Capello, V. Perfetti, F. Fiordaliso, G. Merlini, M. Salmona. "Cardiac light chain amyloidosis: the role of metal ions in oxidative stress and mitochondrial damage". Antioxid Redox Signal. 2017 Jan 28. doi: 10.1089/ars.2016.6848.

- L. Diomede, P. Rognoni, F. Lavatelli, **M. Romeo**, A. di Fonzo, C. Foray, F. Fiordaliso, G. Palladini, V. Valentini, V. Perfetti, M. Salmona, G. Merlini. "Investigating heart-specific toxicity of amyloidogenic immunoglobulin light chains: A lesson from *C. elegans*". Worm 2014; 3; doi:10.4161/21624046.2014.965590.

- L. Diomede L, P. Rognoni, F. Lavatelli, **M. Romeo**, E. del Favero, L.Cantù, E. Ghibaudi, A. di Fonzo, A. Corbelli, F. Fiordaliso, G. Palladini, V. Valentini, V. Perfetti, M. Salmona, G. Merlini. A Caenorhabditis elegans-based assay recognizes immunoglobulin light chains causing heart amyloidosis. Blood. 2014 Jun 5;123(23):3543-52.

**Candidate's publications on topics not associated with the work described in this thesis:**

- F. Morelli, **M. Romeo**, MM. Barzago, M. Bolis, D. Mattioni, G. Rossi, F. Tagliavini, A. Bastone, M. Salmona, L. Diomede. "V363I and V363A mutated tau affect aggregation and neuronal dysfunction differently in *C. elegans*". Neurobiology of Disease, 2018 Sep;117:226-234. doi: 10.1016/j.nbd.2018.06.018.

- A. Sarrica, N. Kirika, **M. Romeo**, M. Salmona, L. Diomede. "Safety and Toxicology of Magnolol and Honokiol". Planta Med. 2018 Jun 20. doi: 10.1055/a-0642-1966.

- Y. Zeinolabediny, F. Caccuri, L. Colombo, F. Morelli, **M. Romeo**, A. Rossi, S. Schiarea, C. Ciaramelli, C. Airoldi, D. Liu, J. Krupinski, S. Sarroca, C. Sanfeliu, M. Slevin, A. Caruso, M. Salmona, L. Diomede. "HIV-1 matrix protein p17 misfolding forms toxic amyloidogenic assemblies that induce neurocognitive disorders". Scientific Reports, 2017 Sep 4;7(1):10313. doi: 10.1038/s41598-017-10875-0.

- M. F. M. Sciacca, V. Romanucci, A. Zarrelli, I. Monaco, F. Lolicato, N. Spinella, C. Galati, G. Grasso, L. D'Urso, **M. Romeo**, L. Diomede, M. Salmona, C.Bongiorno, G. Di Fabio, C. La Rosa and D. Milardi. "Inhibition of Aβ amyloid growth and toxicity by Silybins: the crucial role of stereochemistry". ACS Chemical Neuroscience, 2017 Aug 16;8(8):1767-1778. doi: 10.1021/acschemneuro. 7b00110.

- M. Gobbi, **M. Romeo**, M. Stravalaci, M. Beeg, A. Cagnotto, F.Fiordaliso, M. Salmona and L. Diomede. "An Integrated Approach to Investigate Toxic Oligomers of Amyloidogenic Proteins and Potential Inhibitors: Application to the Effects of Humanin on Aβ Oligomers". The FASEB Journal, *2017* vol. 31 no. 1 Supplement lb98.

- **M. Romeo**, M. Stravalaci, M. Beeg, A. Rossi, F. Fiordaliso, A. Corbelli, M. Salmona, M. Gobbi, A. Cagnotto, L. Diomede. "Humanin Specifically Interacts with Amyloid-β Oligomers and Counteracts Their *in vivo* Toxicity*".* Journal of Alzheimer's Disease, 2017;57(3):857-871. doi: 10.3233/JAD-160951.

- I. Kel, Z. Chang, N. Galluccio, **M. Romeo**, S. Beretta, L. Diomede, A. Mezzelani, L. Milanesi, C. Dieterich, I. Merelli. "Spire: a modular pipeline for eQTL analysis of RNA-Seq data reveals a regulatory hotspot controlling miRNA expression". Molecular Biosystem 2016 Oct 18;12(11):3447-3458.

- M. Beeg, M. Stravalaci, **M. Romeo**, A. D. Carra, A. Cagnotto, A. Rossi, L. Diomede, M. Salmona,M. Gobbi. "Clusterin binds to Aβ1-42 oligomers with high affinity and interferes with peptide aggregation by inhibiting primary and

secondary nucleation". Journal of Biological Chemistry 2016, Mar 25;291(13):6958-66. doi:10.1074/jbc.M115.689539.

- L. Diomede, **M.Romeo**, A. Cagnotto, A. Rossi, M. Beeg, M. Stravalaci, F. Tagliavini, G. Di Fede, M. Gobbi, and M. Salmona. "The new β amyloid-derived peptide Aβ1-6A2V-TAT(D) prevents Aβ oligomer formation and protects transgenic C. elegans from Aβ toxicity". Neurobiology of disease, 2016 Apr; 88, 75-84, doi:10.1016/j.nbd.2016.01.006. Epub 2016 Jan 11.

- I. Sola, E. Viayna, T. Gómez, C. Galdeano, M. Cassina, P. Camps, **M. Romeo**, L. Diomede, M. Salmona, P. Franco, M. Schaeffer, D. Colantuono, D. Robin, D. Brunner, N. Taub, D. Muñoz-Torrero. "Multigram Synthesis and *in Vivo* Efficacy Studies of a Novel Multitarget Anti-Alzheimer's Compound". Molecules 2015, *20*, 4492-4515; doi:10.3390/molecules20034492.

- G. Di Fede, L. Diomede, M. Catania, E. Maderna, F. Moda, M. Ruggerone, **M. Romeo**, M. Morbin, L. Palamara, I. Campagnini, L. Colombo, A. Rossi, A. Cagnotto, M. Messa, A. De Luigi, S. Mancini, M. Stravalaci, M. Gobbi, T. Borsello, M. Salmona, F. Tagliavini. "Targeting beta-amyloid by the A2V Aβ variant: a novel disease-modifying strategy for the treatment of Alzheimer's disease". Journal of Alzheimer's disease 41, 2014, S1-S59; doi: 10.3233/JAD-149999.

- D. Baderna, A. Colombo, **M. Romeo**, F. Cambria, F. Teoldi, M. Lodi, L. Diomede, E. Benfenati. "Soil quality in the Lomellina using in vitro models of human health effects and ecotoxicological assays". Environ Res. 2014 Aug; 133:220-31. doi: 10.1016/j.envres.2014. 05.030. Epub 2014 Jun 24.

- M. Beeg, M. Stravalaci, A. Carra, **M. Romeo**, A. Rossi, M. Salmona, L. Diomede, M. Gobbi. "Clusterin reduces the formation of biological relevant toxic soluble $A\beta_{1\text{-}42}$ oligomers". Alzheimer's and Dementia, 2014 July; Volume 10, Issue 4, Supplement, Pages P651–P652.

# List of abbreviations

| | |
|---|---|
| **Aβ** | Amyloid-β |
| **ANS** | Autonomous nervous system |
| **ATP** | Adenosine triphosphate |
| **AD** | Alzheimer's disease |
| **AL** | Immunoglobulin light chains amyloidosis |
| **BJ** | Bence- Jones protein |
| ***C. elegans*** | *Caenorhabditis elegans* |
| **CQ** | 5-chloro-7-iodo-quinolin-8-ol |
| **cTnI** | Cardiac troponin I |
| **Cu** | Copper |
| **DAF** | Abnormal DAuer Formation |
| ***E. coli*** | *Escherichia coli* |
| **EF** | Ejection fraction |
| **EDTA** | Ethylenediaminetetraacetic acid |
| **EGCG** | Epigallocatechin gallate |
| **F** | Female |
| **Fe** | Iron |
| **FLC** | Free light chains |
| **FOXO** | Forkhead transcription factors |
| **GFP** | Green fluorescent protein |
| **GI** | Gastrointestinal tract |

| | |
|---|---|
| **H** | Heart |
| **Hoechst** | 2'-[4-ethoxyphenyl]-5-[4-methyl-1-piperazinyl]-2,5'-bi-1H-benzimidazole trihydro-chloride trihydrate |
| **HSP** | Heat shock protein |
| **$H_2O_2$** | Hydrogen peroxide |
| **I/IGF-1** | Insulin/insulin growth factor-1 |
| **InsR** | Insulin receptor |
| **IVS** | Interventricular septum |
| **JNK** | c-Jun–N-terminal kinase |
| **LC** | Immunoglobulin light chains |
| **M** | Male |
| **N.A.** | Not available |
| **NGM** | Nematode growth medium |
| **NT-proBNP** | N-terminal prohormone of brain natriuretic peptide |
| **PBS** | Phosphate-buffered saline |
| **PBT2** | 5,7-dichloro-2-dimethylaminomethyl-8-hydroxyquinoline |
| **PI** | Isoelectric point |
| **PNS** | Peripheral nervous system |
| **PW** | Posterior wall |
| **REC** | recombinant protein |
| **ROS** | Reactive oxygen species |
| **SOD** | Superoxide dismutase |
| **TEM** | Transmission electron microscopy |
| **TETRA** | Tetracycline hydrochloride |

| | |
|---|---|
| **TMRM** | Tetramethylrhodamine, methyl ester |
| **Zn** | zinc |

CHAPTER **1**

# Introduction

The central role of proteins in ensuring many biological functions is specifically related to their amino acid sequence and consequently their three-dimensional structure. The correct folding of proteins is finely regulated by different molecular mechanisms which assist them to adopt and maintain their native functional conformational state and inhibit the formation of alternative nonfunctional assemblies (Soto, 2003). In the last decades, an increasing number of human diseases have been identified as associated with changes in protein structure. These pathological conditions referred to as “protein misfolding diseases”, involve the production of proteins that do not achieve their functional conformational state or adopt an alternative one. These disorders can be ascribed to: i) the degradation of a specific precursor protein unable to fold correctly (loss of function disorders, i.e. cystic fibrosis) or ii) the overproduction and aggregation of misfolded proteins in different organs (gain of toxic function disorders) (Blancas-Mejia and Ramirez-Alvarado, 2013). Amyloidoses represent an example of this last category of protein-misfolding diseases.

## 1.1 Amyloidoses

Amyloidoses are a heterogeneous group of protein misfolding diseases whose hallmark is the anomalous extracellular or intracellular deposition of pathogenic proteins in different tissues and/or organs (Chiti and Dobson, 2006, Blancas-Mejia and Ramirez-Alvarado, 2013). The term amyloid, derived from the Latin amiloideus ("starch-like"), was used for the first time in medicine in 1854 by

Rudolf Virchow to indicate small round proteinaceous deposits localized in the nervous system, sharing structural properties similar to starch (Naito, 2014).

The classification of amyloidoses is based on the biochemical nature of the precursor protein involved in the pathology (Perfetti et al., 2001). To date, 37 different proteins with amyloid-like features have been identified, each one associated to a specific hereditary or sporadic pathological disorder (Chiti and Dobson, 2017). Although all these proteins are unrelated and do not share similarities in their amino acid sequence (Falk et al., 1997, Chiti and Dobson, 2006), all of them produce insoluble extracellular or intracellular deposits with a common β-fibrillar structure. It was observed that these aggregates share common biochemical and tinctorial properties (Soto, 2003), including the resistance to denaturants and proteases' degradation and the ability to show apple-green birefringence when they are analyzed by polarized light microscopy after Congo red staining (Howie et al., 2008, Soto, 2003).

The mechanism driving protein aggregation was first described for the amyloid-β (Aβ) peptide, actively involved in Alzheimer's disease (AD), which was then investigated and defined as "amyloid cascade": a multistep process common to all the proteins involved in amyloid diseases (Verma et al., 2015). During the early stages of the aggregation pathway, monomers of a protein can start to self-aggregate leading to the formation of small reactive intermediates known as oligomers (Figure 1).

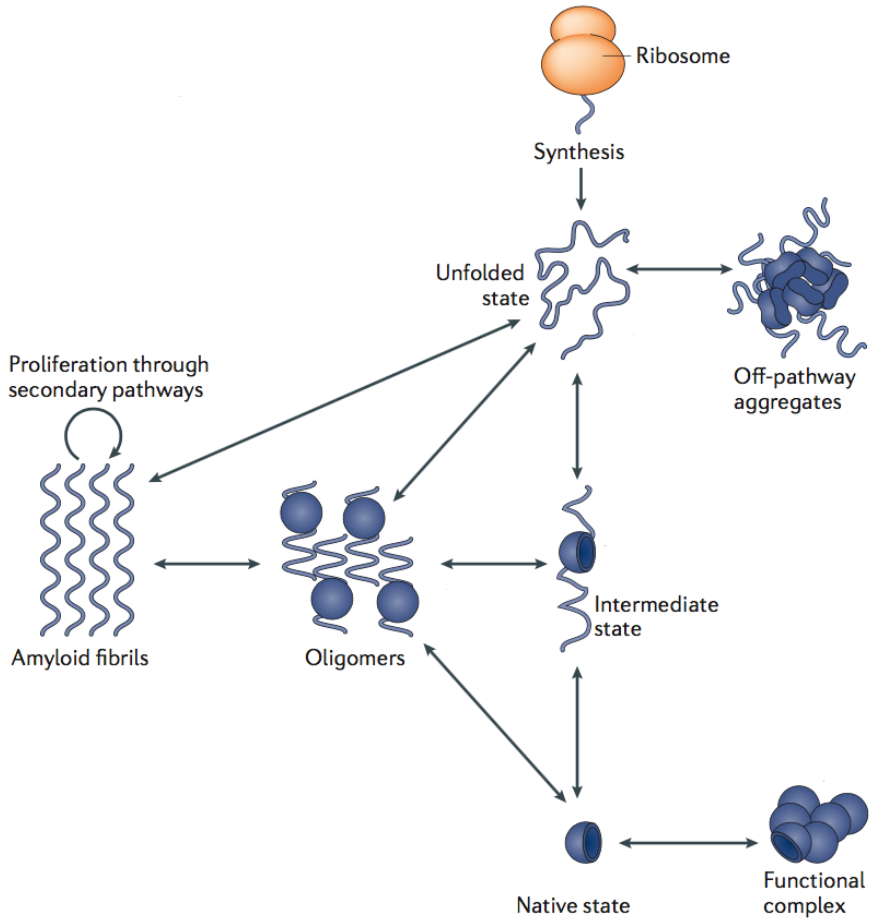


***Figure 1| A schematic representation of protein misfolding and aggregation***

*During misfolding and aggregation, the polypeptide chain undergoes different large conformational rearrangements leading to the formation of unstable misfolded intermediates. These species, through intermolecular interactions with other molecules, assemble to small oligomers which, with further growth, produce amyloid-like fibrils. The molecular mechanisms driving protein oligomerisation and aggregation are not yet clear. Adapted from (Knowles et al., 2014).*

These soluble species can cluster to form beaded chains called protofibrils (Knowles et al., 2014, Chiti and Dobson, 2017). The rearrangement of these assemblies is then involved in the formation of mature fibrils that are highly ordered β-sheet structures prone to aggregate and form amyloidogenic deposits (Knowles et al., 2014, Siddiqi et al., 2017).

Whether oligomers or amyloid fibrils are responsible for the onset and progression of amyloidoses, remain a matter of debate (Nuvolone and Merlini, 2017a). For a long time, researchers believed that fibrillar deposits were the most toxic species in amyloidoses. To date, it is known that, although the accumulation of these species in the extracellular or intracellular compartments alters the tissue architecture, there is not a correlation between the total amount of aggregates and the functional alterations observed (Perfetti et al., 2001). Recently, it was hypothesized that oligomers of different amyloidogenic proteins, due to the exposure of hydrophobic domains, induce toxicity through a common mechanism (Gandy et al., 2010, Sengupta et al., 2016, Chiti and Dobson, 2017, Knowles et al., 2014). For these reasons, they are considered the most relevant species able to induce biological effects such as reactive oxygen species (ROS) production, cell death and tissue damage (Gandy et al., 2010, Sengupta et al., 2016, Chiti and Dobson, 2017, Knowles et al., 2014). The elucidation of the molecular mechanisms determining these pathologies is crucial to clarify and develop new therapeutic approaches to treat and prevent them.

To this end, considerable efforts have been made in the last decade to develop new therapeutic strategies aimed at counteracting Aβ toxicity in AD. Passive immunization, based on the administration of exogenous monoclonal antibodies, is an emerging approach for the treatment of AD (van Dyck, 2018). Different antibodies against Aβ amyloid have been proposed (Schilling et al., 2018) and among them, the human monoclonal antibody aducanumab is particularly promising (Sevigny et al., 2016, Arndt et al., 2018). In a phase 1b study, it was demonstrated that aducanumab targets explicitly Aβ aggregates, including soluble

oligomers and insoluble fibrils, but not monomers (Sevigny et al., 2016, van Dyck, 2018, Arndt et al., 2018). Furthermore, the administration of higher doses of aducanumab once a month for up to 54 weeks reduces the amount of the amyloid burden in the brain of AD patients, also ameliorating their cognitive ability (Sevigny et al., 2016, van Dyck, 2018). To date, the effects of low doses of aducanumab are under evaluation in phase 3 clinical trial for early AD (van Dyck, 2018).

Overall, these data contributed to elucidate the molecular mechanisms involved in the AD and to develop new therapeutic strategies aimed at reducing Aβ toxicity. Moreover, due to the specificity of aducanumab for Aβ aggregates, new antibodies specifically targeting oligomers could also be designed for other protein misfolding diseases.

## 1.2 Systemic amyloidoses

Based on the specific localization of the fibrillary aggregates, amyloidoses can be distinguished in localized or systemic amyloidoses. The presence of deposits in the site of precursor production is known as localized amyloidosis while their localization at one or more sites distant from the site of precursor synthesis is referred to as systemic amyloidosis (Nienhuis et al., 2016). In both cases, the production and accumulation of a large amount of these proteins in a specific tissue cause characteristic clinical symptoms (Chiti and Dobson, 2017).

Systemic amyloidoses are a group of rare, heterogeneous diseases which prognosis depends upon a specific precursor protein and the affected organs (Nuvolone and Merlini, 2017b). In these pathologies, a large quantity of a

misfolded precursor protein is synthetized and then, through the bloodstream, it is deposited in extracellular compartments of different organs as insoluble fibrillar assemblies. The accumulation and deposition of the amyloidogenic proteins lead to cellular death and organ dysfunction (Nuvolone and Merlini, 2017b).

To date, 15 systemic amyloidoses have been identified (Table 1), each one associated to a specific precursor protein.

## 1.3 Immunoglobulin light chains amyloidosis

Immunoglobulin light chains (LC) amyloidosis (AL amyloidosis) is the most common form of systemic amyloidosis in Western countries, with an incidence of 10 new patients per million per year (Blancas-Mejia and Ramirez-Alvarado, 2013, Nuvolone and Merlini, 2017b). A plasma cell dyscrasia causes it, that is the abnormal proliferation of a plasma cell clone in the bone marrow (Patel and Hawkins, 2015).

Under physiological conditions, immunoglobulins are produced and assembled in the bone marrow by plasma cells to form a Y-shaped tetramer consisting of two identical LC (kappa or lambda isotype) covalently linked to two identical heavy chains. LC are physiologically synthesized slightly in excess than heavy chains: most of them are then assembled into intact immunoglobulins while those that do not bind to heavy chains are secreted in the bloodstream as monomers or dimers free LC (Selvaratnam et al., 2016). Due to their small size, most of free LC are filtered by the kidney across the glomerulus, reabsorbed in the proximal tubules and catabolized by proteases (Solling, 1981, Strober and Waldmann, 1974). For this reason, in healthy patients the total amount of LC detected in the urine,

known as Bence-Jones protein (BJ), is low (1–10 mg/24 h) (Selvaratnam et al., 2016, Strober and Waldmann, 1974).

***Table 1| Systemic amyloidoses***

| Precursor Protein | Disease | Type of disease | Affected Organ |
|---|---|---|---|
| Monoclonal immunoglobulin light chain | Light-chain amyloidosis | Sporadic | Heart, kidney, liver, peripheral and autonomous nervous system, gastrointestinal tract, soft tissues |
| Monoclonal immunoglobulin heavy chain | Heavy-chain amyloidosis | Sporadic | Kidney, liver |
| Serum amyloid A protein | AA amyloidosis | Sporadic | Kidney, liver, spleen, heart |
| Transthyretin | Senile systemic amyloidosis | Sporadic and hereditary | Heart, vessels, soft tissues, kidney, central nervous system |
| $\beta_2$-microglobulin | Dialysis-related amyloidosis | Iatrogenic | Joints, heart, gastrointestinal tract, lung |
| Apolipoprotein A-I (ApoA-I) | ApoA-I amyloidosis | Hereditary | Kidney, heart, liver |
| Apolipoprotein A-II (ApoA-II) | ApoA-II amyloidosis | Hereditary | Kidney |
| Apolipoprotein A-IV (ApoA-IV) | ApoA-IV amyloidosis | Sporadic | Kidney |
| Apolipoprotein C-II (ApoCII) | ApoCII amyloidosis | Hereditary | Kidney |
| Apolipoprotein C-III (ApoCIII) | ApoCIII amyloidosis | Hereditary | Kidney |
| Fragments of gelsolin | Gelsolin amyloidosis | Hereditary | Cornea, facial and peripheral nerves, skin |
| Lysozyme | Lysozyme amyloidosis | Hereditary | Kidney, liver, spleen |
| Fibrinogen α-chain | Fibrinogen amyloidosis | Hereditary | Kidney |
| Cystatin C | Cystatin amyloidosis | Hereditary | Cerebral blood vessels |
| Leucocyte chemotactic factor 2 | Renal amyloidosis | Sporadic | Kidney, liver |

*Adapted from Nuvolone et al., 2017 (Nuvolone and Merlini, 2017b) and Chiti and Dobson, 2017 (Chiti and Dobson, 2017).*

In AL amyloidosis a neoplastic plasma cell clone no longer assembles complete immunoglobulins but overproduces amyloidogenic LC, with lambda isotype

predominance (Perfetti et al., 2001). Through the bloodstream, LC are delivered to the kidney causing an increase of the glomerular filtration. However, the resorption capacity of proximal tubules is not sufficient to completely remove the LC burden, leading to the detection of higher concentrations of LC in the urine. At the same time, the increased misfolded LC released into circulation shifts the equilibrium towards fibril formation leading to amyloid deposition in the extracellular space. The persistence of the amyloidogenic aggregates in the tissues disrupts their architecture causing organ failure (Merlini, 2012, Falk et al., 2016, Merlini and Stone, 2006, Kastritis and Dimopoulos, 2016).

AL amyloidosis is closely related to multiple myeloma, a β-cell dyscrasia in which a neoplastic plasma cell clone produces an excess of non-amyloidogenic LC in the bone marrow that infiltrates the bone (Falk et al., 2016). For this reason, myeloma's symptoms include bone lesions, anaemia, hypercalcemia and renal insufficiency, but no amyloid deposits have been ever revealed (Merlini et al., 2011, Ramirez-Alvarado et al., 2007). Contrary, in AL patients a small neoplastic clone typically resides in the bone marrow and secretes LC into the circulation. Therefore, in AL amyloidosis the clinical symptoms are not due to the proliferation of the plasma cell clone in the bone marrow but to the buildup of circulating amyloidogenic LC produced by the neoplastic clone which is the responsible for organ dysfunction (Falk et al., 2016, Merlini et al., 2011, Nuvolone and Merlini, 2017a).

No clear biophysical and biochemical differences have been till now observed among LC from AL- and myeloma-affected patients. The only discriminating characteristic remains the peculiar ability of LC causing AL to form amyloid

assemblies whereas are not formed at all by myeloma LC. For all these reasons, non-amyloidogenic LC purified from myeloma- patients represent the best control for studies involving LC from AL amyloidosis.

**Clinical features of AL amyloidosis**

The prognosis of AL amyloidosis is related to the organ involved in LC deposition, most frequently heart (74%), kidney (65%), liver (17%), gastrointestinal tract (8%), soft tissues (17%) and peripheral (14%) or autonomous nervous system (15%) (Figure 2) (Merlini, 2012, Blancas-Mejia and Ramirez-Alvarado, 2013). However, the molecular mechanism driving the organ tropism it is not yet clear (Westermark, 2012).

AL patients with cardiac involvement show the worst prognosis as compared to other organ involvement, with a median survival of less than a year after diagnosis. Virtually, all AL-affected patients rapidly develop heart failure and ventricular arrhythmias and die from cardiac damage, independently from the localization of amyloid deposits (Merlini, 2012). For this reason, the elucidation of the molecular mechanisms and the development of a new appropriate therapeutic strategy are crucial to limit the LC cardiotoxicity and improve patients' survival.

Great efforts have been made to characterize the amyloidogenic clone involved in AL amyloidosis and to define the mechanisms underlying the LC propensity to aggregate and deposit in specific organs, but with limited success (Sirac et al., 2018). Although it was reported that certain LC germline genes could be associated with specific organ targeting (i.e. IGLV1-44 has been associated with

heart involvement) (Perfetti et al., 2012), the molecular mechanisms involved in LC cardiotoxicity are still under investigation and it is not possible to predict the protein's ability to target specifically the cardiac tissue (Diomede et al., 2014a).

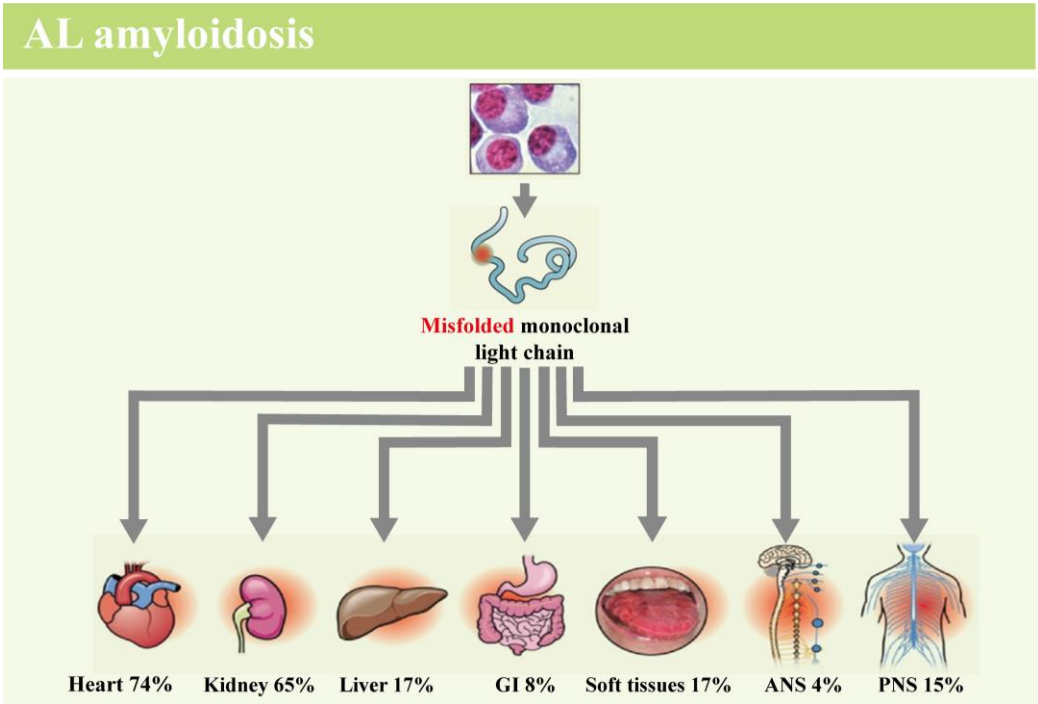


***Figure 2| Schematic representation of tissues involved in AL amyloidosis***

*In AL amyloidosis, a plasma cell clone secretes a large amount of misfolded LC. The wrong folding of this protein is caused by mutations (symbolized by the red dot) in the critical structural sites of LC. These amyloidogenic proteins are prone to aggregate and deposit in different tissues and organs leading to failure organs, mainly in the heart. Adapted from (Merlini, 2012).*

Early diagnosis in AL-affected patients is crucial to stop the progressive organ dysfunction, above all cardiac dysfunction that is mainly involved in patients' survival (Palladini and Merlini, 2009). Nevertheless, although cardiac damage is related to the myocardial fibril deposition, the presence of aggregates alone does not correlate with the severity of the pathology (Liao et al., 2001).

At present, the standard therapy for AL amyloidosis derives from the chemotherapy regimens initially developed for the treatment of multiple myeloma. It is based on the use of a combination of alkylating agents (melphalan, cyclophosphamide), steroids, proteasome inhibitors (bortezomib, ixazomib, carfilzomib), immunomodulatory drugs (thalidomide, lenalidomide, pomalidomide) and monoclonal antibodies (daratumumab, elotuzumab) (Nuvolone and Merlini, 2017a, Kastritis and Dimopoulos, 2016), eventually associated with autologous stem cell transplantation (Hrncic et al., 2000). This approach is aimed to destroy the neoplastic plasma cell clone the new synthesis of LC rapidly, blocking the end-organ damage and leading thus to prolonged patients' survival (Falk et al., 2016).

Although this treatment improved the outcomes of most of AL patients, the prognosis of more than 20% of patients with severe cardiac injury is still poor (Kastritis and Dimopoulos, 2016). They are extremely fragile due to the severe cardiac involvement, and they do not tolerate high-dose of chemotherapeutics (Merlini, 2012). The results are that, although they need urgently of effective therapy, most of them die before starting or during the therapy (Merlini, 2012). For this reason, the elucidation of the mechanisms driving the pathology and consequently develop adequate therapeutics approaches are urgently needed. Clinical findings evidenced that the suppression of the circulating oligomeric LC following chemotherapy is associated with a significant improvement of cardiac function, as demonstrated by the decrease of different cardiac biomarkers, including the N-terminal natriuretic peptide type B (NT-proBNP) and cardiac troponins (cTn) (Nuvolone et al., 2015, Sanchorawala, 2006), resulting in the

extension of the patients' survival. Surprisingly, echocardiography analysis revealed that the amelioration of the clinical signs was not accompanied by a reduction of the amyloid deposits localized in the myocardium, indicating that the standard chemotherapy currently employed prevents the deposition of new LC's aggregates, without removing those already existing (Merlini et al., 2011).

The clinical presentations of AL patients are highly heterogeneous. Moreover, different biological, biochemical, and biophysical factors play a key role in determining the disease (Diomede et al., 2014a). To this end, the generation of appropriate, controllable model animals recapitulating the *in vivo* mechanisms of the pathology is crucial to design and evaluate innovative therapeutic approaches (Diomede et al., 2014b, Sirac et al., 2018, Diomede et al., 2014a).

**Models of LC-induced cardiotoxicity**

Although different groups have made great efforts, no reliable animal models are available to investigate AL amyloidosis (Sirac et al., 2011). This means that the pathogenic role of soluble LC and the mechanisms leading to organ damage are difficult to investigate. *In vitro* and *ex vivo* models have been employed to clarify these processes (Diomede et al., 2014b, Nuvolone and Merlini, 2017a).

In 2004, Brenner et al. investigated the cytotoxicity of LC purified from the urine of AL patients on cardiomyocyte (Brenner et al., 2004). They demonstrated that only soluble cardiotoxic LC, but not control LC purified from multiple myeloma-affected patients, induce oxidative stress by increasing the production of reactive oxygen species (ROS). These reactive species are involved in the impairment of

cell contractility and relaxation through alterations of intracellular calcium homeostasis (Brenner et al., 2004). In 2001, Liao et al. demonstrated that the infusion of BJ LC purified from patients with cardiac involvement causes a rapid and permanent ventricular dysfunction in isolated mouse hearts, independently from fibrils formation (Dispenzieri and Merlini, 2016, Milani et al., 2018, Liao et al., 2001).

Overall, these experimental findings indicate that circulating LC, but not fibrillar deposits, are directly involved in cardiac dysfunction in AL amyloidosis, determining the severity of heart failure and patients survival (Merlini et al., 2011).

The development of suitable animal model steadily overproducing LC and forming amyloid deposits is crucial to elucidate the molecular mechanisms involved in the onset and progression of cardiotoxicity in AL amyloidosis.

## 1.4 *Caenorhabditis elegans*

*C. elegans* is a small, free-living soil nematode, commonly referred to as roundworms. It was used for the first time as a model organism by Sydney Brenner in the mid-1960s, to investigate the mechanisms involved in developmental biology and neurobiology (R. and L., 2008). Since that moment, various groups around the world used the nematode *C. elegans* as simplified *in vivo* animal model for different human pathologies (Table 2), providing considerable insights into the mechanisms of biology including programmed cell death, cell signalling, genomics, metabolism and ageing.

Adult animals are 1-mm long and have a diameter of 80 μm, they are transparent and contain 959 somatic cells, whose 302 are neurons, and its cell lineage is invariant among individuals (Chisholm A. D., 2006). Moreover, *C. elegans* has a short life cycle of about 3 days at 20°C and a lifespan of about 2-3 weeks under suitable living conditions. In the wild, *C. elegans* feeds on available microbes, primarily bacteria and in the laboratory, it is cultivated in large numbers in a liquid medium or on agar plates, seeded with *Escherichia coli (E. coli)* as a food source (Markaki and Tavernarakis, 2010). Its culture requirements are relatively simple and can be preserved cryogenically (Consortium, 1998).

*C. elegans* was the first animal whose genome has been completely sequenced, in 1998 (Consortium, 1998). Although it is a simple organism, it shares similar molecular pathways with mammals. Also, more than 60% of human disease-related genes are homologous in worms (R. and L., 2008, Shen et al., 2018).

**Biology of *C. elegans***

*C. elegans* has two sexes, hermaphrodite and male. Both sexes have five pairs of autosomes and one pair of sex chromosomes. However, while hermaphrodites have two X chromosomes (XX), males are generated by spontaneous non-disjunction in the hermaphrodite germ line, leading to a single X chromosome (XO) (Herman, 2005).

They can be distinguished for the overall body size (male is smaller than the hermaphrodite) and for the morphology of the tail (the hermaphrodite adult tail tip is long and pointed, while the male tail tip is blunt ended) (Figure 3 and Figure 4).

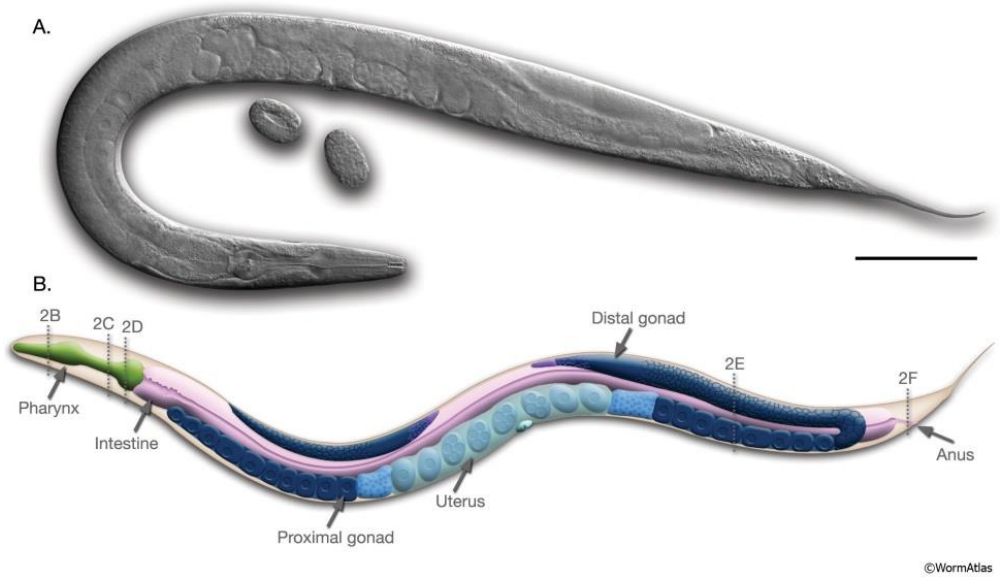


***Figure 3| Anatomy of the adult C. elegans hermaphrodite***
*Adapted from (Palikaras and Tavernarakis, 2013).*

The dominant sexual form is the hermaphrodite that, producing both oocytes and sperm, reproduces by self-fertilization (Zarkower, 2006). During its lifetime, a single hermaphrodite generates a large number of worms (about 300 organisms) all genetically identical to each other (Palikaras and Tavernarakis, 2013).

Males produce only sperm, and under physiological conditions, they arise with a low frequency, usually 0.1%. In adverse conditions, including limited food or high temperature, their number spontaneously rises to increase the chances to survive to the adverse environmental conditions (Palikaras and Tavernarakis, 2013).

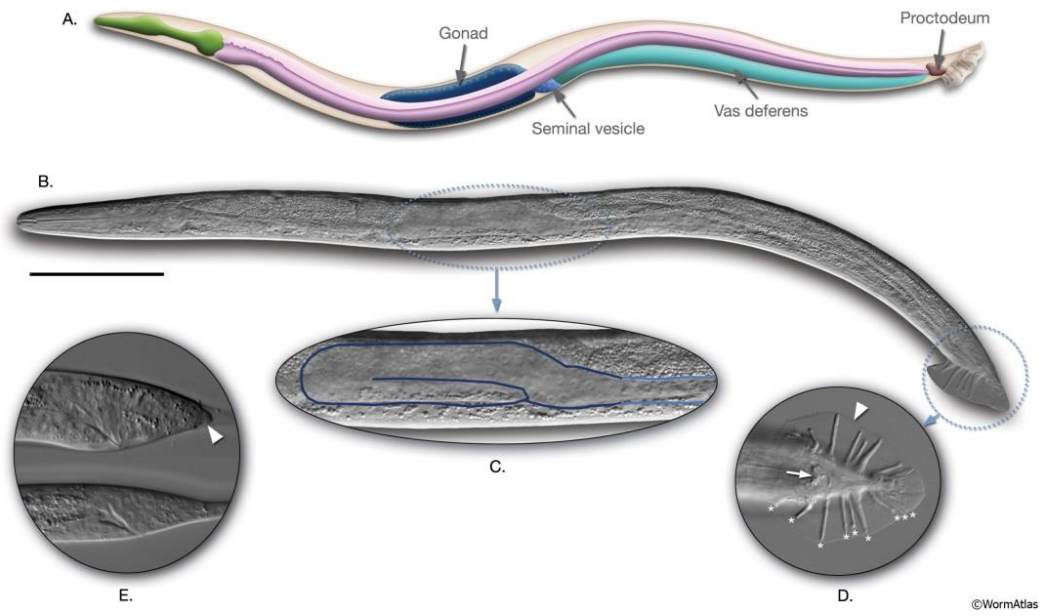


***Figure 4| Anatomy of the adult male***

*Adapted from (Palikaras and Tavernarakis, 2013).*

Under optimal conditions, the life cycle of *C. elegans* occurs in about 3 days at 22°C. It consists of different stages leading to the development of an adult worm, which then lives for about 2 – 3 weeks (Figure 5). After fertilization of an oocyte, through many cell divisions, embryos are formed within the mother's uterus (Altun, 2009). When the embryo reaches the gastrula stage (approximately 30-cell), the worm egg is laid, and the embryonal development proceeds outside the worm. Through additional cell divisions, the cell number of embryo increases leading to the formation of organs. The hatching of the egg occurs when the pharynx starts to pump.

After hatching, *C. elegans* post-embryonic development proceeds through four larval stages ( L1–L4) before it reaching adulthood (Figure 5) (Altun, 2009).

Alternatively, under unfavourable conditions for further growth, including limited food or high temperature, L2 larvae can achieve an alternative larval stage called "dauer" in which feeding is arrested, and locomotion is reduced In this stage, they

can survive for 3–6 months (4–8 times the average lifespan) (Altun, 2009). If the growth conditions improve again, the dauer larvae can resume their normal developmental cycle to reach the sexual maturity (Altun, 2009).

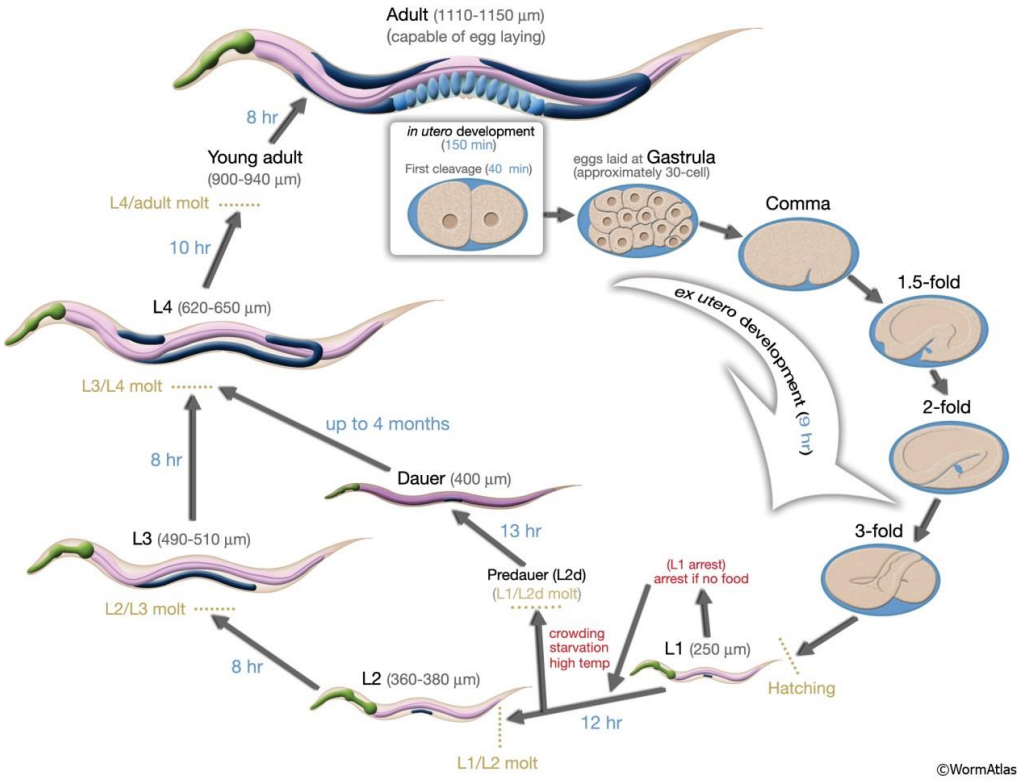


***Figure 5| Life cycle of C. elegans***
*Adapted from (Altun, 2009).*

### *C. elegans* as a model for investigating AL amyloidosis

In the last years, due to the complexity and the limitation of mammalian organisms (e.g. costs, long lifespan), invertebrate models such as *C. elegans* has been used as a rapid and versatile animal model to recapitulate the molecular events occurring in different pathologies, including amyloidosis (Table 2) (Diomede et al., 2014b).

**Table 2| *C. elegans* as animal model to investigate different pathologies**

| Disease | Disease-associated protein | Characteristic pathology in C. elegans | C. elegans findings with potential therapeutic relevance |
|---|---|---|---|
| **AD** | β- amyloid peptide | Muscle-associated human $A\beta_{1-42}$ deposits | Delay of $A\beta_{1-42}$-mediated paralysis by heat shock treatment and ginkgolide |
| | | Neuronal Aβ expression induces defect in chemotaxis | AIRAPL/AIP-1 suppresses Aβ toxicity. |
| | APP/APL-1 | Severe developmental defects induced by inactivation or overexpression of apl-1 | Tetracycline and its analogues protect from β-amyloid- induced toxicity |
| **AD-relevant tau** | PHP-tau | Insoluble highly phosphorylated tau aggregates in neurons linked to a defective pattern of motor neuron development | |
| **PG** | polyQ aggregates | Muscle (polyQm) or neuronal (polyQn) induced toxicity | TOR-2 mediated suppression of polyQ aggregation |
| **HD** | Expression of human Htt (Q>40) in body wall muscle | Motility defects | Rescue of disease phenotype by ubiquilin overexpression |
| | | | Amelioration of the motility defect by Drp-1 knockdown |
| | | | Suppression of proteotoxicity by DR |
| **PD** | Human α-syn expression in dopaminergic neurons | Lewy body formation, selective degeneration of dopaminergic neurons | Co-expression of Rab1 rescue the degeneration |
| | | | Co-expression of TOR-2 ameliorates the aggregate formation |
| | W08D2.5/PARK9, B0432.2/DJ-1, EEED8.9/PINK1 LRRK2/LRK-1 | Knockdown by RNAi enhances misfolding of human a-syn | sir-2.1/SIRT1, lagr-1/LASS2 suppress a-syn inclusion formation |
| | | Enhanced loss of dopaminergic neurons | Autophagy confers neuroprotection |
| **ALS** | SOD1 | Pan-neuronal expression caused severe locomotion defect | |
| | ALS8/VPR-1 | Mild body muscle toxicity influenced by the genetic background | |
| **SMA** | SMN/SMN-1 | Late larval arrest, decreased lifespan, defects in motility and pharyngeal pumping | smn-1(ok355) deletion mutant as a useful platform for functional analysis of human SMN protein |
| **Stroke – Excitotoxicity** | Specific ion channels (DEG-1, MEC-4, DEG-3, GSA-1 in nematode) Specific proteases (calpains CLP-1, TRA-3 and aspartyl proteases ASP-3, ASP-4 in nematode) | Neurodegeneration | Inhibition of executioner proteases (ASP-3, ASP-4) suppresses necrosis Alterations of lysosome biogenesis and functionby genetic or pharmacological treatment could affect necrotic cell death |
| **DMD** | Dystrofin/dys-1 | Muscle degeneration | chn-1/CHIP elimination in the musculature suppresses muscle degeneration |
| **OPMD** | PABPN1 | Muscle cell decline and abnormal motility | Treatment with sirtuin inhibitors protect against mutant PABPN1 |
| **Cancer** | c-Met | Locomotion defects, low fecundity and vulval hyperplasia | |
| | | Anti-apoptotic factor, antagonizes p53/CEP-1, interferes with tumor progression and therapy | |
| | let-60/ras oncogenes | Multivulval phenotype | |
| | vav-1/Vav | | |
| | cep-1/p53 | Apoptotic defects interfere with tumorigenesis and resistance to chemotherapeutic drugs | |
| | HIFa/HIF-1 | Anti-apoptotic factor, antagonizes p53/cep-1, interferes with tumor progression and therapy | Target TYR-2/TRP2 |
| **Metabolic diseases (insulin resistance, type II diabetes** | ogt-1, oga-1 | Null mutations cause alterations in carbohydrate and lipid metabolism | Overexpression or inhibition of specific miRNAs may be a future tool for targeting diabetes |

*Adapted from (Markaki and Tavernarakis, 2010).*

Moreover, *C. elegans* has also been employed as innovative *in vivo* animal model for rapid evaluation of the potential toxicity of different protein assemblies (Diomede et al., 2014b, Stravalaci et al., 2012). In particular, it was demonstrated that the administration of soluble oligomers of Aβ, but not monomers or larger

assemblies, act as "chemical stressors" inhibiting the *C. elegans*' pharyngeal pumping rate (Diomede et al., 2014b, Stravalaci et al., 2012).

These findings are based on the knowledge that sublethal doses of different compounds, including alcohol and heavy metals, are detected as "chemical stressors" by the pharynx of the worm, an organ crucial for the worm's feeding and survival (Jones and Candido, 1999). In 1999, Jones & Candido demonstrated that these molecules, through the production of cellular stress proteins, inhibit the contraction and relaxation of the nematodes' pharynx rapidly to limit the intake of the toxic compounds (Jones and Candido, 1999).

*C. elegans'* pharynx is considered ortholog to the vertebrate heart. Evolutionary conserved cardiac transcription factors finely regulate the development of both organs, and they both possess an automatic contractile activity regulated by similar electrical circuitry and show similar types of ion channels (Avery and Shtonda, 2003, Diomede et al., 2014b, Mango, 2007, Diomede et al., 2014a). Based on this knowledge, we hypothesized that LC directly involved in cardiac injury in AL patients could affect *C. elegans'* pharyngeal motility (Diomede et al., 2014a, Diomede et al., 2014b). To this end, we used for the first time the nematode *C .elegans* as an animal model to investigate *in vivo* the organ tropism of LC in AL amyloidosis (Diomede et al., 2014a, Diomede et al., 2014b). In this study, we demonstrated that cardiotoxic LC, but not myeloma proteins, are detected as chemical stressors from *C. elegans*, which reacts by limiting feeding (Diomede et al., 2014a).

In particular, soluble amyloidogenic LC with different organ tropisms purified from AL patients and non-amyloidogenic LC from multiple myeloma patients as control LC have been used (Diomede et al., 2014a, Diomede et al., 2014b).

After administration to worms, the scoring of the pharyngeal pumping rate has been then used as a powerful tool to determine the potential LC cardiotoxicity (Diomede et al., 2014a, Diomede et al., 2014b).

The pharyngeal impairment caused by cardiotoxic LC, but not non-cardiotoxic LC, is dose-dependent and it became maximal at 100 µg/ml, which is the concentration of circulating levels of free LC measured in the blood of patients with AL amyloidosis [30]. Furthermore, this effect persisted up to 48 hours after administration, indicating that cardiotoxic LC induce a permanent dysfunction (Diomede et al., 2014a).

Cardiotoxic LC obtained from different AL patients specifically impaired the pharyngeal pumping rate of nematodes, independently if they have been purified from urine or serum of AL patients or obtained as recombinant proteins (Diomede et al., 2014a). No toxic effects were observed when nematodes were fed with LC from AL- affected patients involving organs other than the heart (*e.g.* kidney and soft tissue) or with myeloma ones (Diomede et al., 2014a).

Contrary to what observed with the Aβ protein, no differences in oligomerization, secondary structure, stability, and surface hydrophobicity have been observed between cardiotoxic and non cardiotoxic LC. These data indicate that the pharyngeal dysfunction caused by cardiotoxic LC is not due to peculiar protein folding or propensity to form aggregates, compared with the non-toxic LC proteins (Diomede et al., 2014a).

Interestingly, the irreversible impairment of pumping function caused by cardiotoxic LC is related explicitly to mitochondrial ROS production in the worms' pharynx. The administration of cardiotoxic LC, but not myeloma, significantly increased the fluorescence detected by MitoSOX, a mitochondria-specific redox-sensitive dye, indicative of an enhanced oxidant burden. Moreover, similar results were obtained after exposition nematodes to 0.1 mM $H_2O_2$, used as positive control of the experiment. No specific MitoSOX fluorescence has been observed in the pharynx of worms fed myeloma protein or vehicle.

Due to its ability to continuously contract and relax, the pharynx of *C. elegans* is a mitochondrial-rich tissue. Mitochondria continuously supply energy for contraction and play a crucial role in ensuring the physiological function of this organ (Diomede et al., 2014a, Diomede et al., 2014b). However, they are also highly sensitive to oxidative damage. This means that ROS production induced by cardiotoxic LC in the pharynx cause a significant reduction of Adenosine triphosphate (ATP) available for the contraction, leading to loss of organ function (Diomede et al., 2014a, Diomede et al., 2014b).

Moreover, it was demonstrated that cardiotoxic LC, but not myeloma proteins, through ROS generation lead to cell death and reduction in the *C. elegans'* lifespan (Diomede et al., 2014a).

This innovative nematode-based approach is also eligible for the inexpensive screening of candidate drugs counteracting LC toxicity. It was demonstrated that the pharyngeal impairment caused by cardiotoxic LC was counteracted by anti-oxidant molecules able to reduce the mitochondrial ROS burden and restoring the natural lifespan of worms (Diomede et al., 2014b).

Overall, these findings indicate that this approach can be applied to identify the molecular mechanisms are driving the heart tropism in AL amyloidosis, allowing a precise definition of the toxic determinants in LC. The elucidation of their molecular mechanisms of action can accelerate the discovery of eligible drugs targeting critical molecular events of the pathology (Diomede et al., 2014b, Diomede et al., 2014a).

For the first time, *C. elegans* has been used as a "biosensor" to evaluate rapidly the effect of LC potentially cardiotoxic for AL patients. Soluble cardiotoxic LC specifically affect the pharyngeal motility of worms, similarly to Aβ protein. These findings indicate that *C. elegans* recognizes as toxicant the soluble species of different amyloidogenic proteins by common pathways. Furthermore, thanks to the small amount of human LC required to perform the analysis, this nematode-based assay is suitable for basic research and translational applications, and it is also feasible for future routine clinical analysis.

## 1.4 Metal Ions

Metal ions are essentials for life due to their contribution to ensure the physiological activity of most proteins and biological processes (Kozlowski et al., 2009, Andreini et al., 2008). Among them, iron (Fe(III)), copper (Cu(II)) and zinc (Zn(II)) are the most studied ones.

Due to their high reactivity to generate ROS, metal ions are not present in blood plasma in the "free" form but are mainly bound to and transported across the cellular membranes by specific proteins. Zinc is usually bound to albumin and

transferrin, copper is bound to albumin and ceruloplasmin, and iron is carried by transferrin and stored by ferritin (Šuštar and Osredkar, 2011, MacKenzie et al., 2008). To prevent DNA damage, lipid peroxidation and protein oxidation, cell death and pathological disorders, metal ion homeostasis, defined as the balance of uptake, storage and secretion in the different cellular compartments, is strictly regulated by the interplay among transporters, channels, chaperones and metalloregulatory sensors (Angele-Martinez et al., 2014, Bemporad and Chiti, 2012, Roth et al., 1966, Šuštar and Osredkar, 2011, Farooqui, 2016). Severely dysregulation of metal ions homeostasis has been correlated to the onset and progression of cancer, cardiovascular and respiratory diseases, amyotrophic lateral sclerosis and neurodegenerative disorders including AD, Huntington's, Parkinson's and Creutzfeldt-Jakob disease (Angele-Martinez et al., 2014, Bush, 2003). However, the molecular mechanisms triggering an imbalance of metal ion homeostasis in these pathologies, are not yet clear.

**Role of metal ions in AD**

Despite great efforts have been done to elucidate the pathological role of metal ions in different diseases, little information is currently available. Studies have been mainly focused on central amyloidosis whereas the involvement of metal ions in systemic amyloidosis has never been considered. In the past decades, numerous studies investigated the relationship between metal ions and the pathogenesis of AD. Alterations of the physiological concentrations of iron, copper and zinc have been detected in the brains of AD-affected patients, compared to controls patients (Lovell et al., 1998, Cuajungco et al., 2000). In particular, it was observed that metal ions can bind to Aβ protein and promote its

aggregation and deposition (Pithadia and Lim, 2012, Bush, 2003). Accordingly, increased $Zn^{2+}$, $Cu^{2+}$ and $Fe^{3+}$ levels have been measured within the amyloid plaques of AD- affected patients (Table 3) (Bush, 2003, Lovell et al., 1998).

***Table 3| Metal ions' concentrations in amyloid plaques of AD patients, compared to normal age-matched neuropil of control patients***

| **Metal ions (µM)** | | |
|---|---|---|
| | **AD patients** | **Control patients** |
| **$Zn^{2+}$** | 1055 | 350 |
| **$Cu^{2+}$** | 390 | 70 |
| **$Fe^{3+}$** | 940 | 340 |

*Adapted from (Bush, 2003, Cuajungco et al., 2000)*

Different studies reported conflicting data about the concentrations of metal ions in the different cellular compartments (Bush, 2003). The increased levels of $Zn^{2+}$ within the amyloid plaques was accompanied by the presence of low concentrations of $Zn^{2+}$ in the intracellular space (Atwood et al., 1999, Cuajungco et al., 2000), indicating that alterations of the metal ions' distribution among cellular compartments, rather than an increase in their concentration, is involved in the onset and progression of AD (Bush, 2003).

The toxicity of metal ions in AD is also related to their ability to promote ROS generation, *via* Fenton-like reactions (Farooqui, 2016). Aβ monomers bind $Fe^{3+}$ or $Cu^{2+}$ leading to their reduction to $Fe^{2+}$ or $Cu^{+}$, and the formation of Aβ radicals (Aβ•) (Figure 6) (Farooqui, 2016, Opazo et al., 2002). Reactive Aβ•, through the extraction of protons from lipids and proteins, causes the lipid peroxidation,

protein carbonyl modifications and the formation of nucleic acid adducts (Farooqui, 2016).

In the presence of molecular oxygen ($O_2$), $Fe^{2+}$ and $Cu^{+}$ are oxidized to $Fe^{3+}$ and $Cu^{2+}$, thus generating superoxide anion radical ($O^{\bullet-}_2$) and then $H_2O_2$ (Figure 6) (Farooqui, 2016).

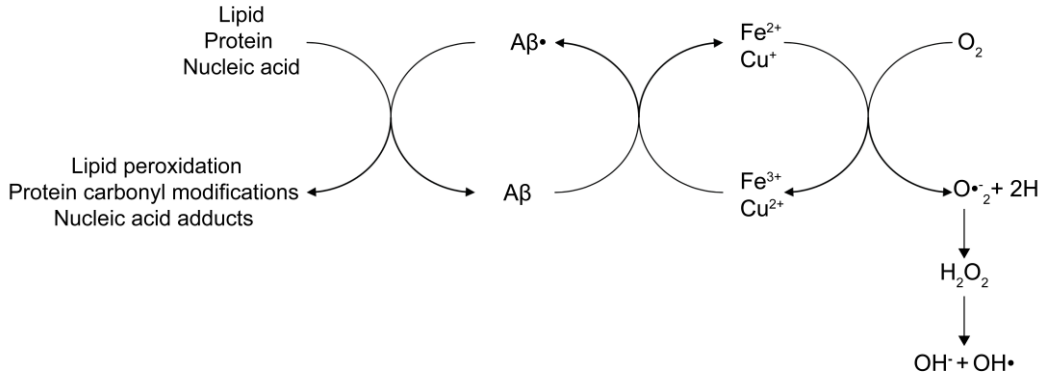


***Figure 6|The binding of Aβ with $Fe^{3+}$ or $Cu^{2+}$ causes the generation of $H_2O_2$***
*After binding of Aβ with $Fe^{3+}$ or $Cu^{2+}$, toxic Aβ radicals (Aβ•) are generated and metal ions are reduced to $Fe^{2+}$ or $Cu^{+}$. Reactive Aβ• extracts protons from lipids, proteins and nucleic acid causing the formation of toxic products. The interactions of reduced metal ions ($Fe^{2+}$ or $Cu^{+}$) with molecular oxygen ($O_2$) lead to the formation of $H_2O_2$ and then hydroxyl radicals (OH•). Adapted from (Farooqui, 2016).*

In the presence of $O^{\bullet-}_2$ or biological reductants (*e.g.* ascorbic acid or glutathione), $Fe^{3+}$ and $Cu^{2+}$ are reduced to $Fe^{2+}$ e $Cu^{+}$ which react with excess $H_2O_2$ to form hydroxyl radicals ($OH^{\bullet}$), *via* Fenton reaction (Farooqui, 2016, Huang et al., 1999).

$$Fe^{3+} + O^{\bullet-}_2 \rightarrow Fe^{2+} + O_2 \qquad Cu^{2+} + O^{\bullet-}_2 \rightarrow Cu^{+} + O_2$$

$$Fe^{2+} + H_2O_2 \rightarrow Fe^{3+} + OH^{-} + OH^{\bullet} \qquad Cu^{+} + H_2O_2 \rightarrow Cu^{2+} + OH^{-} + OH^{\bullet}$$

$Zn^{2+}$ is a redox inert metal ion and thus is not directly involved in redox reactions. However, due its ability to bind monomeric Aβ, promoting its aggregation into

oligomers and plaques, it exerts a crucial role in AD pathogenesis (Farooqui, 2016, Altamura and Muckenthaler, 2009).

Similar interactions have been also demonstrated between metal ions and tau protein (Farooqui, 2016, Sayre et al., 2000), suggesting that the imbalance of metal ions homeostasis and oxidative stress are key elements in AD.

**Metal-binding compounds: clioquinol and PBT2**

Metal-binding compounds have been employed to restore metal ion homeostasis, thus preventing metal-induced ROS generation in several neurodegenerative diseases. These compounds can act as chelators or ionophores (Weekley and He, 2017).

Chelators have been developed to sequester and remove heavy metals after poisoning and then also used to reduce the systemically excess of metals in genetic copper and iron overload disorders (e.g. Wilson's disease, hereditary haemochromatosis) (Helsel and Franz, 2015, Weekley and He, 2017). The binding of chelators to metal ions leads to the formation of metal complexes which are then excreted from the body decreasing the circulating levels of metals (Figure 7) (Flora and Pachauri, 2010).

Due to their hydrophilic nature, chelating compounds cannot cross the blood-brain barrier and are not eligible for the treatment of neurodegenerative diseases (Schimmer, 2011).

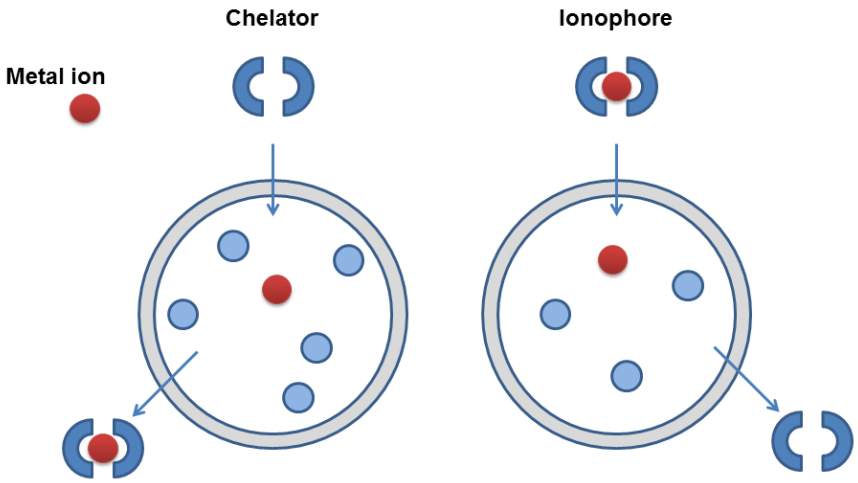


***Figure 7| Chelators and ionophores reduce metal levels through different mechanisms*** *Chelators remove the excess of metals promoting their elimination. Ionophores, through the formation of lipophilic metal complexes, deliver metal ions into the cells. Adapted from (Weekley and He, 2017).*

At variance with chelators, ionophores act as "metal shuttles" (Helsel and Franz, 2015). Through the formation of lipophilic metal complexes, they deliver extracellular metal ions into the cells thus regulating their distribution among the cellular compartments, from regions of excess to regions of deficiency (Figure 7) (Weekley and He, 2017, Helsel and Franz, 2015).

Among ionophores, the two 8-hydroxyquinoline derivatives clioquinol (CQ) and PBT2 have been intensively studied as a potential treatment for neurodegenerative diseases, particularly AD and Huntington's disease.

As shown in Figure 8, despite both compounds have the same coordination site for metals' binding, they have a different substitution pattern around the quinoline ring. In particular, a basic side-chain has been added to PBT2 and iodine (I) at position 5 in CQ has been substituted with chlorine (Cl) in PBT2. These modifications increased the solubility of PBT2 and improved its ability to cross the blood-brain barrier (Adlard et al., 2008)

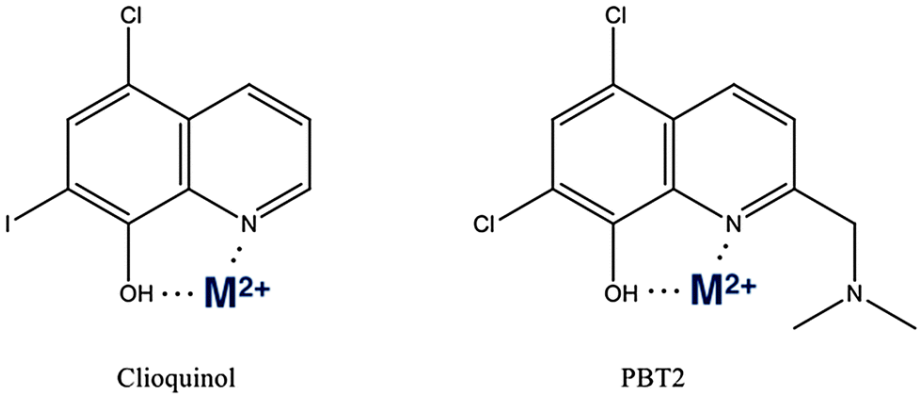


***Figure 8| Structures of clioquinol and PBT2***

*Clioquinol and PBT2 bind metals using oxygen, nitrogen coordination site (Barnham and Bush, 2014)* .

Until the 1970s, CQ has been used as antibiotic for the treatment of intestinal infections caused by amoebas (Budimir, 2011) but in 1985 due to the onset of side effects among the Japanese population, it was withdrawn from sale (Ayton et al., 2017).

The ability of CQ to bind metal ions has been then investigated. CQ is an ionophore able to cross the blood-brain barrier and to bind $Cu^{2+}$ and $Zn^{2+}$ with moderate affinity ($1.2\times10^{-10}$ M and $7\times10^{-8}$ M, respectively) (Ayton et al., 2017, Di Vaira et al., 2004). Although it is weak interaction, it is sufficient to extract metal ions from extracellular Aβ aggregates and release them in the intracellular space, thus regulating and restoring metal neuronal homeostasis (Helsel and Franz, 2015, Ritchie et al., 2003, Ayton et al., 2017, Weekley and He, 2017). In 2001, Cherny et al. demonstrated that CQ prevents Aβ aggregation *in vitro* (Cherny et al., 2001). The pre-clinical study indicated that the daily administration of CQ for 9 weeks to transgenic AD mice reduced of ~49% the Aβ deposits in the brain of mice and counteracted their Aβ-induced memory impairment (Cherny et al., 2001, Ayton et

al., 2017, Grossi et al., 2009). CQ has also been used for a randomized, double-blind, placebo-controlled pilot phase II clinical trial on AD patients (Ritchie et al., 2003). This study showed that chronic treatment with CQ, compared to placebo, attenuated the cognitive impairment in patients suffering from AD. However, this trial was interrupted due to complications with large-scale manufacturing of the compound and to the onset of dyshomeostasis of vitamin B12 in the brain of CQ-treated patients (Barnham and Bush, 2014, Ayton et al., 2017, Yassin et al., 2000). The second-generation 8-hydroxyquinoline compound PBT2 has been then developed for the treatment of AD and Huntington's disease. PBT2 is a Cu/Zn ionophore restoring metal homeostasis inside the cells (Adlard et al., 2008, Crouch et al., 2011). *In vivo* experiments demonstrated that the oral administration of PBT2 to transgenic AD mice reduced the cerebral levels of Aβ and improved the cognitive impairment (Adlard et al., 2008). Furthermore, PBT2 reduced the aggregation of mutant huntingtin in transgenic mice used as a model of Huntington's disease and prolonged their survival (Huntington Study Group Reach, 2015).

Based on these pre-clinical findings, PBT2 has been employed for clinical studies on AD and Huntington's disease affected patients (Lannfelt et al., 2008, Huntington Study Group Reach, 2015). Results obtained from a 12 weeks-phase IIa clinical trial on early AD-patients, demonstrated that PBT2, orally administered at 250 mg/day, reduced the Aβ levels in the cerebrospinal fluid of AD patients and improved their memory impairment (Lannfelt et al., 2008). A 26weeks-phase II randomized, double-blind, placebo-controlled trial has been performed on Huntington's diseases. In this study no side effects have been

observed, indicating that PBT2, at the dose of 250 mg/day, is safe and well-tolerated Despite the fact that some cognitive functions were improved in PBT2-treated Huntington patients, these effects need to be confirmed in a more extensive study (Huntington Study Group Reach, 2015).

**Metal ions stimulate daf-16/FoxO signalling**

Transition metal ions and oxidative stress are reported to regulate the expression of the forkhead box O (FoxO) transcription factors in insulin/insulin growth factor (IGF)-1 signalling (IIS) pathway (Eckers and Klotz, 2009). IIS pathway is highly conserved from *C. elegans* to mammals (Eckers and Klotz, 2009). IIS pathway is highly conserved from *C. elegans* to mammals (Lin et al., 2001) and it is involved in the regulation of different cellular processes including proliferation, apoptosis, metabolism, ageing, longevity, proteostasis and stress resistance (Hay, 2011).

In the presence of a lower concentration of insulin or insulin-like molecules, FoxO in its unphosphorylated form is localized in the nucleus of the cells and promotes the transcription of its target genes (Lee and Dong, 2017). When insulin or insulin-like molecules increased, the binding to the insulin receptor (InsR) results in the phosphorylation and activation of phosphoinositide 3-kinases (PI3K) and the serine/threonine kinase Akt (Eckers and Klotz, 2009) (Figure 9). After activation, Akt phosphorylates nuclear FoxO thus promoting its exclusion into the cytoplasm and causing the down-regulation of its target genes (Hay, 2011, Eckers and Klotz, 2009). Transition metal ions, such as copper and zinc, can act as insulin- like molecules able to bind to InsR and promote the nuclear exclusion of FoxO into the cytoplasm (Eckers and Klotz, 2009) .

As stated before, the IIS pathway plays a crucial role also in protecting cells from oxidative stress (Lee and Dong, 2017). In 2004, Essers et al. demonstrated that the $H_2O_2$-induced oxidative stress leads to the c-Jun–N-terminal kinase (JNK)-mediated phosphorylation of threonine 447 and threonine 451 in FoxO (Essers et al., 2004). Phosphorylated FoxO translocated and, to improve cell resistance to stress, activated the transcription of genes coding for anti-oxidative enzymes, including SOD, catalase and glutathione peroxidase (Figure 9) (Essers et al., 2004).

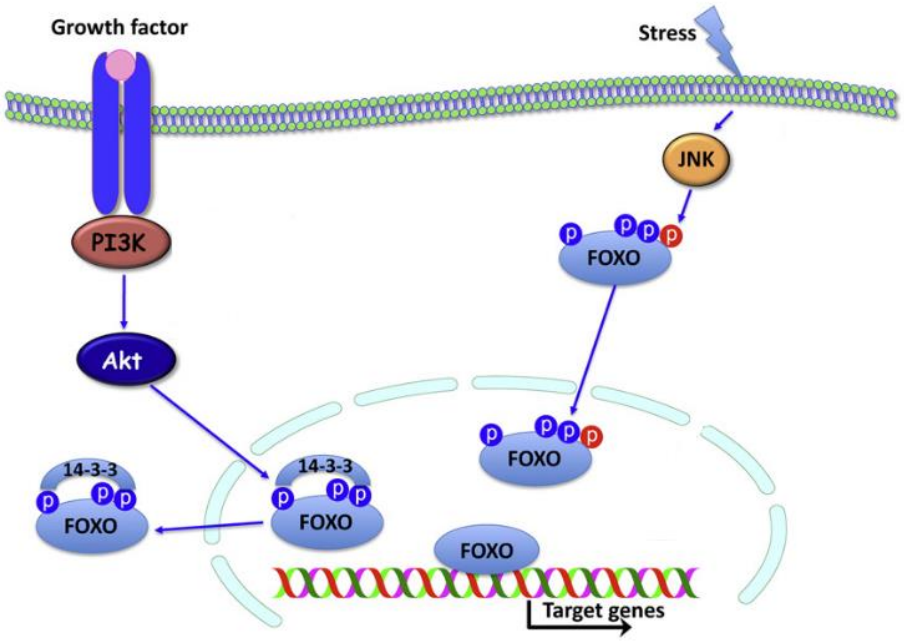


***Figure 9| Schematic representation of the IIS pathway in vertebrates***

*The binding of insulin to its receptor activates the PI3K and Akt kinases, leading to the nuclear exclusion of FoxO into the cytoplasm. Oxidative stress promotes an alternative pathway through the activation of JNK which induced FoxO phosphorylation and its nuclear translocation. This results in the activation of transcription of genes coding for anti-oxidant proteins. Adapted from (Hay, 2011).*

CHAPTER 2

# Aims

For a long time, amyloid deposits were thought to be causative agents in the degenerative process (Roth et al., 1966). Recent studies suggest that the pre-fibrillar, oligomeric assemblies of the amyloidogenic proteins, more than fibrils, are mainly responsible of the toxicity and organ dysfunction observed in patients affected by amyloid-related diseases (Bemporad and Chiti, 2012, Treusch et al., 2009).

The research program of my PhD was aimed to elucidate the molecular mechanisms underlying the ability of *C.elegans'* pharynx to recognize as toxicant the soluble, pre-fibrillar assemblies of the amyloidogenic proteins, particularly LC able to cause heart damage in patients suffering from AL amyloidosis.

Based on the knowledge that the *in vivo* toxicity exert by cardiac LC are specifically related to their ability to generate higher amount of ROS and promote oxidative damage, the aims of the work described in this thesis were to identify the molecular mediators driving ROS production and investigate about the proteins/pathways that are deterministically involved in protein-related pharyngeal damage.

The elucidation of the molecular mechanisms occurring in AL amyloidosis will be crucial to design an effective pharmacological strategy aimed at interrupting the vicious cycle of oxidative stress, blocking the mechanism of heart damage thus improving life expectancy of AL patients with cardiac involvement.

CHAPTER 3

# Materials and Methods

## 3.1 Media, solutions and buffers used for *C. elegans* studies

All media, solutions and buffers were sterilized before the use and diluted using sterile dd$H_2O$.

**Nematode Growth Medium (NGM)-Agar**

| | |
|---|---|
| NaCl | 3.0 g |
| Bacteriological Agar | 17.0 g |
| Bactopeptone | 2.5 g |
| $H_2O$ to 1 litre | |

After sterilization in autoclave, the following solutions were added:

| | |
|---|---|
| Cholesterol (5 mg/ml in EtOH) | 1.0 ml |
| 1M $CaCl_2$ | 1.0 ml |
| 1M $MgSO_4$ | 1.0 ml |
| 1M potassium phosphate, pH 6 | 25.0 ml |

**M9 buffer**

| | |
|---|---|
| $KH_2PO_4$ | 6.0 g |
| $Na_2HPO_4$ | 6.0 g |
| NaCl | 5.0 g |
| 1M $MgSO_4$ | 1.0 ml |
| $H_2O$ to 1 litre. | |

**1X Bleach solution**

| | |
|---|---|
| 5% Bleach | 1.0 ml |
| 10N NaOH | 250 µl |

| | |
|---|---|
| $H_2O$ | 3.75 ml |

**1X Egg buffer**

| | |
|---|---|
| NaCl | 6.9 g |
| KCl | 3.6 g |
| $MgCl_2$ | 190.4 g |
| 1M Hepes, pH 7.3 | 25 ml |
| $H_2O$ to 1 litre. | |

## 3.2 Immunoglobulin light chains purification

Urines were obtained from patients during routine diagnostic procedures performed at the Amyloid Research and Treatment Centre, Foundation IRCCS Policlinico San Matteo (Pavia, Italy). The institutional review board approved the acquisition, storage, and use of biological samples for research purposesppproved by the institutional review board. Written informed consent was received from participants before inclusion in the study. The presence of tissue amyloid deposits and amyloid organ involvement were defined according to the International Consensus Panel Criteria (Gertz et al., 2005). LC cardiotoxicity has been evaluated by clinical, echocardiography, and biochemical parameters. Non-amyloidogenic LC from myeloma patients were used as controls. All LC included in the study were k isotype, which represents about the 75% of amyloidogenic LC. Human monoclonal LC have been isolated from urine (BJ) and by

production, as recombinant proteins (Perfetti et al., 1996, Rognoni et al., 2013), were provided by Amyloid Research and Treatment Centre, Foundation IRCCS Policlinico San Matteo (Pavia, Italy). Overall, seven LC were obtained (six BJ and one recombinant) (Diomede et al., 2017).

## 3.3 Hydrogen peroxide determination

To determine the role of metal ions in AL amyloidosis, cardiotoxic (H7-BJ) and myeloma (MM2-BJ) proteins (1 mg/ml) in 10 mM phosphate-buffered saline (PBS), pH 7.4, have been incubated in the presence or absence of chelex 100 chelating resin (5 mg/ml, Bio-Rad Laboratories, München, Germany) for 1 h at 4°C with shaking, according to the manufacturer's instructions. In the same experimental conditions, PBS and bidistilled water have been incubated with chelex and used as controls for the experiments. After incubation, all samples have been centrifuged at 8700 x *g* for 5 min at 4°C. Supernatants have been collected, and the protein content has been determined (Bio-Rad Laboratories GmbH, München, Germany).

The ability of LC to generate $H_2O_2$ has been then evaluated by using the Amplex® Red Hydrogen Peroxide/Peroxidase Assay Kit (Catalog no. A22188; Molecular Probes, Life Technologies, Thermo Fisher, Milan, Italy), according to the manufacturer's instructions. Proteins have been diluted at 100 µg/ml with 10 mM PBS, pH 7.4 in a volume of 50 µl and moved into a 96-well black plate. Fifty µl of 100 µM Amplex® Red reagent and 0.2 U/ml HRP working solution has been added to each microplate well-containing samples (final concentration of protein

50 µg/ml). To determine the amount of $H_2O_2$ produced by proteins, a standard curve from 0 to 10 µM $H_2O_2$ in 1X Reaction Buffer has been prepared just before use.

Also, 10 µM $H_2O_2$ solution in 1X Reaction Buffer was used as a positive control, and 1X Reaction Buffer without $H_2O_2$ was used as a negative control. Additional controls included 10 mM PBS (pH 7.4) and bidistilled water, incubated or not with chelex.

All samples have been incubated at room temperature for 30 minutes, protected from the light. The fluorescence has been then measured at different time using Tecan Infinite M200 microplate reader (Tecan, Austria) at an excitation wavelength of 563 nm and an emission wavelength of 587 nm.

Additional experiments have been carried out incubating proteins in the presence of 50 µM $CuCl_2$, 50 µM $ZnCl_2$, 50 µM $FeCl_2$, 25 µM CQ (dissolved in DMSO at 250 µM; Sigma Aldrich, MO), or 2 nM PBT2 (dissolved in absolute ethanol at 250 µM; Prana Biotechnology Ltd, Parkville, Australia). $CuCl_2$, $ZnCl_2$, $FeCl_2$, CQ, and PBT2 alone have been used as controls. To investigate the role of thiols in driving metal-induced toxicity, proteins have been incubated with iodoacetamide (1:10 molar ratio) for 3 h at 20°C (Winterbourn and Carrell, 1977). Iodoacetamide alone was used as a control.

## 3.4 *C. elegans* studies

### Commercial strains

N2 ancestral worms (wild type) and transgenic CL2070, CF1553 and TJ356 nematodes were used. They were all obtained from the *Caenorhabditis elegans* Genetic Center (CGC; University of Minnesota, Minneapolis, USA) and propagated at 20°C on solid nematode growth medium (NGM) seeded with OP50 *Escherichia coli (E.coli)* (CGC; University of Minnesota, Minneapolis, USA) for food. The genotype and the description of the transgenic strains are summarized in Table 4.

**Table 4| Summary of the transgenic strains used for the experiments.**

| Strain name | Construct details | Use |
|---|---|---|
| **CL2070** | dvIs70 [hsp-16.2p::GFP + rol-6(su1006)]<br><br>Nematodes express the green fluorescent protein (GFP) under control of the *hsp-16.2* promoter (Link et al., 1999). | To visualize HSP-16.2 expression after oxidative stress (Link et al., 1999). |
| **CF1553** | muIs84 [(pAD76) sod-3p::GFP + rol-6(su1006)]<br><br>Nematodes express GFP under control of the *sod-3* promoter (REF). | To visualize SOD-3 expression after oxidative stress (Libina et al., 2003). |
| **TJ356** | zIs356 [daf-16p::daf-16a/b::GFP + rol-6(su1006)]<br><br>Nematodes express the full length *daf-16* fused to GFP. DAF-16/GFP expression is under the control of the *daf-16* promoter (Lin et al., 2001). | To monitor the translocation of DAF-16 (Hartwig et al., 2009). |

dvIs70= Integrated (Is) transgene ("dv" allele designation from the Reiner Lab; the 70th allele generated in the Reiner Lab). muIs84= Integrated (Is) transgene ("mu" allele designation from the Wightman Lab; the 84th allele generated in the Wightman Lab). zIs356= Integrated (Is) transgene ("z" allele designation from the Johnson Lab; the 356th allele generated in the Johnson Lab). rol-6= dominant collagen mutation that causes animals to roll and move in circles. su1006= ("su" allele designation from the Epstein Lab; the 1006th allele generated in the Epstein Lab).

**Synchronization of *C. elegans* strains**

To prepare age-synchronized nematodes, adult animals were collected with M9 buffer into 50 ml tube, centrifuged at 290 x *g* for 3 minutes at room temperature and washed 4 times to eliminate bacteria. After that supernatant was removed, worms were moved into 15 ml tube and resuspended in 5 ml of bleach solution prepared immediately before use. Nematodes were incubated on orbital shaking at room temperature for 5-10 minutes until the worms appeared damaged and the eggs released from the adult bodies.

Eggs were washed 4 times with 1X egg buffer, then resuspended in 1 ml of 1X egg buffer and left overnight on orbital shaking at 20°C in the absence of bacteria. In these conditions, due to food deprivation, the newly hatched L1 larvae cannot evolve to the next developmental stages. Next day, L1 larvae were moved to fresh NGM plates seeded with OP50 *E. coli* for food.

**Protein administration and pharyngeal pumping rate**

L3 age-synchronized nematodes were collected with M9 buffer, centrifuged, and washed twice with 10 mM PBS, pH 7.4 to eliminate bacteria avoiding any potential interference between bacteria and the LC (Diomede et al., 2014a). Worms were incubated 2 hours with 100 µg/ml BJ or recombinant LC (100

worms/100 µl) in 10 mM PBS, pH 7.4. Control worms were incubated with 10 mM PBS, pH 7.4 (vehicle) only. After incubation on orbital shaking, worms were transferred onto fresh NGM plates seeded with OP50 *E. coli*. The pharyngeal pumping rate, measured by counting the number of times the terminal bulb of the pharynx contracted over a 1-minute interval, was scored 20 h later (Diomede et al., 2014a).

To evaluate the role of metal ions in LC-induced toxicity, additional experiments were carried out by feeding worms for 2 h with 100 µg/ml of LC alone or with 5 mM NAC (Sigma-Aldrich) or 2050 µM TETRA (Sigma-Aldrich) in 10 mM PBS, pH 7.4; 5 mg/ml chelex in 10 mM PBS, pH 7.4; 10 µM EDTA (Sigma Aldrich) in metal-free water (Sigma Aldrich), 0–25 µM CQ, or 0–25 nM PBT2 dissolved as described above; 50–100 µM copper (from $CuCl_2$) in metal-free water, 50–100 µM zinc (from $ZnCl_2$) in metal-free water, 50–100 µM iron (from $FeCl_2$) in metal-free water. Control worms were exposed, in the same experimental conditions, to metal ions alone. Although metals' concentrations are well above the physiological levels in humans, they are not toxic to worms (Boyd et al., 2003, Rebolledo et al., 2011). However, higher doses of chelex, EDTA, CQ, and PBT2 were toxic to nematodes (Harrington et al., 2012, Imbert et al., 1990).

To investigate the role of $H_2O_2$ in LC-induced pharyngeal dysfunction, additional experiments were carried out using 1 mM $H_2O_2$ for 30 min, alone, or together with 5 mg/ml chelex, 25 µM CQ, or 2 nM PBT2. Furthermore, 1 mM $H_2O_2$, 100 µg/ml cardiotoxic and myeloma LC were diluted in 50 mM phosphate buffer, pH 7.0, and incubated with 100 U/ml catalase (Sigma Aldrich) for 15 min at room temperature in dark conditions before nematodes' administration. Worms were

then fed with these solutions (100 worms/100 µl) for 30 min on orbital shaking in dark conditions and then moved onto fresh NGM plates seeded with bacteria. The pharyngeal pumping rate was measured 2 h later.

The combined effect of TETRA and metal binding compounds were then investigated feeding nematodes (100 worms/100 µl) with 100 µg/ml H7-BJ alone for 2 h and then treated for 30 min with CQ (25 µM), PBT2 (0.5–2 nM), 20 µM TETRA alone, or together with 0.5–2 nM PBT2. Worms were then transferred onto NGM plates seeded with OP50 *E. coli* in the presence of the same drug concentration, and the pharyngeal pumping rate was scored 20 h later.

Control worms were exposed, under the same conditions, to the drugs alone or the vehicle.

**Life span studies**

N2 nematodes (100 worms/100 µl), at the L3 larval stage, were fed for 2 h 100 µg/ml of cardiotoxic LC in presence or absence of 25 µM CQ or 2 nM PBT2. Worms were then moved onto fresh NGM plates seeded with *E. coli* in the presence of the same drug concentration. Control worms were exposed, under the same conditions, to the vehicle or the drugs alone. After 20 h nematodes were transferred to fresh NGM plates seeded with bacteria and the number of live worms was scored (considered as day 0). To avoid overlapping generations, the worms were then transferred every day until they stopped laying eggs. Fresh 2 nM PBT2 was daily added to PBT2-treated worms. The number of live worms was determined for each consecutive day until all worms were dead.

**Mitochondrial membrane potential**

N2 nematodes were fed with 100 µg/ml cardiotoxic or myeloma proteins (100 worms/100 µl) in 10 mM PBS, pH 7.4. Negative control worms were incubated with 10 mM PBS, pH 7.4 (vehicle) alone and positive control worms were incubated with 1mM $H_2O_2$. Nematodes were incubated 2h on orbital shaking at room temperature in dark conditions and then transferred on fresh NGM plates seeded with OP50 *E. coli*, pre-treated for 2 h with 20 µM TMRM (Molecular Probes, Thermo Fisher Scientific). After 24 h, worms were collected with M9 buffer, centrifuged at 2000 x g for 5 min and immobilized with 20 mM levamisole. Nematodes were immediately used for microscopic examination with an inverted fluorescent microscope (IX-71 Olympus) equipped with a CCD camera. Images of the pharynges were taken at 40X magnification with a TRITC filter set (Olympus).

**Mitochondrial production of ROS**

Feeding worms evaluated the effect of LC on mitochondrial oxidant burden with MitoSOX Red (Molecular Probes, Italy) (Molecular Probes, Italy) (Diomede et al., 2014a). Worms at the L3-L4 larval stage were incubated for 2 h with 100 µg/ml cardiotoxic and myeloma protein in 10 mM PBS, pH 7.4 in the absence or presence of 25 µM CQ or 2 nM PBT2. Negative control worms were fed vehicle alone whereas positive controls were fed 1 mM $H_2O_2$ for 30 min. The effect of drugs alone was also determined. Experiments were also carried out incubating worms with 1 mM $H_2O_2$ for 30 min, alone, or together with 25 µM CQ, or 2 nM

PBT2. Nematodes were then transferred to NGM plates seeded with fresh bacteria as food and 10 μM MitoSOX Red. After 20 h, nematodes were transferred to fresh NGM plates seeded with OP50 and left for 1 h, so that residual dye could be washed out from the pharynx lumen. Nematodes were paralyzed by adding 20 mM levamisole (Sigma-Aldrich) and left for 30 min on orbital shaking in dark conditions. Nematodes were then centrifuged at 2000 x g for 5 min at room temperature and fixed in 4% paraformaldehyde for 24 h at 4°C. Worms were then mounted on slides for microscopy and observed by epifluorescence using an inverted fluorescent microscope (IX-71 Olympus) equipped with a CDD camera.

**Transmission electron microscopy analysis**

N2 worms fed 100 μg/ml cardiotoxic LC or myeloma proteins (100 worms/100 μl) in 10 mM PBS, pH 7.4, alone or with 5 mM NAC, 50 μM TETRA, 25 μM CQ or 2 nM PBT2. Control worms were incubated with vehicle alone (Vehicle) only. After 2 h of incubation on orbital shaking, worms were transferred onto NGM plates seeded with OP50 *E. coli* in the presence of the same drug concentration. After 20 h, nematodes were picked, washed in 10 mM PBS, pH 7.4, and fixed with 2% glutaraldehyde in 0.12 M phosphate buffer, pH 7.4. Worms were then cut open at the level of the second bulb of the pharynx, to improve access to the fixative. After post-fixation at room temperature overnight, samples were incubated in a solution of 1% $OsO_4$ and 1.5% ferrocyanide in 0.12 M cacodylate buffer (ferrocyanide-reduced $OsO_4$) at room temperature for 1 h, then 0.3%

thiocarbohydrazide in $H_2O$ for 5 min, and finally 2% $OsO_4$ in 0.12 M cacodylate buffer for 1 h.

*C. elegans* pharynx was then placed into 2% agarose gel, and small cubes were cut and dehydrated in graded series of ethanol for 10 min each, cleared in propylene oxide and embedded in Epoxy medium (Epon 812 Fluka) and polymerized at 60°C for 72 h. From each sample, one semithin (1 μm) section was cut with a Leica EM UC6 ultramicrotome and mounted on glass slides for light microscopic inspection. Ultrathin (60-80 nm thick) sections of areas of interest were obtained, counterstained with uranyl acetate and lead citrate, and examined with an Energy Filter Transmission Electron Microscope (EFTEM, ZEISS LIBRA® 120) equipped with a YAG scintillator slow-scan CCD camera.
TEM analysis was performed in collaboration with Dr. Fabio Fiordaliso, Head of the Bio-imaging Unit, Department of Cardiovascular Research, Istituto di Ricerche Farmacologiche Mario Negri IRCCS, Milan, Italy.

**DAF-16 translocation assay and pharyngeal expression of heat-shock protein (HSP)-16.2 and manganese superoxide dismutase (SOD)-3**

DAF-16/GFP nuclear translocation was evaluated in TJ356 nematodes. Pharyngeal expression of HSP-16.2 and SOD-3 was determined in CL2070 and CF1553 worms, respectively.

Age-synchronized nematodes at L3 larval stage were incubated for 2 h at 20°C with 100 μg/ml cardiotoxic (H7-BJ) or myeloma (MM2-BJ) protein (100

worms/100 µl) in 10 mM PBS, pH 7.4, in the absence or presence of 25 µM CQ, 2 nM PBT2, 50 µM TETRA and 5 mM NAC. Control worms were incubated with 10 mM PBS, pH 7.4, (vehicle) or drugs alone. After 2-20 h, nematodes were paralyzed by adding 20 mM levamisole, centrifuged at 2000 x *g* for 5 min at room temperature, and fixed in 4% paraformaldehyde in 10 mM PBS, pH 7.4, for 24 h at 4°C in dark conditions. Nuclear translocation of DAF-16 was visualized with an inverted fluorescent microscope (IX-71 Olympus) equipped with a CDD camera. Organisms were scored as positive for nuclear localization when green foci were observed throughout the entire body from head to tail and as cytosolic when DAF-16/GFP was diffused.

The number of worms with each level of translocation was counted (n=100 worms/ condition). The assay was repeated at least four times.

To prove the nuclear localization of activated DAF-16/GFP, nuclear counterstaining was performed with 2'-[4-ethoxyphenyl]-5-[4-methyl-1-piperazinyl]-2,5'-bi-1H-benzimidazole trihydrochloride trihydrate (Hoechst 33342; Thermo Fisher Scientific). Nematodes were fed 100 µg/ml of cardiotoxic (H7-BJ) LC (100 worms/100 µl) in 10 mM PBS, pH 7.4. Control worms were incubated with 10 mM PBS, pH 7.4 (vehicle) only. Worms were incubated 2 h with orbital shaking and then paralyzed by adding 20 mM levamisole. After centrifugation at 2000 x *g* for 3 min, nematodes were fixed in 4% paraformaldehyde for 24 h at 4°C on orbital shaking in dark conditions. Nematodes were then centrifuged at 2000 x *g* for 3 min, washed twice with 10 mM PBS, pH 7.4, and resuspended in 0.5 ml of 125 mM Tris- HCl solution, pH 7.4, containing 1% Triton X- 100 and 5% β-mercaptoethanol. After overnight

incubation at 4°C, worms were washed with 10 mM PBS, pH 7.4 and incubated at room temperature for 30 min in 0.5 ml of Hoechst (1 mg/ml in 10 mM PBS, pH 7.4). Nuclear translocation of DAF-16 and Hoechst was visualized at 40X magnification with a GFP and a UV filter, respectively, with an inverted fluorescent microscope (IX-71 Olympus) equipped with a CCD camera. At least 10 worms were photographed per group.

Images for HSP-16.2 and SOD-3 GFP-expression in the pharynx of worms were acquired using the same exposure settings. Sampling images of different animals calculated average pixel intensity values. Mean pixel intensity for each experimental group was calculated using Cell-F software (Olympus). For each experiment at least 25 worms were examined for each strain/condition. Each experiment was repeated 3 times.

## 3.4 Circular dichroism (CD) spectroscopy and thermal stability analysis

Far-UV circular dichroism (CD) spectra of cardiotoxic LC (H7-BJ) and myeloma (MM2-BJ) proteins treated or not with 5 mg/ml chelex, 25 μM CQ, or 2 nM PBT2. All samples, at a protein concentration of 0.4 mg/ml in 50 mM sodium phosphate, pH 7.4, were incubated overnight at room temperature. Far-UV CD measurements were performed at 25°C in 50 mM sodium phosphate, pH 7.4, with a Jasco J-700 spectropolarimeter (Jasco Europe, Cremella, Italy) using a quartz cuvette with a path length of 1 mm. Scans were conducted from 250 to 200 nm at a speed of 100 nm/min with a spectral band width of 2 nm, a sensitivity of 20 degrees, and response time of 1 s. The α-helical and β-sheet contents were

calculated with K2D, CDSSTR, and CONTIN software applications CD. CD spectra represent the average of 10 scans. Data are shown as mean residue ellipticity (MRE, deg $cm^2$ $dmol^{-1}$) as a function of wavelength.

Melting data were recorded at 202 nm to monitor β-sheet unfolding on sample heating from 37°C to 80°C. Analyses were performed in a 1 mm path length quartz cuvette, temperature slope of 1°C/min, band width of 2 nm, data pitch of 0.2° C, and response time of 2 s. The thermal melt value (Tm) for each condition was calculated at the midpoint of the unfolding transition.

CD analysis was performed in collaboration with Dr. Paola Rognoni, at the Amyloid Research and Treatment Centre, Foundation IRCCS Policlinico San Matteo, Pavia, Italy.

## 3.5 Statistical analysis

Data were analyzed using GraphPad Prism 7.0 software (CA, USA) by an independent Student's t-test, one-way and two-way ANOVA and Bonferroni's post-test analysis. The values of $IC_{50}$ and median survival were determined using Prism version 6.0 for Windows (GraphPad Software, CA, USA). A *p*-value <0.05 was considered statistically significant.

CHAPTER **4**

# Results

## 4.1 Cardiotoxic LC affect pharyngeal motility through ROS generation

Cardiotoxic LC specifically impair the pharynx of *C. elegans* through ROS generation, particularly within mitochondria (Diomede et al., 2014a). To evaluate the ability of cardiotoxic and myeloma proteins to promote ROS generation, amplex red has been employed in cell-free conditions as a fluorescent reporter. As reported in Figure 10, cardiotoxic LC generated significantly higher levels of ROS, particularly $H_2O_2$, compared to myeloma ones (725 ± 55.8 *vs* 278 ± 61.9 fluorescence intensity [FI] value for cardiotoxic LC and myeloma, respectively, $p<0.01$) (Diomede et al., 2017).

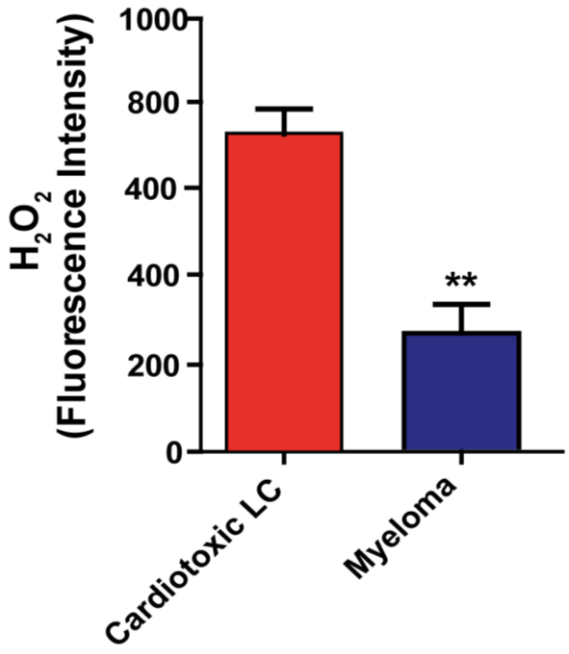


***Figure 10| Detection of reactive oxygen species generated by cardiotoxic LC***

*Detection of $H_2O_2$ produced by cardiotoxic LC and myeloma by Amplex red. Data are expressed as mean ± SE of fluorescence intensity (FI), n=6, **p<0.01 vs cardiotoxic LC, one-way ANOVA and Bonferroni's post hoc test. Adapted from (Diomede et al., 2017).*

Similar results were obtained using different cardiotoxic and myeloma proteins derived from unrelated germline gene confirming that the ability of cardiotoxic LC to promote ROS generation is not linked to a specific amino acid sequence (Diomede et al., 2017).

To elucidate the role of $H_2O_2$ in driving the pharyngeal dysfunction caused by cardiotoxic LC, catalase has been employed (Figure 11). Catalase is an oxidoreductase enzyme that, through the hydrolyzation of $H_2O_2$ into oxygen and water, scavenges hydrogen peroxide when it is present in high concentrations (Djordjevic, 2004).

To this end, worms were fed with cardiotoxic and myeloma proteins previously incubated for 15 min with 100 U/ml of catalase. In these experimental conditions, catalase completely abolished the toxicity induced by exogenous $H_2O_2$, used as a positive control, and counteracted the pharyngeal dysfunction caused by cardiotoxic LC (Figure 11). No changes were observed with myeloma-fed worms (Figure 11) (Diomede et al., 2017).

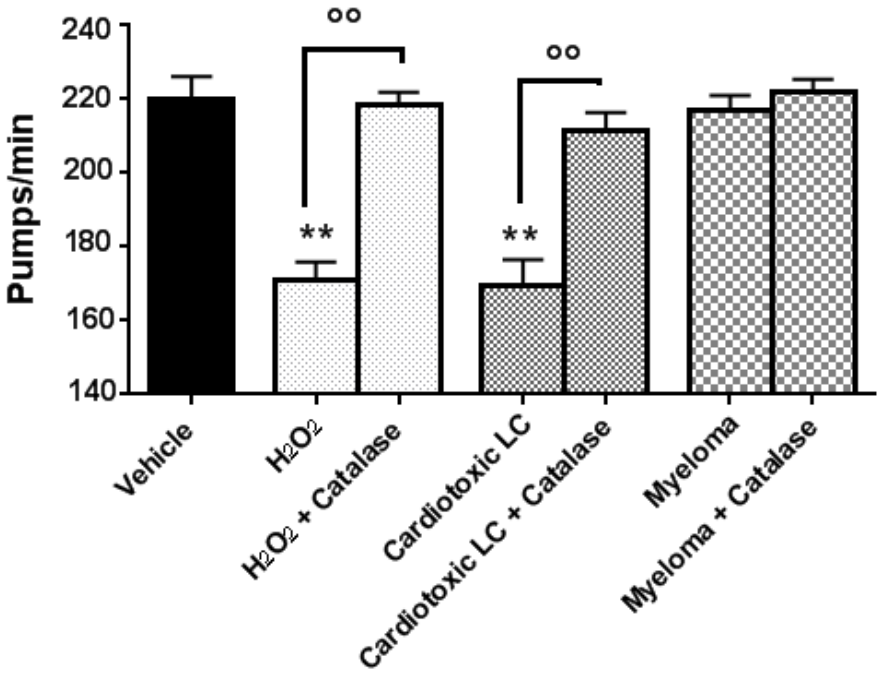


***Figure 11| Effect of catalase on cardiotoxic LC-induced pharyngeal dysfunction***

*Worms were fed for 30 min with 100 µg/ml cardiotoxic LC or myeloma, or 1 mM $H_2O_2$ (used as positive control) previously incubated or not with 100 U/ml catalase for 15 min at room temperature in dark conditions. Control worms received 50 mM phosphate buffer, pH 7.0 (Vehicle). Pumping rate as mean pumps/min ± SE (3 independent assays, n= 30 worms/assay). **p<0.01 vs Vehicle, °°p<0.01 vs the corresponding $H_2O_2$ or cardiotoxic LC not treated with catalase, one-way ANOVA, and Bonferroni's post hoc test (Diomede et al., 2017).*

To investigate the effects of ROS on pharyngeal subcellular compartments, transmission electron microscopy (TEM) analyses were performed after LC administration (Figure 12).

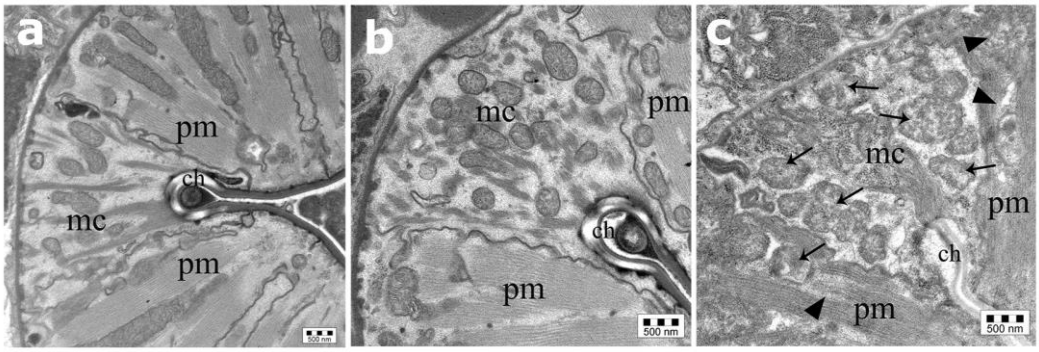


***Figure 12| ROS-induced cardiotoxic LC severely disrupt C. elegans pharyngeal ultrastructure***

*Representative images of worm's pharynx obtained from the ultrastructural analysis by TEM in C. elegans fed for 2 h with (A) Vehicle, (B) myeloma protein and (C) cardiotoxic LC. Images showed two pharyngeal muscles (pm) separated by a marginal cell (mc), placed at the corner of the pharyngeal channel (ch). Arrows indicate mitochondria. Scale bar, 500 nm. Pharyngeal muscles of worms fed cardiotoxic LC resulted in damage to mitochondria, which exhibited a clustering pattern, irregular shape, swelling, and massive disruption of the internal components (i.e., cristae). Marginal cells, which contain many mitochondria due to their active role in contractile motor function, were severely compromised and myofilaments connected to the marginal cells, which were perfectly aligned in vehicle-fed worms, were deranged. Adapted from (Diomede et al., 2017).*

Due to the vital role of mitochondria in providing energy for contractile activity, the effects of ROS on these organelles have been evaluated. As reported in Figure 12 B, cardiotoxic LC-fed worms, showed severe pharyngeal ultrastructure alterations, particularly in muscles and mitochondria, compared with vehicle-treated nematodes (Figure 12 A). In particular, mitochondria were enlarged and also the cristae, formed by the internal membrane, were almost lost entirely (Figure 12 B). No alterations in mitochondria, both in size and morphology, have been detected when worms were fed with myeloma proteins (Figure 12 C) (Diomede et al., 2017).

Moreover, tetramethylrhodamine methyl ester (TMRM) was then used to evaluate the effect of cardiac and myeloma proteins on mitochondrial membrane potential. Under physiological conditions, TMRM accumulates in healthy mitochondria with intact membrane potentials revealing a bright signal. On the contrary, unhealthy mitochondria lose their membrane potential causing a reduction of the TMRM signal.

In our experimental conditions, cardiotoxic LC-fed worms, similarly to the $H_2O_2$-fed worm, showed a reduction of mitochondrial membrane potential, demonstrating that the morphological alterations caused by cardiotoxic LC were accompanied by impaired mitochondrial function (Figure 13). No modifications of the mitochondrial membrane potential have been detected in myeloma-fed worm (Figure 13 C) (Diomede et al., 2017).

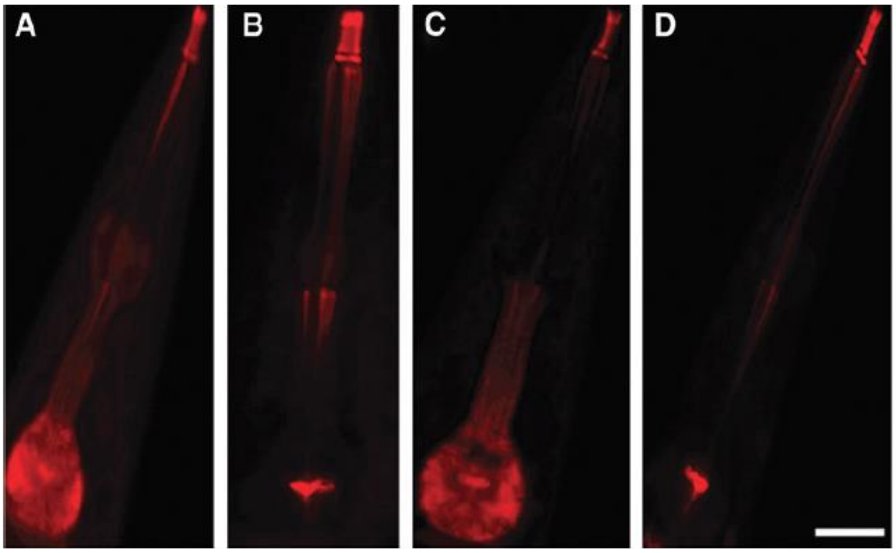


***Figure 13| Effect of cardiotoxic LC on pharyngeal mitochondrial membrane potential***
*Representative images illustrate the TMRM accumulation, which appeared brighter in healthy pharyngeal cells of vehicle-fed worms (A), and was lost after the treatment with cardiotoxic LC (B), but not myeloma protein (C), as an indication of depolarization of the*

*mitochondrial membrane potential. A similar effect was observed with $H_2O_2$ used as positive control (D). Scale bar, 50 µm (Diomede et al., 2017).*

To establish if the functional and structural alterations caused by cardiotoxic LC were ascribed to a specific protein or intrinsic features of cardiac LC, different cardiotoxic LC derived from unrelated germline gene were used. Results obtained in the same experimental conditions revealed similar toxic effects for all the cardiac proteins considered in the study, with no restriction to a particular germline gene or set of genes (Diomede et al., 2017).

## 4.2 Cardiotoxic LC regulate genes involved in oxidative stress resistance

The effects of ROS generation on oxidative stress pathways have been then evaluated.

In *C. elegans*, oxidative stress conditions promote the phosphorylation and translocation of a FOXO gene, called *daf-16*, from cytosol to nucleus of the cell. This leads to the transcription of different genes involved in oxidative stress response and survival, including *sod-3* and *hsp 16.2* (Back et al., 2012, Hartwig et al., 2009, Mukhopadhyay et al., 2006).

To determine if the translocation of DAF-16 mediates the toxicity caused by cardiac LC, transgenic TJ356 *C. elegans* nematodes expressing *daf-16* fused with the green fluorescent protein (DAF-16/GFP) - under the control of the daf-16 promoter - has been used (Hartwig et al., 2009).

When worms were fed with vehicle or myeloma proteins, DAF-16 is detected mainly in the cytosol of the cells (Figure 14 A-C-D). The exposure to high amounts of ROS generated by cardiac LC modulated the FOXO signalling pathway promoting the nuclear translocation of DAF-16. This process is detectable as the appearance of condensed green foci in the body of the worms (Figure 14 B-C-D). Similar results were obtained when worms were fed with exogenous $H_2O_2$ (Appendix 2 A) (Diomede et al., 2017).

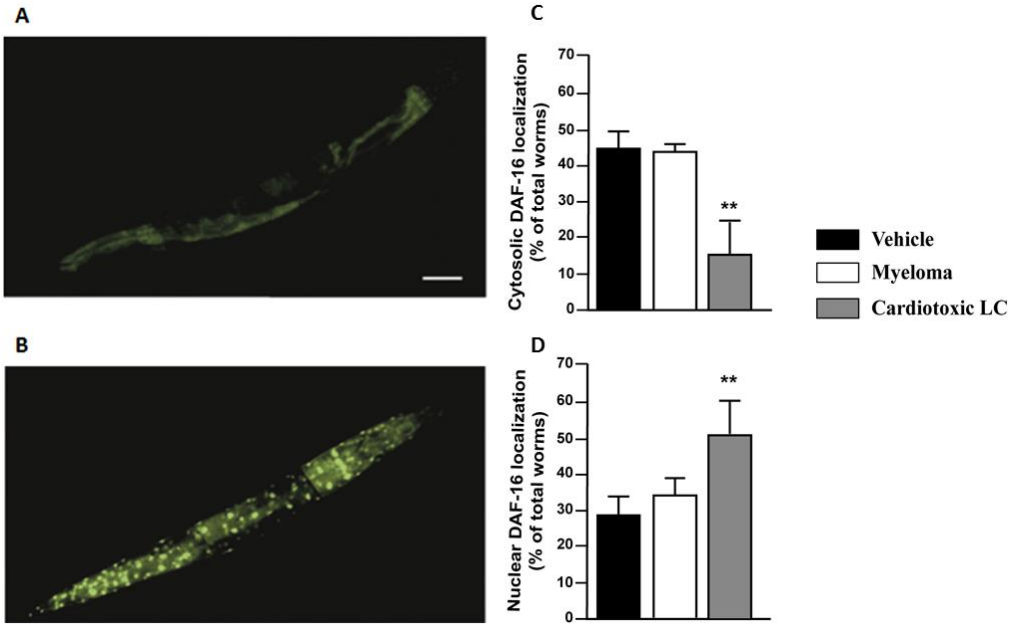


***Figure 14| Cardiotoxic LC promote DAF-16 translocation from cytoplasm to nucleus in TJ356 transgenic worms***

*(A, B) Image of DAF-16/GFP expression in (A) control vehicle-fed and (B) cardiotoxic LC- fed worms. (C, D) The subcellular distribution of DAF-16 expression in worms fed 2 h: vehicle, 100 µg/ml cardiotoxic or myeloma LC. According to DAF-16 localization, worms were divided into two phenotypes, including "cytosolic" and "nuclear". The percentage of DAF-16 localization concerning vehicle-fed worms was calculated based on three experiments, n=100. Mean ± SE. **p<0.01 vs vehicle, one-way ANOVA, and Bonferroni's post hoc test. Adapted from (Diomede et al., 2017).*

Furthermore, the nuclear localization of DAF-16 has been confirmed by co-localization experiments, carried out using a blue fluorescent dye specific for nuclei (Figure 15) (Diomede et al., 2017).

After translocation in the nucleus, DAF-16 activates the transcriptions of proteins involved in the adaptive responses of the antioxidant defence system that protects against oxidative stress (Hartwig et al., 2009).

To demonstrate the activation of this defence system after cardiotoxic LC-feeding, the expression of two genes transcriptionally regulated by DAF-16 has been evaluated. In particular, the involvement of the HSP 16.2, acting as a ROS sensor and also affects the lifespan of worms (Hartwig et al., 2009), and the activity of the enzyme SOD-3, a mitochondrial enzyme converting superoxide into less toxic hydrogen peroxide and oxygen, was investigated. *C. elegans* expresses five SOD enzymes. Among them, both SOD-2 and SOD-3 are Mn-SOD enzymes localised in the mitochondria of cells (Back et al., 2012, Hunter et al., 1997, Moreno-Arriola et al., 2014).

However, only *sod-3* is upregulated explicitly by ROS through *daf-16* translocation, whereas *sod-2* is activated during normal developmental stages.

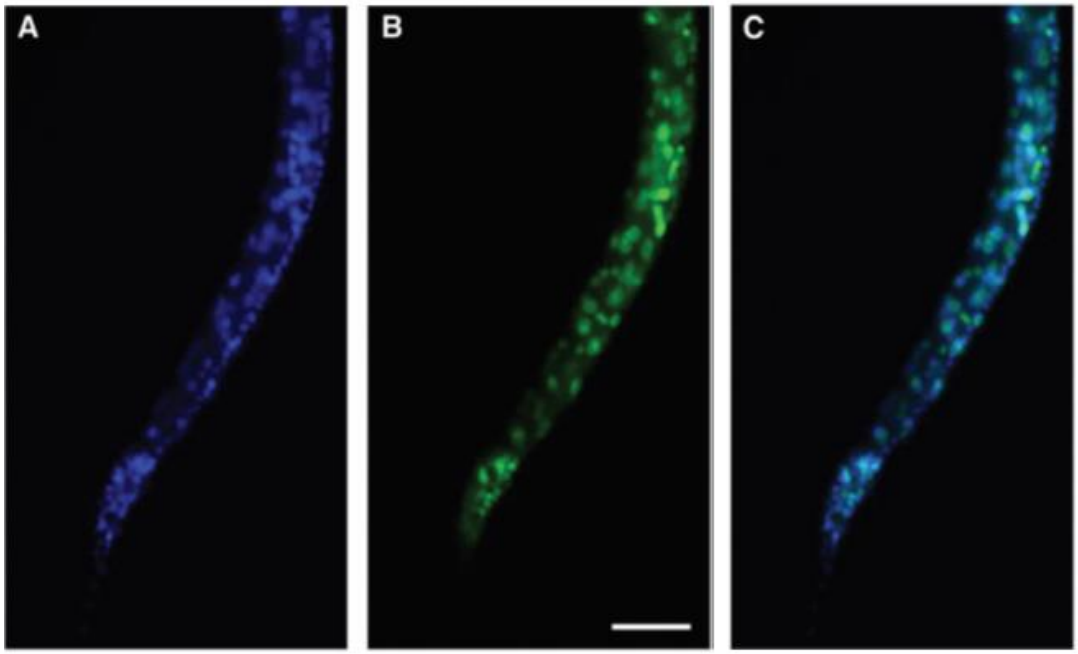


***Figure 15| Co-localization of nuclear staining and DAF-16/GFP in transgenic TJ356 worms fed cardiotoxic LC***

*Representative images depict in (A) the blue fluorescence of nuclear staining and in (B) the green fluorescence provided by DAF-16/GFP labelling. The nuclear localization of DAF-16/GFP was demonstrated by the co-localization of the two stainings in panel (C). Scale bar = 100 µm (Diomede et al., 2017).*

To confirm the activation of HSP-16.2 after cardiac LC-feeding, transgenic CL2070 worms, expressing GFP under the control of *hsp-16.2* promoter, has been used (Hartwig et al., 2009). As shown in Figure 16, cardiotoxic LC, induced a significant increase in HSP-16.2 signal in the pharynx of worms, similar to that caused by the $H_2O_2$ administration (Appendix 2 B). No effects have been detected in myeloma-fed worms (Figure 16) (Diomede et al., 2017).

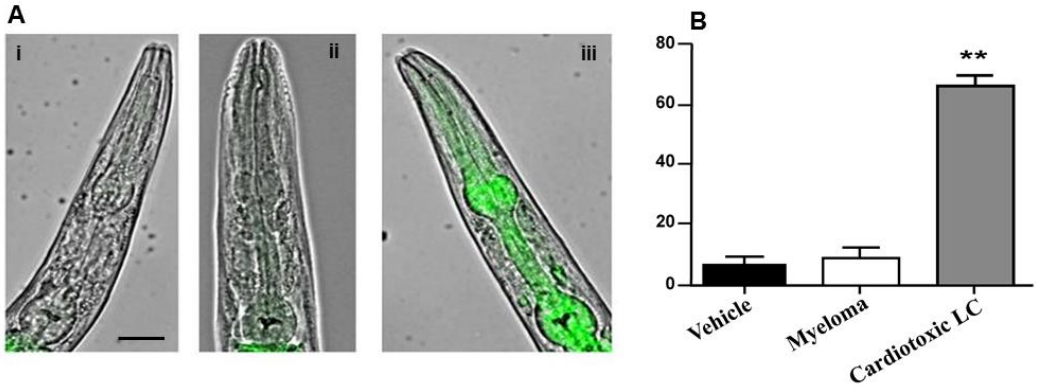


***Figure 16| Cardiotoxic LC induce the pharyngeal expression of HSP-16.2***

*Transgenic worms were fed for 2 h with (i) Vehicle, (ii) 100 µg/ml myeloma or (iii) 100 µg/ml cardiotoxic LC. (A) Images of HSP-16.2 expression as overlays of GFP fluorescence and light microscopy in CL2070 transgenic worms. Scale bar, 50 µm. (B) Quantified GFP intensity in CL2070. FI in each group was calculated as mean grey value ± SE based on three experiments, n = 25. **p<0.01 vs Vehicle, one-way ANOVA, and Bonferroni's post hoc test. Adapted from (Diomede et al., 2017).*

In the same experimental condition, the activation of SOD-3 has been then investigated using transgenic CF1553 worms, expressing GFP under the control of *sod-3* promoter (Anbalagan et al., 2012). As reported in Figure 17, cardiotoxic LC-fed worms, but not myeloma-ones, caused the activation of SOD-3 protein expression in the pharynx of nematodes. Similar effects have been observed when nematodes were fed with exogenous $H_2O_2$ (Appendix 2 B) (Diomede et al., 2017).

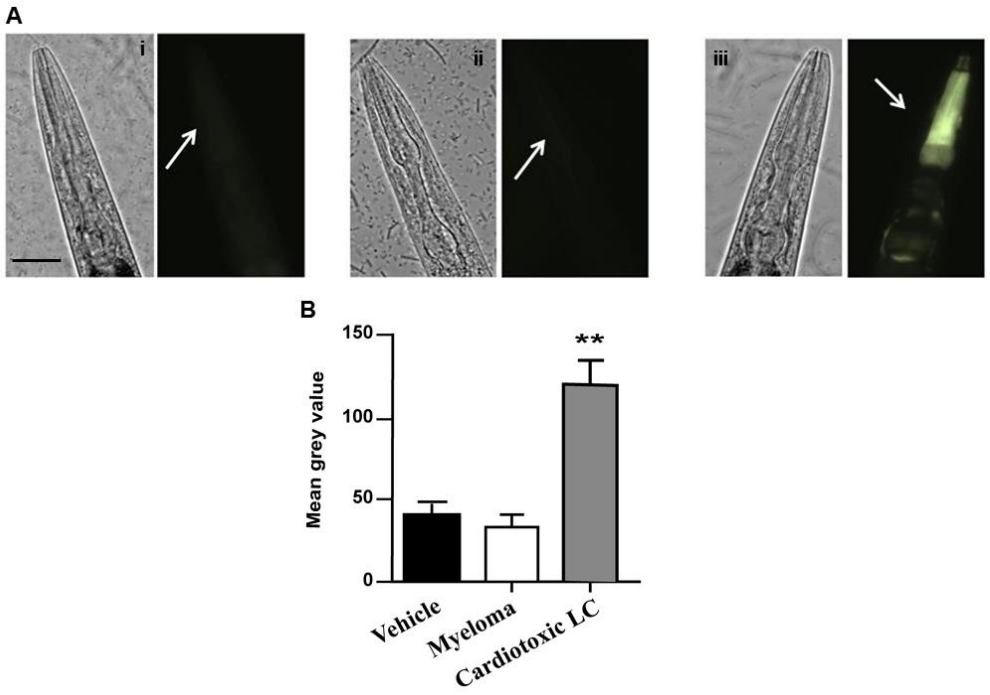


***Figure 17| Cardiotoxic LC induce the pharyngeal expression of SOD-3***

*Transgenic worms were fed for 2 h with (i) Vehicle (10 mM PBS, pH 7.4), (ii) 100 µg/ml myeloma or (iii) 100 µg/ml cardiotoxic LC. (A) Images of SOD-3 expression as GFP fluorescence (arrows) in CF1553 transgenic worms. Scale bar, 50 µm. (B) Quantified GFP intensity in CF1553 worms in response to treatments. FI in each group was calculated as mean grey value ± SE based on three experiments, n=25. **p<0.01 vs Vehicle, one- way ANOVA, and Bonferroni's post hoc test. Adapted from (Diomede et al., 2017).*

These findings indicated that the specific ability of cardiotoxic LC to damage sub-cellular pharyngeal structures, particularly mitochondria, derived from their ability to generate ROS and consequently, to activate pharyngeal expression of different proteins involved in oxidative stress pathways (Diomede et al., 2017).

## 4.3 Metal ions drive ROS generation and pharyngeal damage

To elucidate the molecular mechanisms driving the ability of cardiotoxic LC to generate ROS, the role of metal ions has been investigated employing three monoclonal LC purified from urine (BJ) of AL patient with cardiac involvement and three negative control patients with multiple myeloma (MM) (Diomede et al., 2017).

To clarify the molecular mechanisms involved in ROS generation, experiments were carried out in cell-free conditions by using amplex red assay. As reported in Figure 10, cardiotoxic LC generate significantly higher levels of ROS, particularly $H_2O_2$, at variance with myeloma ones (725 ± 55.8 *vs* 278 ± 61.9 fluorescence intensity [FI] value for cardiotoxic LC and myeloma, respectively, $p<0.01$).

The involvement of metal ions in this process has been then explored by eluting cardiotoxic LC and myeloma proteins on chelex, a metal-chelating resin (Diomede et al., 2017).

To monitor conformational changes of the secondary structure caused by metal chelation, far-UV circular dichroism (CD) has been used. As shown in Figure 18, the presence of a metal ion chelating agent did not affect the secondary structure of cardiotoxic LC and myeloma proteins. They shared similar β- sheet content, consistent with the pattern of a typical immunoglobulin (Diomede et al., 2017).

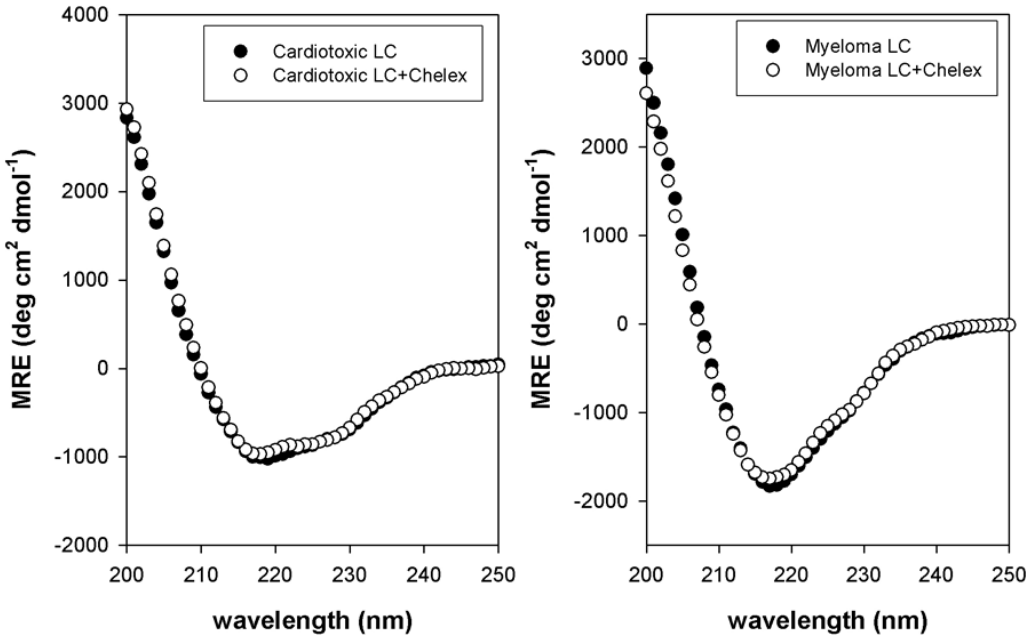


**Figure 18| Effect of metal ion chelators on the secondary structure of LC**

*Far- UV CD spectra of cardiotoxic and myeloma LC treated or not with 5 mg/ml chelex. Proteins were used at 0.4 mg/ml in 50 mM sodium phosphate, pH 7.4, were incubated overnight at room temperature. Far-UV CD measurements were performed at 25°C in 50 mM sodium phosphate, pH 7.4, with a Jasco J-700 spectropolarimeter (Jasco Europe, Cremella, Italy) using a quartz cuvette with a path length of 1 mm. Scans were conducted from 250 to 200 nm at a speed of 100 nm/min with a spectral bandwidth of 2 nm, a sensitivity of 20 degrees, and response time of 1 s. The α-helical and β-sheet content were calculated with K2D, CDSSTR, and CONTIN software applications CD. CD spectra represent the average of 10 scans. Data are shown as mean residue ellipticity (MRE, deg cm$^2$ dmol$^{-1}$) as a function of wavelength. All spectra presented a robust negative band at 216–218 nm. Both cardiotoxic and myeloma proteins had a similar β-sheet content, consistent with the pattern of a typical immunoglobulin, which was not modified by the presence of a metal ion chelating agent. Adapted from (Diomede et al., 2017).*

Furthermore, the thermal stability of cardiotoxic LC and myeloma proteins after metal chelation was explored using guanidinium chloride (GdnHCl) as a denaturant. As shown in Figure 19, treatment with chelex resin did not affect the thermostability of proteins (Diomede et al., 2017).

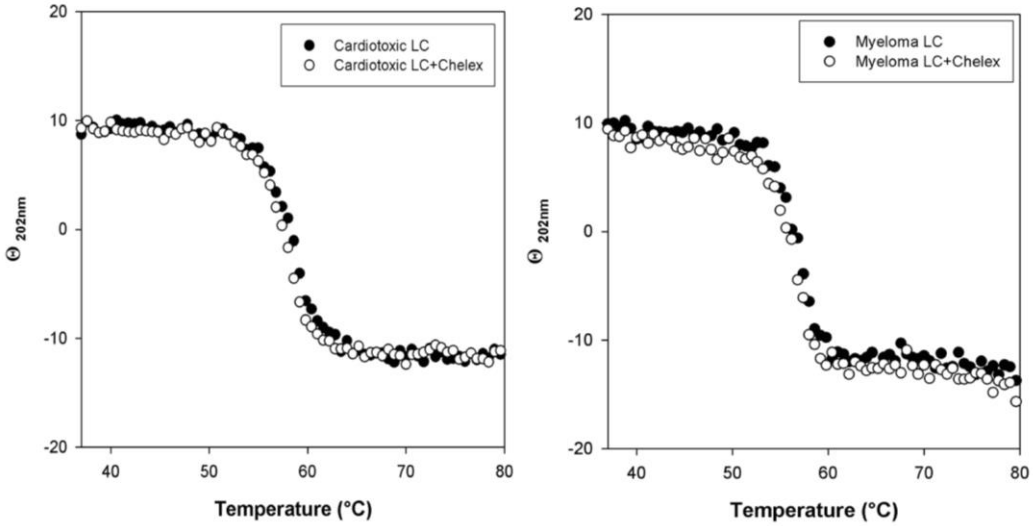


| | Tm |
|---|---|
| **Cardiotoxic LC** | 58.3 |
| **Cardiotoxic LC + Chelex** | 57.7 |

| | Tm |
|---|---|
| **Myeloma** | 56.8 |
| **Myeloma+ Chelex** | 56.3 |

***Figure 19| Effect of metal ion chelators on the thermal stability of LC***

*Melting data were recorded at 202 nm to monitor b-sheet unfolding on sample heating from 37°C to 80°C. Analyses were performed in a 1 mm path length quartz cuvette, temperature slope of 1°C/min, band width of 2 nm, data pitch of 0.2°C, and response time of 2 s. The thermal melt value (Tm) for each condition was calculated at the midpoint of the unfolding transition. No statistical difference among the various conditions tested was observed. No significant perturbations in thermostability were observed in LC after metal ion chelation. Adapted from (Diomede et al., 2017).*

Chelex treatment significantly attenuated the ability of cardiotoxic LC to produce hydrogen peroxide (725 ± 55.8 FI in cardiotoxic LC and 222 ± 101 FI in cardiotoxic LC + chelex) and entirely abolished ROS production caused by myeloma (278 ± 61.9 FI in myeloma and 4.17 ± 4.09 in myeloma + chelex) (Figure 20) (Diomede et al., 2017).

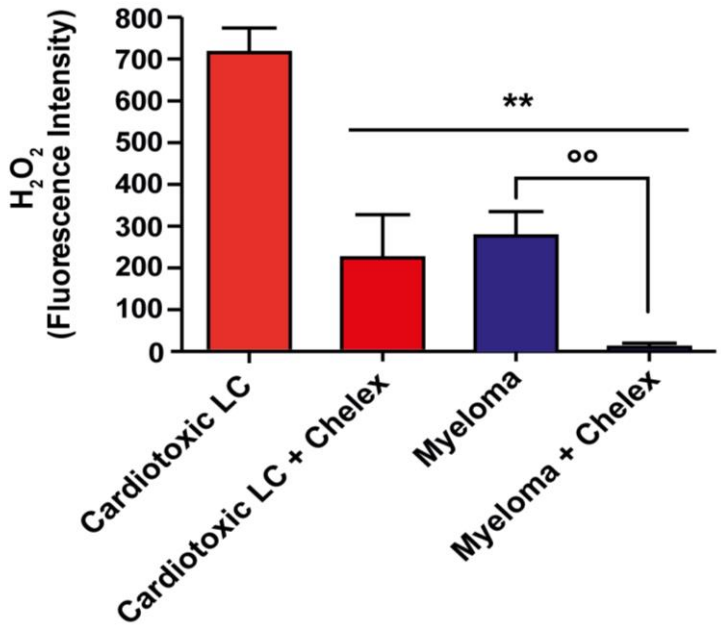


***Figure 20| Effect of metal chelation on the ability of LC to generate ROS***

*$H_2O_2$ produced by cardiotoxic LC and myeloma incubated 2 h with or without 5 mg/ml chelex. Mean ± SE of fluorescence intensity (FI), n=6, **p<0.01 vs cardiotoxic LC and °°p<0.01 vs myeloma, one-way ANOVA and Bonferroni's post hoc test (Diomede et al., 2017).*

However, the treatment with the chelex resin did not completely abolish the ROS production by cardiotoxic LC probably because some traces of metal ions might contain residue after the elution (Diomede et al., 2017).

To evaluate the effect of metal chelation on *C. elegans*, cardiotoxic and myeloma proteins were incubated with chelex or ethylenediaminetetraacetic acid (EDTA) as metal- chelating compounds, and then diluted in metal-free water before administration to worms. In these experimental conditions, the pharyngeal impairment caused by cardiotoxic LC was wholly abolished by chelex or EDTA, whereas no changes were observed when worms were fed with myeloma proteins (Figure 21) (Diomede et al., 2017).

To understand the role of metal ions in driving the toxicity of cardiotoxic LC, proteins were first eluted on chelex resin and then incubated with different metal ions including copper (II), iron (II) and zinc (II). Amplex red assay revealed that the addition of copper and iron, but not zinc, to cardiotoxic and myeloma proteins restored their native ability to produce $H_2O_2$ (Figure 22) (Diomede et al., 2017).

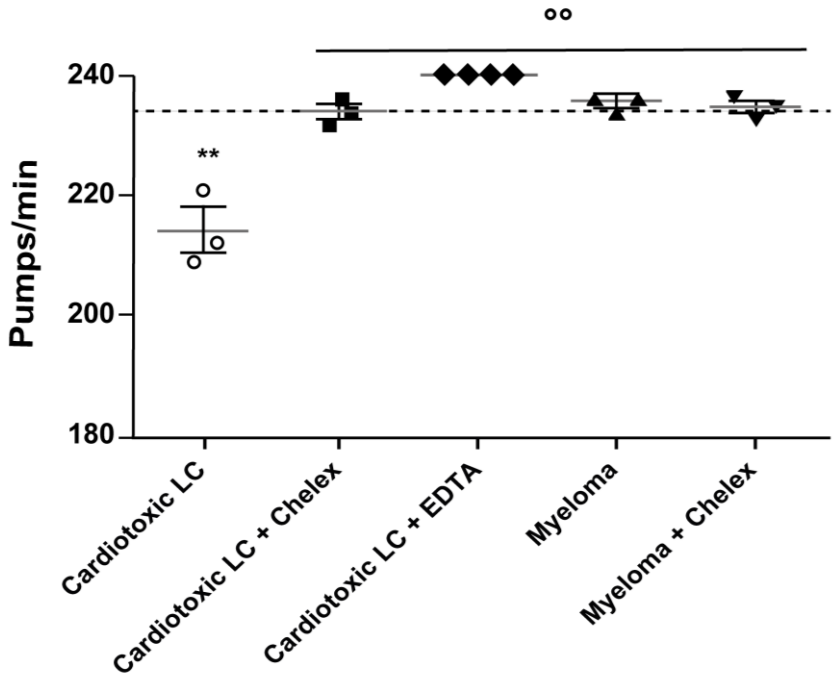


***Figure 21| Metal-chelating compounds prevent the pharyngeal impairment caused by cardiotoxic LC***

*Worms were fed for 2 h with 100 µg/ml cardiotoxic LC, myeloma proteins with or without 5 mg/ml chelex or 10 µM EDTA. Control worms were incubated with 10 mM PBS, pH 7.4 (Vehicle) only (dotted line). The mean ± 95% CI of pumps/min was calculated (horizontal line). Each dot is the mean of pumps/min for each protein (3 independent assays, n=30 worms/assay). **p<0.01 vs Vehicle, °°p<0.01 vs cardiotoxic LC, one-way ANOVA, and Bonferroni's post hoc test (Diomede et al., 2017).*

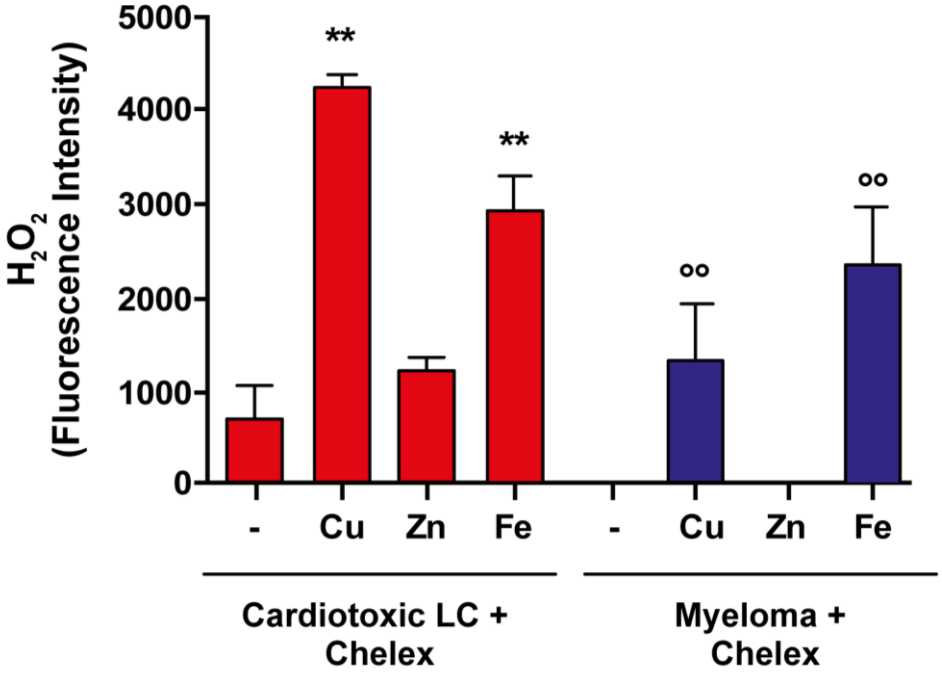


***Figure 22| Effect of chelex on the ability of LC to generate ROS***

*$H_2O_2$ produced by 45 µM cardiotoxic LC and myeloma treated with chelex and incubated 2 h with 50 µM $CuCl_2$, $ZnCl_2$, or $FeCl_2$. Control samples were incubated with chelex-treated 10 mM PBS, pH 7.4. Mean ± SE of FI, n=12, **p<0.01 vs cardiotoxic LC incubated with chelex-treated PBS, pH 7.4, °°p<0.01 vs myeloma LC + chelex-treated PBS, pH 7.4, one- way ANOVA, and Bonferroni's post hoc test (Diomede et al., 2017).*

However, only the addition of copper to cardiotoxic LC, but not to myeloma ones, caused a worsening of the pharyngeal dysfunction induced by cardiotoxic LC, whereas iron and zinc did not exert additional toxic effect (Figure 23) (Diomede et al., 2017).

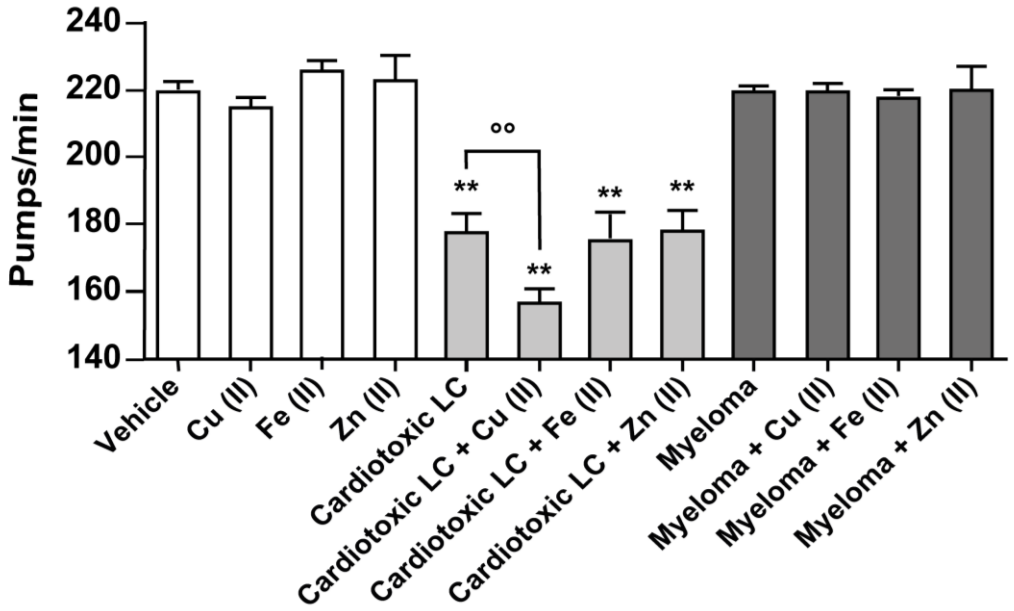


***Figure 23| Effect of metal ions on the ability of LC to affect pharyngeal pumping in worms***

*Worms were fed for 2h with 100 µg/ml cardiotoxic LC, myeloma with or without 50 µM $CuCl_2$, $ZnCl_2$, or $FeCl_2$. Control worms were incubated with 10 mM PBS, pH7.4 (Vehicle) only or 50 µM $CuCl_2$, $ZnCl_2$, and $FeCl_2$. Pumping rate as mean pumps/min ± SE (n=20 worms/assay, three assays). **p<0.01 vs vehicle, one-way ANOVA, and Bonferroni's post hoc test. °°p<0.0001 vs cardiotoxic LC, two-way ANOVA, and Bonferroni's post hoc test (Diomede et al., 2017).*

According to these findings, the addition of copper to chelex-treated cardiotoxic LC, but not zinc or iron, restores the toxicity of cardiotoxic LC and impairs the pharyngeal motility of *C. elegans* (Figure 24). In the same experimental conditions, it was observed that the pumping rate of *C. elegans*-fed myeloma protein was not affected by either copper or iron and zinc (Figure 23 and Figure 24) (Diomede et al., 2017).

All these findings indicate that, although iron and copper can drive the generation of $H_2O_2$ in cell-free conditions both in cardiotoxic and myeloma proteins, only

copper causes a pharyngeal dysfunction *in vivo*, when incubated with cardiotoxic LC (Diomede et al., 2017).

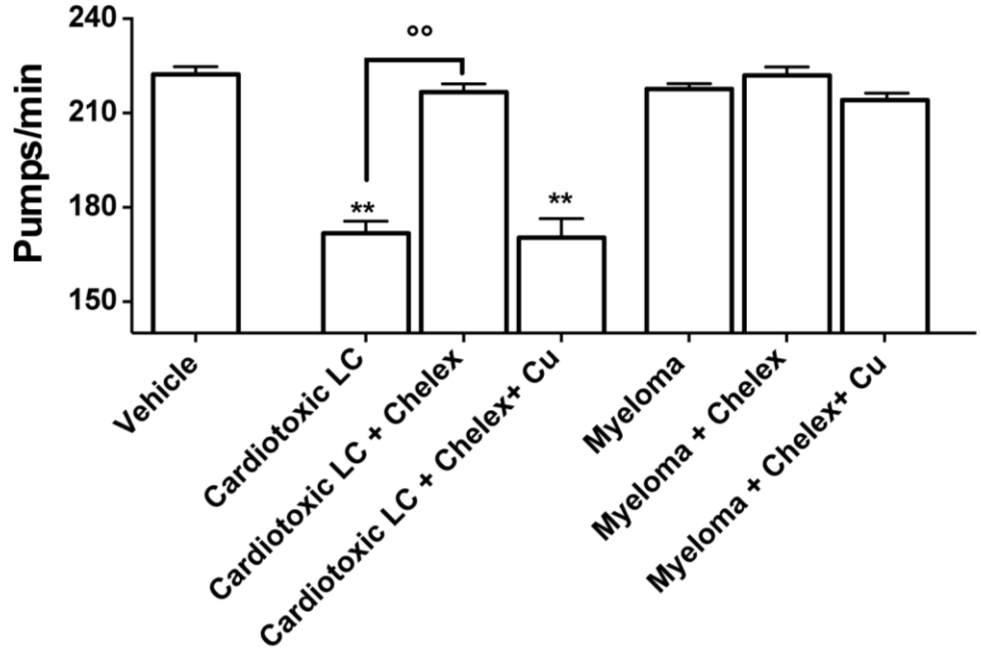


***Figure 24| Effect of chelex and copper on LC-induced toxicity***

*Worms were fed for 2 h with 100 µg/ml cardiotoxic LC or myeloma treated or not with 5 mg/ml of chelex and 50 µM copper. Control worms received 50 mM phosphate buffer, pH 7.4, alone (Vehicle). Pumping rate as mean pumps/min ± SE (3 independent assays, n=30 worms/assay). **p<0.01 vs Vehicle, °°p<0.01 vs cardiotoxic LC, one-way ANOVA, and Bonferroni's post hoc test (Diomede et al., 2017).*

The ability of cardiotoxic LC to increase $H_2O_2$ production in the presence of copper indicates that the metal can be reduced from $Cu^{2+}$ to $Cu^{+}$ by the protein, suggesting that cardiotoxic LC possess reducing species to donate electrons, as the thiol group of cysteine. To prove this hypothesis, proteins were pre-incubated with iodoacetamide, an alkylating molecule able to bind the thiol group of cysteine, preventing copper binding and ROS generation. In this experimental condition, pre-incubation with iodoacetamide significantly prevents the $H_2O_2$

generation caused by the addition of copper to cardiotoxic LC solution (Figure 25) (Diomede et al., 2017).

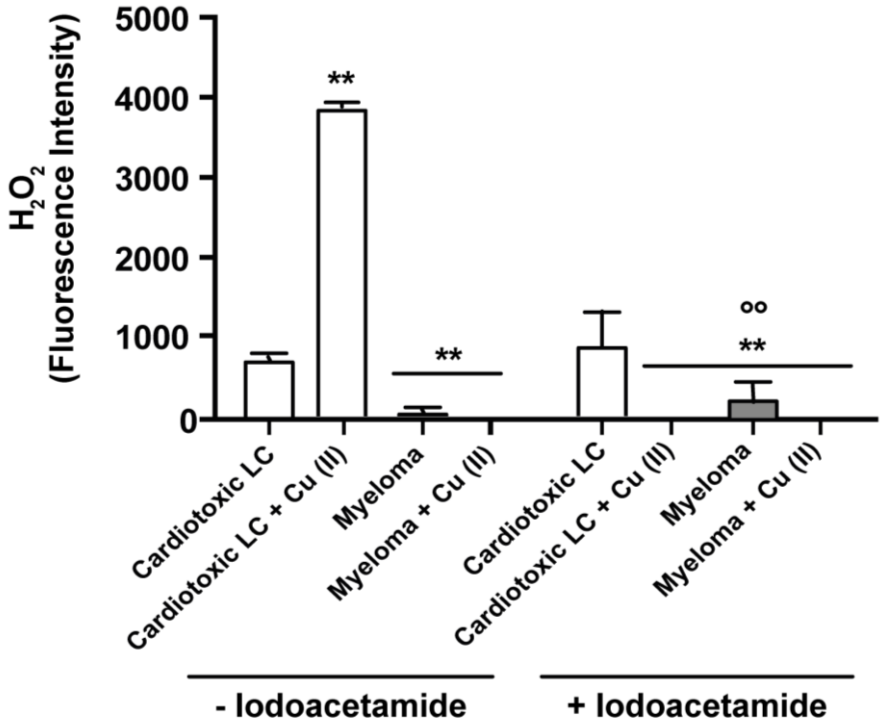


***Figure 25| Iodoacetamide cleared the copper-induced increased production of $H_2O_2$***

*$H_2O_2$ produced by cardiotoxic LC and myeloma previously treated for 3 h at 20°C with iodoacetamide and then incubated 2 h with 50 µM $CuCl_2$. Mean ± SE of FI, n=9, **p<0.01 vs cardiotoxic LC not treated with iodoacetamide and °°p<0.01 vs cardiotoxic LC treated with iodoacetamide, one-way ANOVA, and Bonferroni's post hoc test. ANOVA, analysis of variance (Diomede et al., 2017).*

All these data demonstrate that metal ions, particularly copper, play a crucial role in driving ROS generation caused by cardiotoxic LC (Diomede et al., 2017).

## 4.4 Metal- binding compounds counteracted the cardiotoxic LC-induced functional and structural damage on the worm's pharynx

To confirm the role of metal ions in driving oxidative stress in AL amyloidosis and to develop a pharmacological strategy aimed at restoring the metal homeostasis, 5-chloro-7-iodo-quinoline-8-ol (CQ) and PBT2 have been used (Diomede et al., 2017).

As showed in Figure 26, both CQ and PBT2 counteracted the toxicity caused by cardiotoxic LC in a dose-dependent manner. In particular, PBT2 being significantly more effective than CQ, with an $IC_{50}$ about 7000-fold lower ($IC_{50}$= 1.08 ± 1.1 nM and 7.5 ± 1.0 µM for PBT2 and CQ, respectively; $p<0.01$, Student's t-test) (Diomede et al., 2017).

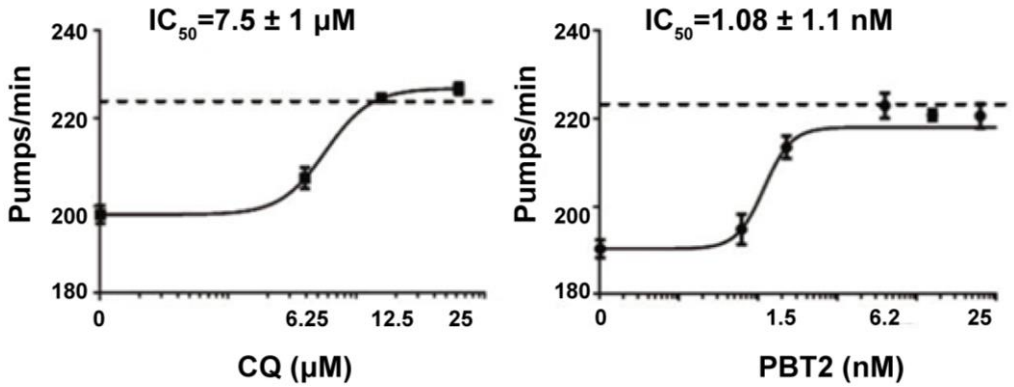


***Figure 26| Dose-response effect of metal ions chelating agents on LC-induced pharyngeal dysfunction***

*Worms were fed 2 h 100 µg/ml cardiotoxic LC in the absence or presence of 0-25 µM CQ or 0-25 nM PBT2. Control worms received vehicle alone (dotted line). Mean ± SE, N=30. $IC_{50}$ ± SD is reported (Diomede et al., 2017).*

Based on these data, CQ and PBT2 have been used at the optimal concentration of 25 µM and 2 nM, respectively. At these concentrations, drugs alone did not alter

the pharyngeal motility of worms and prevented the pharyngeal dysfunction caused by cardiotoxic LC (Figure 27 A). To confirm that the protective effects exerted by CQ and PBT2 against cardiotoxic LC were not related to general antioxidant activity, additional experiments were carried out co-incubating both compounds with exogenous $H_2O_2$. Neither compounds counteracted $H_2O_2$-induced pharyngeal toxicity, indicating that their protective effect is explicitly related to their ability to chelate metal ions (Figure 27 A). Moreover, both compounds counteracted $H_2O_2$ production, as revealed by amplex red assay (Figure 27 B) (Diomede et al., 2017).

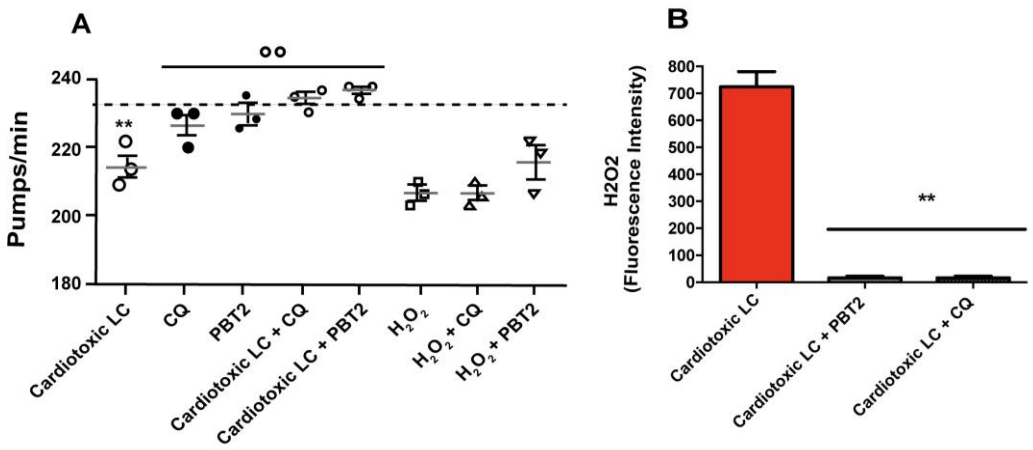


***Figure 27| Effect of metal-binding compounds CQ and PBT2 on LC-induced pharyngeal dysfunction and $H_2O_2$ production***

*(**A**) Effect of CQ and PBT2 on LC-induced pharyngeal dysfunction. Worms were fed for 2 h with 100 µg/ml cardiotoxic LC in the absence or presence of 0–25 µM CQ or 0–25 nM PBT2. Control worms received vehicle alone (dotted line). Each value is the mean ± SE, n=30. $IC_{50}$ ± SD is reported, p<0.01, Student's t-test. (**B**) $H_2O_2$ produced by cardiotoxic LC incubated 2 h with or without 2 nM PBT2 or 25 µM CQ. Mean ± SE of FI, n=6, **p<0.01 vs cardiotoxic LC, one-way ANOVA and Bonferroni's post hoc test. Adapted from (Diomede et al., 2017).*

In all of these experimental conditions, the treatment with CQ and PBT2 did not affect the secondary structure and the thermal stability of the proteins (Figure 28) (Diomede et al., 2017).

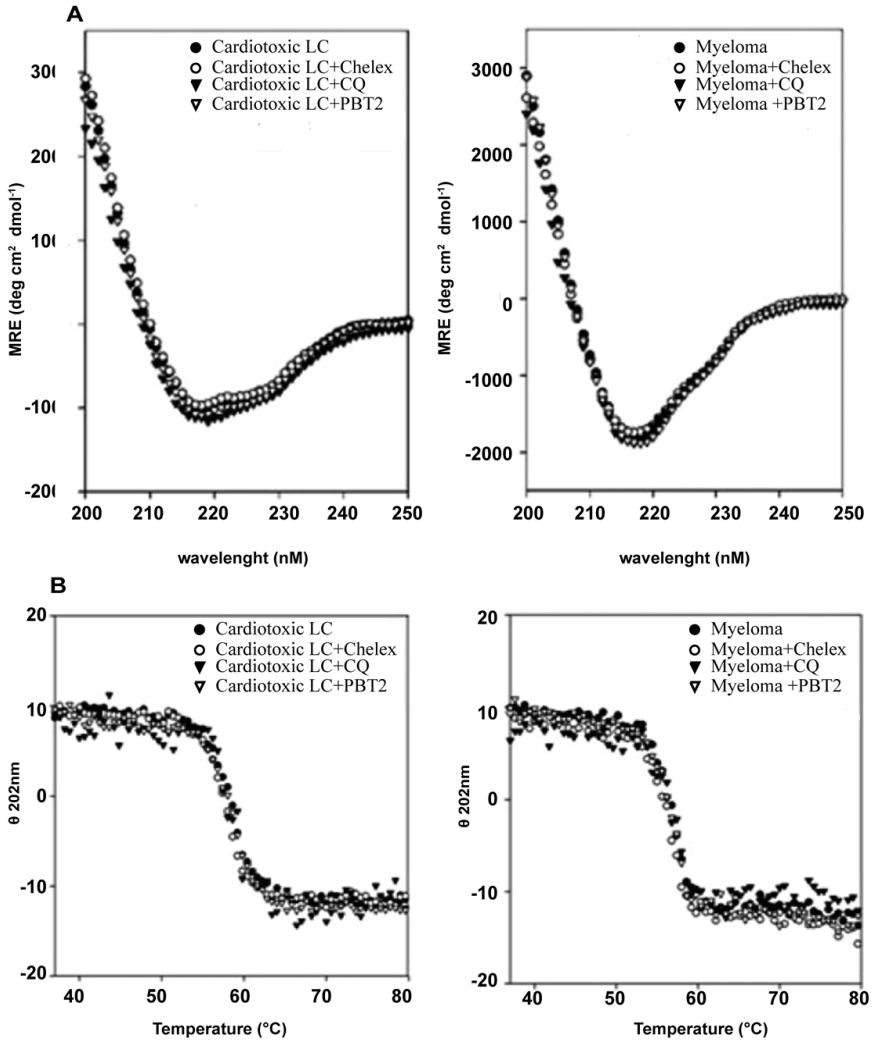


| | Tm |
|---|---|
| **Cardiotoxic LC** | 58.3 |
| **Cardiotoxic LC+Chelex** | 57.7 |
| **Cardiotoxic LC+CQ** | 58.4 |
| **Cardiotoxic LC+PBT2** | 58.3 |

| | Tm |
|---|---|
| **Myeloma** | 58.3 |
| **Myeloma+Chelex** | 57.7 |
| **Myeloma+CQ** | 58.4 |
| **Myeloma+PBT2** | 58.3 |

***Figure 28| Effect of metal ion chelators on the secondary structure and thermal stability of LC***

*(A) Far-UV CD spectra of cardiotoxic LC and myeloma proteins treated or not with 5mg/ml chelex, 25 µM CQ, or 2 nM PBT2. All samples, at the protein concentration of 0.4 mg/ml in 50 mM sodium phosphate, pH 7.4, were incubated overnight at room temperature. Far-UV CD measurements were performed at 25°C in 50 mM sodium phosphate, pH 7.4, with a Jasco J-700 spectropolarimeter using a quartz cuvette with a path length of 1 mm. Scans were conducted from 250 to 200nm at a speed of 100 nm/min*

*with a spectral bandwidth of 2 nm, a sensitivity of 20 mdegrees, and response time of 1 sec. The α-helical and β-sheet content was calculated with K2D, CDSSTR, and CONTIN software applications CD. CD spectra represent the average of 10 scans. Data are shown as mean residue ellipticity (MRE, deg cm2 dmol-1) as the function of wavelength. All spectra presented a strong negative band at 216–218 nm. Both cardiotoxic and myeloma proteins had similar β-sheet content, consistent with the pattern of a typical immunoglobulin, which were not modified by the presence of metal ion chelating agent. (**B**) Melting data were recorded at 202 nm to monitor β-sheet unfolding on sample heating from 37°C to 80°C. Analyses were performed in a 1mmpath length quartz cuvette, temperature slope of 1°C/min, the bandwidth of 2 nm, data pitch of 0.2°C, and response time of 2 sec. The thermal melt value (Tm) for each condition was calculated at the midpoint of the unfolding transition. No statistical difference among the various conditions tested was observed. No significant perturbations in thermostability were observed in LC after metal ion chelation (Diomede et al., 2017).*

The protective effects exerted by CQ and PBT2 against cardiac LC-induced toxicity were also confirmed by mitosox red staining. As shown in Figure 29, both CQ and PBT2 protected nematodes from pharyngeal mitochondrial ROS generation caused by cardiotoxic LC but not against $H_2O_2$-induced toxicity (Figure 29) (Diomede et al., 2017).

The protective effects of CQ and PBT2 on mitochondria of the pharynx of *C.elegans* have been then explored with TEM analysis. As shown in Figure 30, cardiotoxic LC at variance with myeloma, severely damage mitochondria in *C. elegans'* pharynx. However, when cardiotoxic LC was administered in the presence of 2 nM PBT2 or 25 µM CQ a protective effect in pharyngeal cells has been observed (Figure 30 D-E).

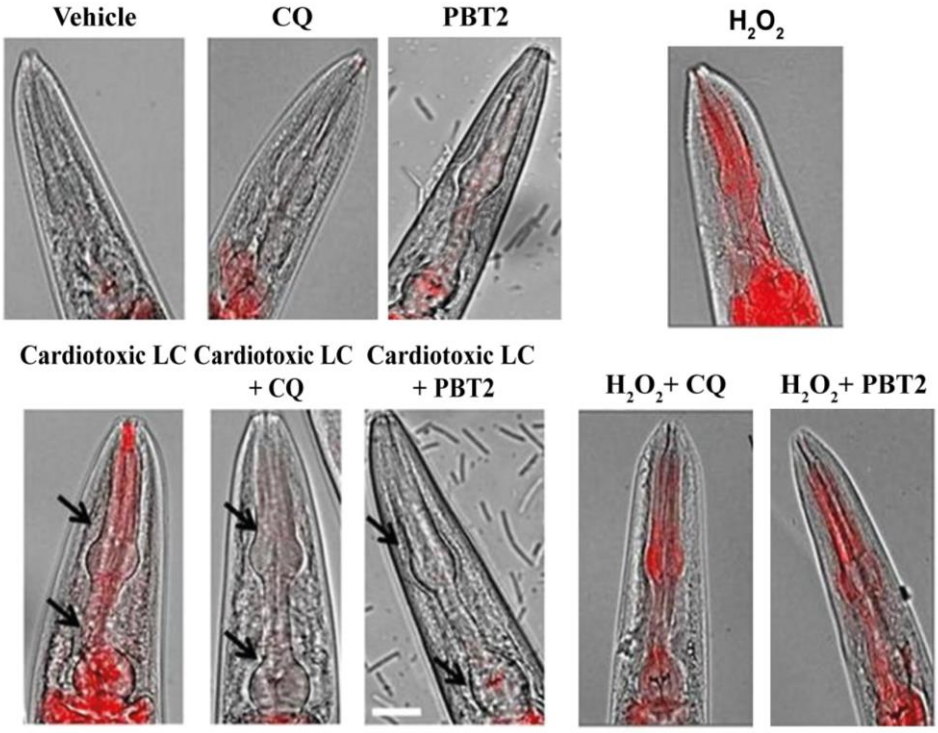


***Figure 29| Effect of CQ and PBT2 on LC-induced ROS generation***

*Worms were fed for 2 h with 100 µg/ml cardiotoxic LC with or without 25 µM CQ or 2 nM PBT2. $H_2O_2$ (1mM) was administered for 30 min with or without the drugs. Control worms received vehicle alone. Images obtained from the overlay of a contrast phase and MitoSOX fluorescence (arrows). Scale bar, 50 µm (Diomede et al., 2017).*

Similar protective effects have also been obtained when worms were fed with cardiotoxic LC in the presence of 50 µM TETRA, an antibiotic that has also antioxidant and metal ion chelator activity (Chin and Lach, 1975, Stoilova et al., 2013), or 5 mM n-acetylcysteine (NAC), a prototypic antioxidant compound. Both compounds protect pharyngeal cells from mitochondria-induced damage (Figure 30 F-G) and counteract the pharyngeal dysfunction caused by cardiotoxic LC (Figure 31) (Diomede et al., 2017).

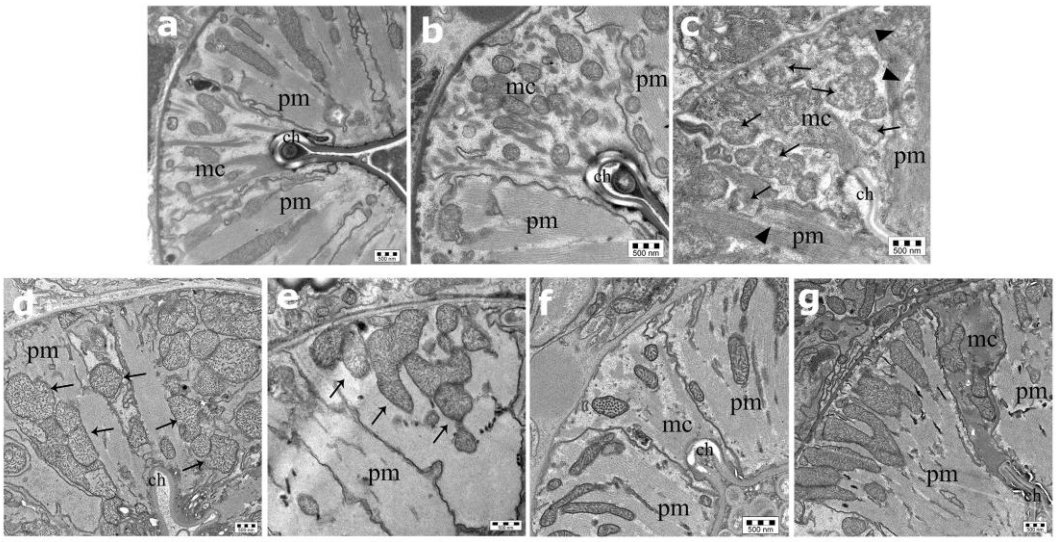


***Figure 30| ROS-induced cardiotoxic LC severely disrupt C. elegans pharyngeal ultrastructure***

*Representative images of worm's pharynx obtained from the ultrastructural analysis by TEM in C. elegans fed for 2 h with (a) Vehicle, (b) myeloma protein, (c) cardiotoxic LC alone, or with (d) 25 µM CQ, (e) 2 nM PBT2, (f) 50 µM TETRA, or (g) 5 mM NAC. Images showed two pharyngeal muscles (pm) with their mitochondria (arrowheads) separated by a marginal cell (mc) and its mitochondria (arrows), placed at the corner of the pharyngeal channel (ch). Scale bar, 500 nm. Pharyngeal muscles of worms fed cardiotoxic LC resulted in damage to mitochondria, which exhibited a clustering pattern, irregular shape, swelling, and massive disruption of the internal components (i.e., cristae). Marginal cells, which contain many mitochondria due to their active role in contractile motor function, were severely compromised and myofilaments connected to the marginal cells, which were perfectly aligned in vehicle-fed worms, were deranged (Diomede et al., 2017).*

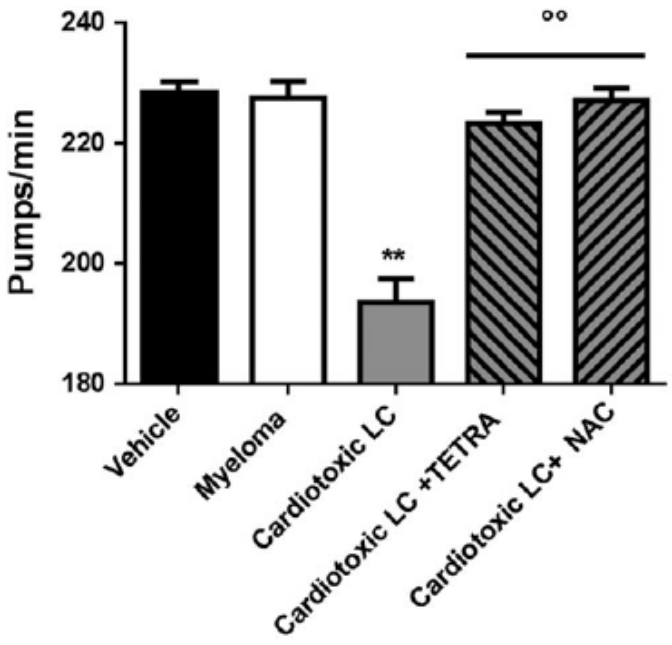


***Figure 31| Antioxidant compounds counteract the pharyngeal impairment caused by cardiotoxic LC***

*Cardiotoxic LC and myeloma in 10 mM phosphate-buffered saline, pH 7.4 were administered to worms (100 worms/100 µl) at 100 µg/ml alone or with 50 µM TETRA or 5 mM NAC. Control worms received vehicle alone (Vehicle). After incubation for 2 h in the absence of OP50 E. coli, worms were plated on NGM plates seeded with bacteria. Pharyngeal pumping was evaluated 20 h after plating and expressed as pumps/minute. **p<0.01 vs vehicle and °°p < 0.01 vs cardiotoxic LC, according to one-way ANOVA and Bonferroni's post hoc test. Adapted from (Diomede et al., 2017).*

To assess that the protective effects of CQ and PBT2 were not related to the specific purification procedure for BJ proteins, new experiments were carried out employing recombinant LC obtained from the same cardiac amyloid patients (Diomede et al., 2017). As reported in Table 5, both CQ and PBT2 similarly prevent from the pharyngeal dysfunction caused by the same cardiotoxic LC (H7), obtained from the urine of an AL-affected patient (BJ) or recombinantly (rec).

These data indicate that the damage mediated by metal ions was not an artefact of the protein purification procedure (Diomede et al., 2017).

***Table 5| Effect of CQ and PBT2 on the pharyngeal impairment caused by the natural Bence Jones and Recombinant LC from the Same Cardiac Amyloid Patient.***

| Treatment | Pharyngeal pumping (Pumps/min ± SE) |
|---|---|
| Vehicle | 233.2 ± 1.5 |
| H7-BJ | 209.5 ± 1.6* |
| H7-rec | 212.4 ± 1.0* |
| H7-BJ + CQ | 235.2 ± 1.2 |
| H7-BJ + PBT2 | 238.0 ± 1.4 |
| H7-rec + CQ | 237.0 ± 1.0 |
| H7-rec + PBT2 | 233.3 ± 1.7 |

*Human monoclonal amyloidogenic cardiotoxic LC obtained as natural Bence Jones (H7-BJ) and recombinant (H7-r) from the same cardiac amyloid patient were administered to worms (100 worms/100 µl) at 100 µg/ml in 10 mM PBS, pH 7.4, in the absence or presence of 25 µM CQ or 2 nM PBT2. Control worms received vehicle alone (Vehicle). After incubation for 2 h in the absence of OP50 E. coli, worms were plated on NGM plates seeded with bacteria. Pharyngeal functionality evaluated 20 h after plating. Pharyngeal pumping is expressed as pumps/minute ± SE. *p<0.01 vs vehicle, according to one-way analysis of variance followed by Bonferroni's post hoc test. Adapted from (Diomede et al., 2017).*

Overall, these findings indicate that cardiotoxic LC, though the disruption of metal ion homeostasis, generate ROS which directly damages the subcellular pharyngeal structures, notably mitochondria (Diomede et al., 2017).

## 4.5 Metal ions regulate the expression of genes involved in oxidative stress resistance

To determine if CQ or PBT2 prevents the activation of the antioxidant defence system caused by ROS generation, transgenic TJ356, CL2070 and CF1553 strains have been used. To this end, cardiotoxic and myeloma proteins were administered to worm with or without 25 µM CQ or 2 nM PBT2, and the fluorescence intensities have been then measured. As reported in Figure 33, both CQ and PBT2 counteracted the activation of DAF-16 induced by the cardiotoxic LC, preventing its nuclear translocation (Figure 32). A similar effect was observed after administration of 50 µM TETRA, but not 5 mM NAC (Figure 32) (Diomede et al., 2017).

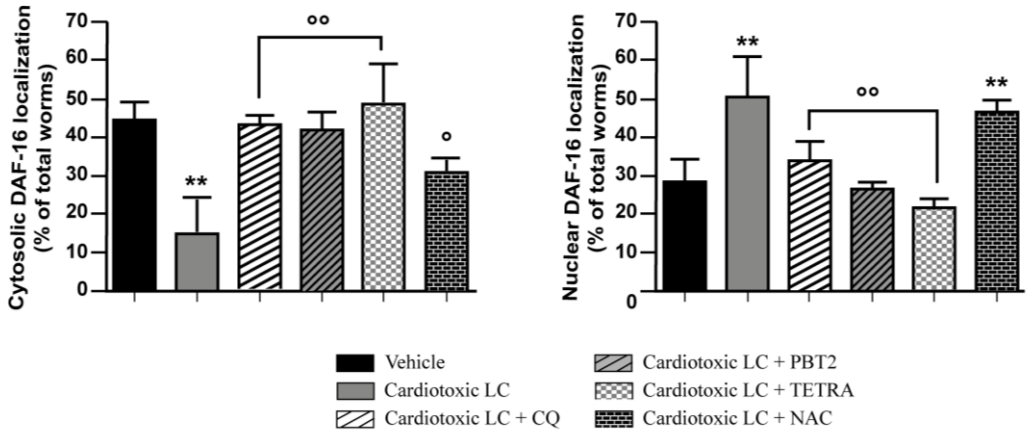


***Figure 32| Metal ions drive the ability of cardiotoxic LC to promote DAF-16 translocation from cytoplasm to nucleus in TJ356 transgenic worms***

*The subcellular distribution of DAF-16 expression in worms fed 2 h: vehicle,100 µg/ml cardiotoxic LC with or without 25 µM CQ, 2 nM PBT2, 50 µM TETRA, or 5 mM NAC. According to DAF-16 localization, worms were divided into two phenotypes, including ''cytosolic'' and ''nuclear.'' The percentage of DAF-16 localization concerning vehicle-fed worms was calculated based on three experiments, n=100. Mean ± SE. **p<0.01 vs vehicle, °p<0.05 and °°p<0.01 vs cardiotoxic LC, one-way ANOVA, and Bonferroni's post hoc test. Adapted from (Diomede et al., 2017).*

According to this data, the co-incubation with CQ and PBT2 significantly reduced the HSP-16.2 and SOD-3 protein expression caused by cardiotoxic LC, reducing the GFP signal in the pharynx of CL2070 and CF1553 worms, respectively (Figure 33) (Diomede et al., 2017).

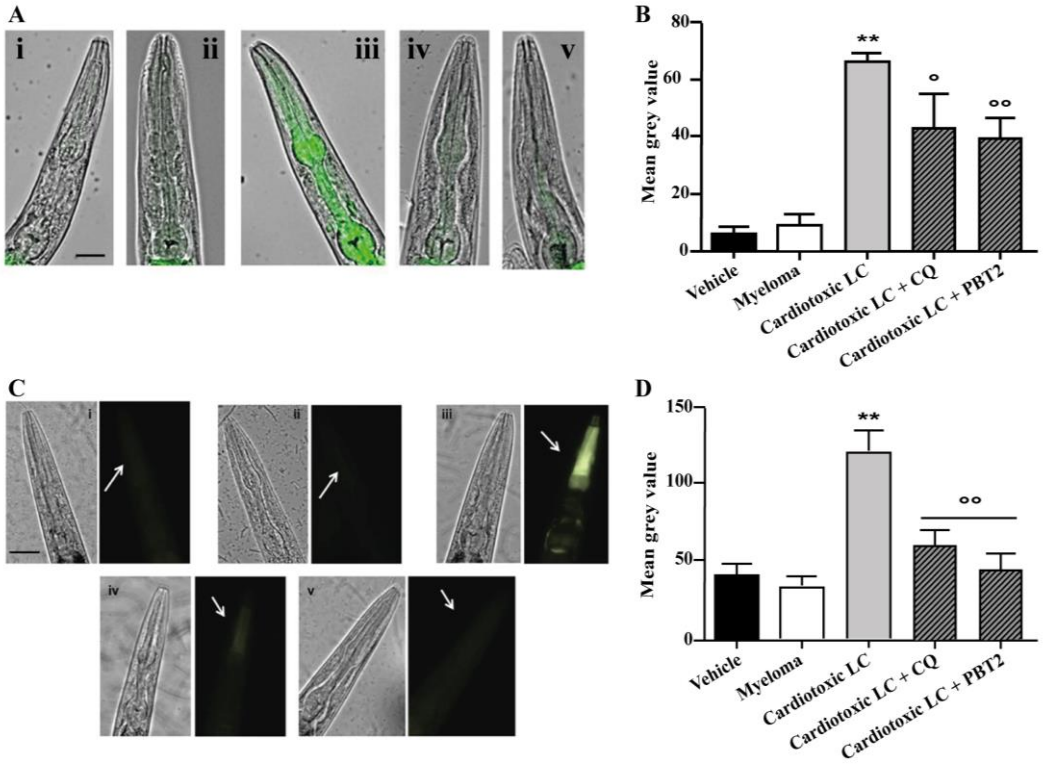


***Figure 33| Metal ions drive the ability of cardiotoxic LC to induce the pharyngeal expression of HSP-16.2 and SOD-3***

*(**A–D**) Transgenic worms were fed for 2 h with (i) Vehicle (10mM PBS, pH 7.4), (ii) 100 µg/ml myeloma, (iii)100 µg/ml cardiotoxic LC, (iv) cardiotoxic LC +25 µM CQ or (v) cardiotoxic LC + 2 nM PBT2. (**A**) Images of HSP-16.2 expression as overlays of GFP fluorescence and light microscopy in CL2070 transgenic worms. (**C**) Images of SOD-3 expression as GFP fluorescence (arrows) in CF1553 transgenic worms. Scale bar, 50 µm. Quantified GFP intensity in (**B**) CL2070 and (D) CF1553 worms in response to treatments. FI in each group was calculated as mean grey value ± SE based on three experiments, n=25. **p<0.01 vs Vehicle, °p<0.05 and °°p<0.01 vs cardiotoxic LC, one-way ANOVA, and Bonferroni's post hoc test (Diomede et al., 2017).*

The effect of CQ and PBT2 on survival was then evaluated. It was already reported that cardiotoxic LC- fed worms show a significant reduction of lifespan compared to vehicle-fed worms (median survival: 13 and 9 days for vehicle- and

cardiotoxic LC-fed worms, respectively, p = 0.0001, Log-rank test) (Figure 34). The administration of a single dose of 25 µM CQ and 2 nM/day PBT2 prolonged the survival of cardiotoxic LC- treated worms, restoring their natural lifespan (median survival: 14 days for cardiotoxic LC + CQ-treated worms (p=0.036 *vs* cardiotoxic LC) and 13 days for cardiotoxic LC + 2 nM/day PBT2 (p=0.025 *vs* cardiotoxic LC) (Figure 34) (Diomede et al., 2017).

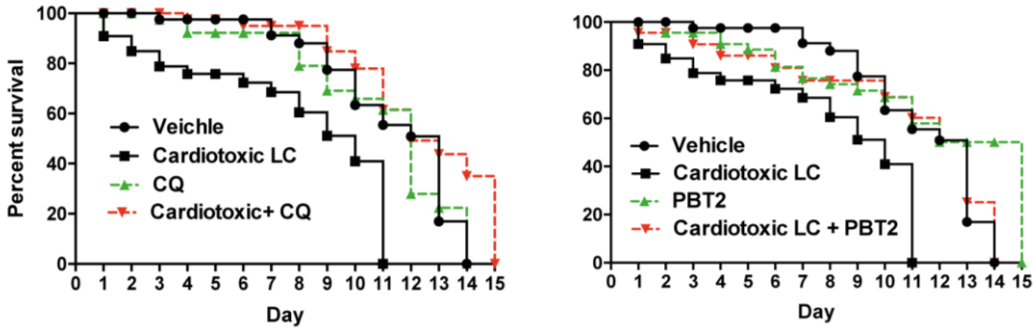


***Figure 34| Metal-binding compounds restore the natural nematode survival***

*Kaplan–Meier survival curves treated with vehicle, 100 µg/ml of cardiotoxic LC or myeloma, in the absence or presence of 25 µM CQ or 2 nM PBT2. Survival is expressed as a percentage of the initial population (n=30 worms/group, three independent experiments) (Diomede et al., 2017).*

Overall, these results indicated that cardiotoxic LC through metal ion-mediated ROS production, activate consequent FOXO/DAF-16 pathway stimulating the genes involved in the control of the oxidative stress response and lifespan. The co-incubation of cardiac LC with metal-binding compounds, such as CQ and PBT2, abolished the worm stress response and indicating that metal chelating compounds can be considered as innovative candidates for the treatment of AL patients with severe cardiac involvement (Diomede et al., 2017).

## 4.6 Synergic beneficial effect of PBT2 and TETRA

In 2014, Diomede et al. demonstrated the protective effect of tetracyclines against toxicity exerts by cardiac LC in *C. elegans* (Diomede et al., 2014a). Based on these pre-clinical findings, Wechalekar et al. designed a clinical study to evaluate the cardioprotective effect of doxycycline in AL patients (Wechalekar and Whelan, 2017). Preliminary data indicated that orally administration of 100 mg of doxycycline (corresponding to about 100 µM/day) in addition to standard chemotherapy, cause a significant reduction of the early deaths in patients with cardiac AL (Wechalekar and Whelan, 2017).

To develop a feasible clinical approach for AL amyloidosis, the combination of metal- binding compounds and tetracyclines have been evaluated in *C. elegans*. To reflect clinical conditions, worms were first incubated with cardiotoxic LC to induce damage of their pharynx. Then, drugs have been administered to worms for 30 min. The effects of 20 µM TETRA, a dose lower than that used in the clinic, 2 nM PBT2 and 25 µM CQ have been evaluated. As reported in Figure 35A, in these experimental conditions TETRA was ineffective, whereas PBT2 but not CQ, restore the pharyngeal dysfunction caused by cardiotoxic LC (Diomede et al., 2017).

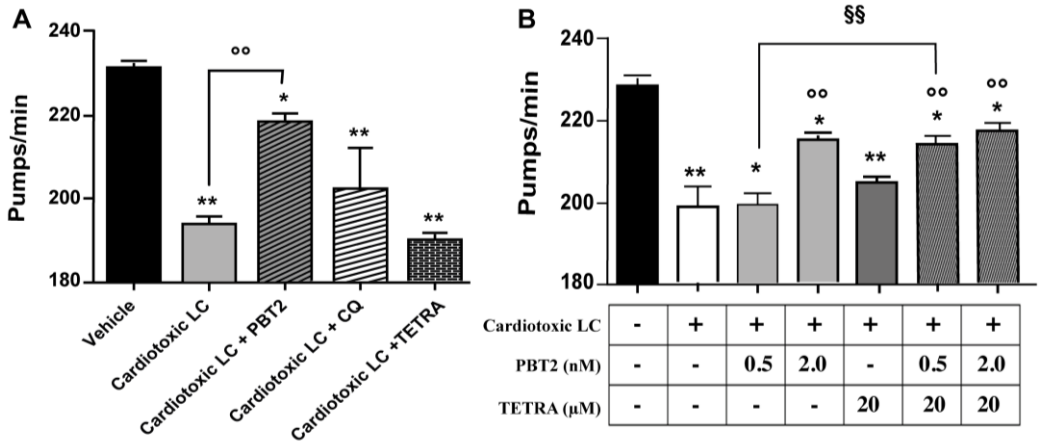


***Figure 35| Co-administration of PBT2 and TETRA causes a synergic effect against pharyngeal dysfunction***

*(**A, B**) Pharyngeal performance of worms fed 100 µg/ml cardiotoxic LC for 2 h and then treated for 30 min with (**A**) 25 µM CQ, 20 µM TETRA, or 2 nM PBT2 or with (**B**) 0.5–2 nM PBT2 alone or together with 20 µM TETRA. Control worms fed vehicle alone. **p<0.001, *p<0.005 vs vehicle, °°p<0.001 vs cardiotoxic LC, one-way ANOVA, and Bonferroni's post hoc test. §§p<0.01 significant interaction vs worms fed cardiotoxic LC + 0.5 nM PBT2, two-way ANOVA, and Bonferroni's post hoc test (Diomede et al., 2017).*

To determine the lowest effective dose of PBT2 able to improve the effect of TETRA, this metal-binding compound was administered at 2 or 0.5 nM concentrations. As reported in Figure 35 B, the single administration of PBT2 alone at the lower concentration, it results ineffective. However, when it was used in combination with TETRA, they exert a synergistic and beneficial effect on the pharyngeal motility of worms (Figure 35 B). Moreover, when higher concentrations of PBT2 were used in combination with TETRA, no additional protective effects have been observed (Diomede et al., 2017).

Although this combined treatment did not reverse the pharyngeal dysfunction to normal levels, these results indicate that the combined administration of low doses of PBT2 and TETRA may represent an innovative pharmacological approach to

break the vicious cycle of oxidative stress and heart damage induced by cardiotoxic LC (Diomede et al., 2017).

# CHAPTER 5

# Discussion

To date, the therapeutic approach used for AL amyloidosis, similarly to that employed for multiple myeloma, is aimed at the suppression of the plasma cell clone overproducing amyloidogenic LC (Merlini et al., 2011). This pharmacological treatment resulted in the reduction of the circulating LC although an effect on pre-formed amyloid deposits was not observed (D'Souza et al., 2017, Palladini et al., 2012). Eligible patients can also undergo autologous stem cell transplantation (D'Souza et al., 2017). It was estimated that about the 25% of the total AL- affected patients, due to their end-stage cardiac damage, is too fragile to receive chemotherapeutic treatment and transplantation (Milani et al., 2018).In the absence of any cure, the median survival of these patients is less than one year after diagnosis (Milani et al., 2018). This is why the accessibility to methods allowing the early diagnosis of AL as well as the development of innovative therapeutic approaches are needed to counteract the rapid progressing cardiac failure in patients suffering from AL amyloidosis, particularly in most compromised ones (Diomede et al., 2017).

Actually no transgenic animals steadily overproducing LC and forming amyloid deposits are available. In the last years, various attempts have been made to develop AL transgenic mice, employing different pathogenic LC. However, no successful results have been reported because no fibrils formation has been observed (Buxbaum, 2009, Sirac et al., 2011). This might be due to the low concentrations of proteins synthesized and secreted in these animal models, at variance with human physiological conditions (Sirac et al., 2011). In 2000, Hrncic et al. developed a mouse model by injecting intraperitoneally of massive amounts of LC purified from AL-affected patients (Hrncic et al., 2000). Although it was

the only mouse model in which amyloid deposits have been detected, it was also reported that macrophages and neutrophils then surrounded these aggregates and then resorbed (Hrncic et al., 2000). This means that this model is not eligible for *in vivo* study on AL amyloidosis (Hrncic et al., 2000). New *in vivo* approaches have been used to investigate the toxicity of the different protein assemblies (Diomede et al., 2014b). In 2013, Mishra et al. used zebrafish (*Danio renio*) embryos as an animal model to investigate the effects of LC purified from the urine of AL patients with cardiac injury (Mishra et al., 2013). In agreement to the clinical finding, the *in vivo* and *ex vivo* experiments, they demonstrated that through increased of oxidative stress, cardiotoxic LC cause cardiac damage, cell death and the reduction of overall survival of injected organisms, in the absence of fibrillary deposits (Mishra et al., 2013).

Similar results were also obtained in 2014 by Diomede et al. employing the nematode *C.elegans* as a novel animal model to investigate the cardiotoxicity of LC (Diomede et al., 2014a). Although the main limitation of this model is the evolutionarily distance from vertebrates, in this worm many human stress pathways are conserved. This means that, although the translation to human pathology requires caution, this nematode is suitable to investigate the molecular mechanisms of different complex diseases (Diomede et al., 2014b, Diomede et al., 2014a).

Although the presence of amyloidogenic deposits is one of the main features of AL amyloidosis, soluble assemblies of LC, due to their ability to generate ROS, play a vital role in the onset and progression of the pathology (Diomede et al., 2014a). Counteracting the toxic effects of ROS with antioxidants or tetracyclines,

resulted in a protective effect against the LC-induced damage both in vitro and in vivo (Diomede et al., 2014a, Liao et al., 2001). Based on these findings, doxycycline, has been used in a case-matched clinical study in which AL patients with severe cardiac involvement received doxycycline (100 mg, twice daily) in addition to the standard chemotherapy (Wechalekar and Whelan, 2017). As reported by Wechalekar et al., adjuvant doxycycline extended survival in AL-affected patients with cardiac damage and NT-proBNP levels lower than 8500 ng/L (stage IIIa) (Wechalekar and Whelan, 2017, Palladini et al., 2015). Unfortunately, this approach is ineffective in IIIb patients, with severe cardiac damage and NT-proBNP levels above 8500 ng/L (Wechalekar and Whelan, 2017, Palladini et al., 2015).

In this study, I used the nematode *C. elegans* to investigate the molecular mechanisms involved in ROS generation, and in particular the role of metal ions in promoting the oxidative-mediated damage caused by cardiotoxic LC.

The data obtained demonstrate that the ROS species generated by cardiac LC caused severe mitochondrial damage in the pharynx of worms (Diomede et al., 2017). The translational relevance of this observation is supported by the TEM analysis performed on human cardiac biopsies from AL patients with severe cardiac involvement and admitted to heart transplantation. In these samples, the presence of a severe mitochondrial ultrastructural damage comparable to that observed in the pharynx of worms fed with cardiotoxic LC indicated that the impairment of mitochondria is actively involved in cardiac AL amyloidosis (Diomede et al., 2017).

The ability of cardiotoxic LC to co-localize with mitochondria was already described *in vitro*, in human primary cardiac fibroblasts and stem cell-derived cardiomyocytes (Lavatelli et al., 2015). Using a proteomic approach, it was also demonstrated that cardiotoxic LC, but not myeloma one, specifically interact with intracellular proteins involved in cell viability and metabolism, leading to severe alteration of mitochondrial morphology (Lavatelli et al., 2015). Overall, these findings indicate that LC affect the mitochondria of *C. elegans*' pharynx and the vertebrate heart similarly. It should be noted that both these organs are rich in mitochondria due to their crucial role in providing the energy required for contraction (Diomede et al., 2017).

Metal ions, particularly copper, play a crucial role in different neurodegenerative disorders due to their ability to interact and promote the aggregation of different amyloidogenic proteins, including Aβ protein and α-synuclein (Hunter et al., 1997, Ostrerova-Golts et al., 2000). Studies conducted *in vitro* on recombinant LC reported that copper might promote their aggregation (Davis et al., 2001, Diomede et al., 2017). In this study it has been demonstrated that redox-active transition metal ions, particularly copper, specifically interact with cardiotoxic LC, driving their ability to generate ROS (Diomede et al., 2017).

The ROS production is entirely unrelated to the germline gene of LC and to the purification' method employed to obtain the proteins.

The interaction of LC with metal ions is pivotal for the ROS-induced damage within the pharyngeal cells, particularly at the mitochondrial level (Diomede et al., 2017). In *C. elegans*, cells react to this insult by activating the transcription of different protective pathways. To gain insight into the molecular mechanism

driving cardiotoxic LC, the activation of the DAF-16/FOXO transcription factor, as a defence mechanism against the ROS-induced damage and devoted to re-establish the cellular homeostasis, has been here demonstrated (Fonte et al., 2002, Heidler et al., 2010). It is known that in *C. elegans*, the phosphorylation and the nuclear translocation of DAF-16 trigger the transcription of genes involved in stress resistance and longevity, including *sod-3* and *hsp-16.2* (Fonte et al., 2002, Heidler et al., 2010). I demonstrated that cardiotoxic LC, but not myeloma, increase the expression of *sod-3*, mainly localized in the mitochondria of pharyngeal cells (Giglio et al., 1994, Hunter et al., 1997), and *hsp-16.2* (Diomede et al., 2017).

All these data have been collected and summarized in Figure 36.

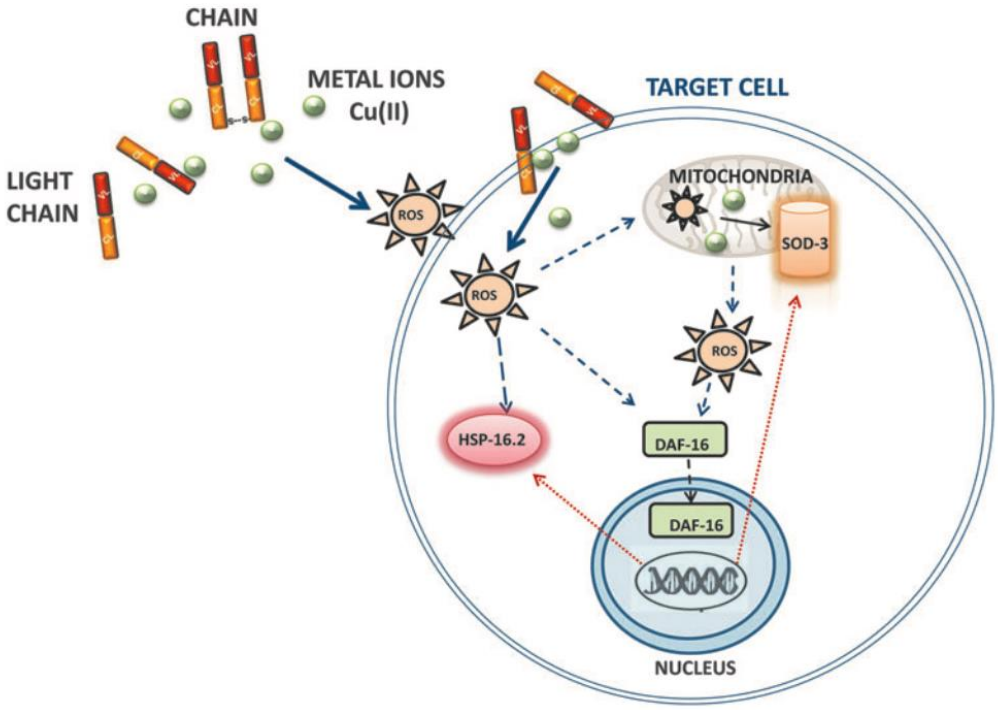


***Figure 36| Proposed model for metal ion involvement in the mechanism underlying the LC-induced toxicity***

*Redox-active transition metals, particularly copper, drive the ability of cardiotoxic LC to produce ROS in vivo. The excessive production of ROS can directly target the pharyngeal cells, damaging the organelle functions and the ultrastructure, particularly at the*

*mitochondrial level. Mitochondria react to ROS by inducing the expression of the scavenger protein SOD-3. Also, the nuclear translocation of the FOXO/DAF-16 transcription factor is activated, triggering a secondary ROS-induced cellular response by inducing the transcription of stress-responsive genes, including hsp- 16.2 and sod-3, and controlling longevity.*

To definitively block the ROS production, a new pharmacological strategy aimed not only at chelating metal ions but also to restore correct metal homeostasis, was here designed (Diomede et al., 2017). CQ and the new derivative PBT2 have been considered because both compounds specifically act as metal chelators and re-establish metal homeostasis across the plasma membrane into cells (Crouch et al., 2011). PBT2 has been recently developed for the treatment of Huntington disease and is currently under evaluation for the treatment of other neurodegenerative disorders characterized by cognitive impairment, neuronal degeneration and protein aggregation, including AD (Huntington Study Group Reach, 2015, Adlard et al., 2008).

Both CQ and PBT2 protected *C. elegans* from the pharyngeal dysfunction, and the mitochondrial impairment caused by cardiotoxic LC blocking their ability to produce ROS. PBT2 was active at a concentration 7000-fold lower than CQ (Diomede et al., 2017). Interestingly, neither compounds protected from the pharyngeal dysfunction nor mitochondrial damage caused by exogenous $H_2O_2$, demonstrating that their effect is not related to an antioxidant activity (Diomede et al., 2017). Also, these two drugs prevented the activation of the DAF-16/FOXO pathway and inhibited the transcription of *sod-3* and *has-16.2* genes (Diomede et al., 2017). The protective activity of PBT2 and CQ was not related to any antioxidant activity since they were not effective against the pharyngeal

dysfunction and mitochondrial damage caused by exogenous $H_2O_2$. The only antioxidant activity, as that exerted by NAC, was not sufficient to block the nuclear translocation of DAF-16 and the activation of SOD-3 and HSP-16.2 in cardiotoxic LC-fed worms, confirming that the regulation of metal ions homeostasis is crucial to abolish the worm stress response (Diomede et al., 2017). When PBT2 was co-administered with TETRA, a synergic protective effect was obtained. This allows reducing the doses of each drug to be employed significantly. These findings suggest that this approach can also be applied to improve the median survival of AL patients, particularly those of stage IIIb which have no benefits from the administration of doxycycline alone (Diomede et al., 2017).

Although this evidence are obtained in a simple multicellular organism, their relevance is supported by the evolutionary conservation of fundamental biological processes between *C. elegans* and humans and the similar subcellular alterations caused by cardiac LC in human heart and worms. This new conceptual advance paves the way for new pharmacological strategies aimed at totally inhibiting the vicious cycle of redox damage.

CHAPTER **6**

# Concluding remarks

Overall, the results obtained in this thesis demonstrated that *C. elegans* could be used for rapid screening of LC in basic research and translational applications, to discriminate their cardiotoxic potential.

I identify the mechanism by which cardiotoxic LC, but not myeloma proteins, are recognized as toxic by *C. elegans.* Moreover, using this nematode, I gain insight into the molecular mechanisms involved in AL amyloidosis identifying metal ions, already proposed to be involved in some central amyloidosis, as novel mediators of the LC toxicity (Gaeta and Hider, 2005, Wong and Duce, 2014).

Based on these findings, I contributed to design and develop a new pharmacological strategy based on the use of metal chelating compound PBT2 in combination with tetracycline in addition to standard bortezomib-based chemotherapy. This approach, aimed at restoring the metal homeostasis and interrupting the vicious cycle of oxidative stress production caused by metal ions, can be used to improve cardiac response rate in newly diagnosed patients with AL amyloidosis, improving their life expectancy.

CHAPTER 7

# Bibliography

ADLARD, P. A., CHERNY, R. A., FINKELSTEIN, D. I., GAUTIER, E., ROBB, E., CORTES, M., VOLITAKIS, I., LIU, X., SMITH, J. P., PEREZ, K., LAUGHTON, K., LI, Q. X., CHARMAN, S. A., NICOLAZZO, J. A., WILKINS, S., DELEVA, K., LYNCH, T., KOK, G., RITCHIE, C. W., TANZI, R. E., CAPPAI, R., MASTERS, C. L., BARNHAM, K. J. & BUSH, A. I. 2008. Rapid restoration of cognition in Alzheimer's transgenic mice with 8-hydroxy quinoline analogs is associated with decreased interstitial Abeta. *Neuron,* 59**,** 43-55.

ALTAMURA, S. & MUCKENTHALER, M. U. 2009. Iron toxicity in diseases of aging: Alzheimer's disease, Parkinson's disease and atherosclerosis. *J Alzheimers Dis,* 16**,** 879-95.

ALTUN, Z. F. A. H., D.H. 2009. *Introduction. In WormAtlas.* [Online].

ANBALAGAN, C., LAFAYETTE, I., ANTONIOU-KOUROUNIOTI, M., HAQUE, M., KING, J., JOHNSEN, B., BAILLIE, D., GUTIERREZ, C., MARTIN, J. A. & DE POMERAI, D. 2012. Transgenic nematodes as biosensors for metal stress in soil pore water samples. *Ecotoxicology,* 21**,** 439-55.

ANDREINI, C., BERTINI, I., CAVALLARO, G., HOLLIDAY, G. L. & THORNTON, J. M. 2008. Metal ions in biological catalysis: from enzyme databases to general principles. *J Biol Inorg Chem,* 13**,** 1205-18.

ANGELE-MARTINEZ, C., GOODMAN, C. & BRUMAGHIM, J. 2014. Metal-mediated DNA damage and cell death: mechanisms, detection methods, and cellular consequences. *Metallomics,* 6**,** 1358-81.

ARNDT, J. W., QIAN, F., SMITH, B. A., QUAN, C., KILAMBI, K. P., BUSH, M. W., WALZ, T., PEPINSKY, R. B., BUSSIERE, T., HAMANN, S., CAMERON, T. O. & WEINREB, P. H. 2018. Structural and kinetic basis for the selectivity of aducanumab for aggregated forms of amyloid-beta. *Sci Rep,* 8**,** 6412.

ATWOOD, C. S., HUANG, X., MOIR, R. D., TANZI, R. E. & BUSH, A. I. 1999. Role of free radicals and metal ions in the pathogenesis of Alzheimer's disease. *Met Ions Biol Syst,* 36**,** 309-64.

AVERY, L. & SHTONDA, B. B. 2003. Food transport in the C. elegans pharynx. *J Exp Biol,* 206**,** 2441-57.

AYTON, S., BELAIDI, A. A., LEI, P. & BUSH, A. I. 2017. Chapter 10 - Targeting Transition Metals for Neuroprotection in Alzheimer's Disease. *In:* GOZES, I. (ed.) *Neuroprotection in Alzheimer's Disease.* Academic Press.

BACK, P., BRAECKMAN, B. P. & MATTHIJSSENS, F. 2012. ROS in aging Caenorhabditis elegans: damage or signaling? *Oxid Med Cell Longev,* 2012**,** 608478.

BARNHAM, K. J. & BUSH, A. I. 2014. Biological metals and metal-targeting compounds in major neurodegenerative diseases. *Chem Soc Rev,* 43**,** 6727-49.

BEMPORAD, F. & CHITI, F. 2012. Protein misfolded oligomers: experimental approaches, mechanism of formation, and structure-toxicity relationships. *Chem Biol,* 19**,** 315-27.

BLANCAS-MEJIA, L. M. & RAMIREZ-ALVARADO, M. 2013. Systemic amyloidoses. *Annu Rev Biochem,* 82**,** 745-74.

BOYD, W. A., COLE, R. D., ANDERSON, G. L. & WILLIAMS, P. L. 2003. The effects of metals and food availability on the behavior of Caenorhabditis elegans. *Environ Toxicol Chem,* 22**,** 3049-55.

BRENNER, D. A., JAIN, M., PIMENTEL, D. R., WANG, B., CONNORS, L. H., SKINNER, M., APSTEIN, C. S. & LIAO, R. 2004. Human amyloidogenic light chains directly impair cardiomyocyte function through an increase in cellular oxidant stress. *Circ Res,* 94**,** 1008-10.

BUDIMIR, A. 2011. Metal ions, Alzheimer's disease and chelation therapy. *Acta Pharm,* 61**,** 1-14.

BUSH, A. I. 2003. The metallobiology of Alzheimer's disease. *Trends Neurosci,* 26**,** 207-14.

BUXBAUM, J. N. 2009. Animal models of human amyloidoses: are transgenic mice worth the time and trouble? *FEBS Lett,* 583**,** 2663-73.

CHERNY, R. A., ATWOOD, C. S., XILINAS, M. E., GRAY, D. N., JONES, W. D., MCLEAN, C. A., BARNHAM, K. J., VOLITAKIS, I., FRASER, F. W., KIM, Y., HUANG, X., GOLDSTEIN, L. E., MOIR, R. D., LIM, J. T., BEYREUTHER, K., ZHENG, H., TANZI, R. E., MASTERS, C. L. & BUSH, A. I. 2001. Treatment with a copper-zinc chelator markedly and rapidly inhibits beta-amyloid accumulation in Alzheimer's disease transgenic mice. *Neuron,* 30**,** 665-76.

CHIN, T. F. & LACH, J. L. 1975. Drug diffusion and bioavailability: tetracycline metallic chelation. *Am J Hosp Pharm,* 32**,** 625-9.

CHISHOLM A. D. 2006. Nematode ( C. elegans ), Molecular Biology of. *Reviews in Cell Biology and Molecular Medicine.*

CHITI, F. & DOBSON, C. M. 2006. Protein misfolding, functional amyloid, and human disease. *Annu Rev Biochem,* 75**,** 333-66.

CHITI, F. & DOBSON, C. M. 2017. Protein Misfolding, Amyloid Formation, and Human Disease: A Summary of Progress Over the Last Decade. *Annu Rev Biochem,* 86**,** 27-68.

CONSORTIUM, C. E. S. 1998. Genome sequence of the nematode C. elegans: a platform for investigating biology. *Science,* 282**,** 2012-8.

CROUCH, P. J., SAVVA, M. S., HUNG, L. W., DONNELLY, P. S., MOT, A. I., PARKER, S. J., GREENOUGH, M. A., VOLITAKIS, I., ADLARD, P. A., CHERNY, R. A., MASTERS, C. L., BUSH, A. I., BARNHAM, K. J. & WHITE, A. R. 2011. The Alzheimer's therapeutic PBT2 promotes amyloid-beta degradation and GSK3 phosphorylation via a metal chaperone activity. *J Neurochem,* 119**,** 220-30.

CUAJUNGCO, M. P., FAGET, K. Y., HUANG, X., TANZI, R. E. & BUSH, A. I. 2000. Metal chelation as a potential therapy for Alzheimer's disease. *Ann N Y Acad Sci,* 920**,** 292-304.

D'SOUZA, A., FLYNN, K., CHHABRA, S., DHAKAL, B., HAMADANI, M., JACOBSEN, K., PASQUINI, M., WEIHRAUCH, D. & HARI, P. 2017. Rationale and design of DUAL study: Doxycycline to Upgrade response in light chain (AL) amyloidosis (DUAL): A phase 2 pilot study of a two-pronged approach of prolonged doxycycline with plasma cell-directed therapy in the treatment of AL amyloidosis. *Contemp Clin Trials Commun,* 8**,** 33-38.

DAVIS, D. P., GALLO, G., VOGEN, S. M., DUL, J. L., SCIARRETTA, K. L., KUMAR, A., RAFFEN, R., STEVENS, F. J. & ARGON, Y. 2001. Both the environment and somatic mutations govern the aggregation pathway of pathogenic immunoglobulin light chain. *J Mol Biol,* 313**,** 1021-34.

DI VAIRA, M., BAZZICALUPI, C., ORIOLI, P., MESSORI, L., BRUNI, B. & ZATTA, P. 2004. Clioquinol, a drug for Alzheimer's disease specifically interfering with brain metal metabolism: structural characterization of its zinc(II) and copper(II) complexes. *Inorg Chem,* 43**,** 3795-7.

DIOMEDE, L., ROGNONI, P., LAVATELLI, F., ROMEO, M., DEL FAVERO, E., CANTU, L., GHIBAUDI, E., DI FONZO, A., CORBELLI, A., FIORDALISO, F., PALLADINI, G., VALENTINI, V., PERFETTI, V., SALMONA, M. & MERLINI, G. 2014a. A Caenorhabditis elegans-based assay recognizes immunoglobulin light chains causing heart amyloidosis. *Blood,* 123**,** 3543-52.

DIOMEDE, L., ROGNONI, P., LAVATELLI, F., ROMEO, M., DI FONZO, A., FORAY, C., FIORDALISO, F., PALLADINI, G., VALENTINI, V., PERFETTI, V., SALMONA, M. & MERLINI, G. 2014b. Investigating heart-specific toxicity of amyloidogenic immunoglobulin light chains: A lesson from C. elegans. *Worm,* 3**,** e965590.

DIOMEDE, L., ROMEO, M., ROGNONI, P., BEEG, M., FORAY, C., GHIBAUDI, E., PALLADINI, G., CHERNY, R. A., VERGA, L., CAPELLO, G. L., PERFETTI, V., FIORDALISO, F., MERLINI, G. & SALMONA, M. 2017. Cardiac Light Chain Amyloidosis: The Role of Metal Ions in Oxidative Stress and Mitochondrial Damage. *Antioxid Redox Signal,* 27**,** 567-582.

DISPENZIERI, A. & MERLINI, G. 2016. Immunoglobulin Light Chain Systemic Amyloidosis. *In:* ROCCARO, A. M. & GHOBRIAL, I. M. (eds.) *Plasma Cell Dyscrasias.* Cham: Springer International Publishing.

DJORDJEVIC, V. B. 2004. Free radicals in cell biology. *Int Rev Cytol,* 237**,** 57-89.

ECKERS, A. & KLOTZ, L. O. 2009. Heavy metal ion-induced insulin-mimetic signaling. *Redox Rep,* 14**,** 141-6.

ESSERS, M. A., WEIJZEN, S., DE VRIES-SMITS, A. M., SAARLOOS, I., DE RUITER, N. D., BOS, J. L. & BURGERING, B. M. 2004. FOXO transcription factor activation by oxidative stress mediated by the small GTPase Ral and JNK. *EMBO J,* 23**,** 4802-12.

FALK, R. H., ALEXANDER, K. M., LIAO, R. & DORBALA, S. 2016. AL (Light-Chain) Cardiac Amyloidosis: A Review of Diagnosis and Therapy. *J Am Coll Cardiol,* 68**,** 1323-41.

FALK, R. H., COMENZO, R. L. & SKINNER, M. 1997. The systemic amyloidoses. *N Engl J Med,* 337**,** 898-909.

FAROOQUI, A. A. 2016. Neurochemical Aspects of Alzheimer Disease. *Therapeutic Potentials of Curcumin for Alzheimer Disease.* Cham: Springer International Publishing.

FLORA, S. J. & PACHAURI, V. 2010. Chelation in metal intoxication. *Int J Environ Res Public Health,* 7**,** 2745-88.

FONTE, V., KAPULKIN, W. J., TAFT, A., FLUET, A., FRIEDMAN, D. & LINK, C. D. 2002. Interaction of intracellular beta amyloid peptide with chaperone proteins. *Proc Natl Acad Sci U S A,* 99**,** 9439-44.

GAETA, A. & HIDER, R. C. 2005. The crucial role of metal ions in neurodegeneration: the basis for a promising therapeutic strategy. *Br J Pharmacol,* 146**,** 1041-59.

GANDY, S., SIMON, A. J., STEELE, J. W., LUBLIN, A. L., LAH, J. J., WALKER, L. C., LEVEY, A. I., KRAFFT, G. A., LEVY, E., CHECLER, F., GLABE, C., BILKER, W. B., ABEL, T., SCHMEIDLER, J. & EHRLICH, M. E. 2010. Days to criterion as an indicator of toxicity associated with human Alzheimer amyloid-beta oligomers. *Ann Neurol,* 68**,** 220-30.

GERTZ, M. A., COMENZO, R., FALK, R. H., FERMAND, J. P., HAZENBERG, B. P., HAWKINS, P. N., MERLINI, G., MOREAU, P., RONCO, P., SANCHORAWALA, V., SEZER, O., SOLOMON, A. & GRATEAU, G. 2005. Definition of organ involvement and treatment response in immunoglobulin light chain amyloidosis (AL): a consensus opinion from the 10th International Symposium on Amyloid and Amyloidosis, Tours, France, 18-22 April 2004. *Am J Hematol,* 79**,** 319-28.

GIGLIO, M. P., HUNTER, T., BANNISTER, J. V., BANNISTER, W. H. & HUNTER, G. J. 1994. The manganese superoxide dismutase gene of Caenorhabditis elegans. *Biochem Mol Biol Int,* 33**,** 37-40.

GROSSI, C., FRANCESE, S., CASINI, A., ROSI, M. C., LUCCARINI, I., FIORENTINI, A., GABBIANI, C., MESSORI, L., MONETI, G. & CASAMENTI, F. 2009. Clioquinol decreases amyloid-beta burden and reduces working memory impairment in a transgenic mouse model of Alzheimer's disease. *J Alzheimers Dis,* 17**,** 423-40.

HARRINGTON, J. M., BOYD, W. A., SMITH, M. V., RICE, J. R., FREEDMAN, J. H. & CRUMBLISS, A. L. 2012. Amelioration of metal-induced toxicity in Caenorhabditis elegans: utility of chelating agents in the bioremediation of metals. *Toxicol Sci,* 129**,** 49-56.

HARTWIG, K., HEIDLER, T., MOCH, J., DANIEL, H. & WENZEL, U. 2009. Feeding a ROS-generator to Caenorhabditis elegans leads to increased expression of small heat shock protein HSP-16.2 and hormesis. *Genes Nutr,* 4**,** 59-67.

HAY, N. 2011. Interplay between FOXO, TOR, and Akt. *Biochim Biophys Acta,* 1813**,** 1965-70.

HEIDLER, T., HARTWIG, K., DANIEL, H. & WENZEL, U. 2010. Caenorhabditis elegans lifespan extension caused by treatment with an orally active ROS-generator is dependent on DAF-16 and SIR-2.1. *Biogerontology,* 11**,** 183-95.

HELSEL, M. E. & FRANZ, K. J. 2015. Pharmacological activity of metal binding agents that alter copper bioavailability. *Dalton Trans,* 44**,** 8760-70.

HERMAN, R. K. 2005. Introduction to sex determination. *In:* COMMUNITY, T. C. E. R. (ed.) *Wormbook.* Wormbook.

HOWIE, A. J., BREWER, D. B., HOWELL, D. & JONES, A. P. 2008. Physical basis of colors seen in Congo red-stained amyloid in polarized light. *Lab Invest,* 88**,** 232-42.

HRNCIC, R., WALL, J., WOLFENBARGER, D. A., MURPHY, C. L., SCHELL, M., WEISS, D. T. & SOLOMON, A. 2000. Antibody-mediated resolution of light chain-associated amyloid deposits. *Am J Pathol,* 157**,** 1239-46.

HUANG, X., ATWOOD, C. S., HARTSHORN, M. A., MULTHAUP, G., GOLDSTEIN, L. E., SCARPA, R. C., CUAJUNGCO, M. P., GRAY, D. N., LIM, J., MOIR, R. D., TANZI, R. E. & BUSH, A. I. 1999. The A beta peptide of Alzheimer's disease directly produces hydrogen peroxide through metal ion reduction. *Biochemistry,* 38**,** 7609-16.

HUNTER, T., BANNISTER, W. H. & HUNTER, G. J. 1997. Cloning, expression, and characterization of two manganese superoxide dismutases from Caenorhabditis elegans. *J Biol Chem,* 272**,** 28652-9.

HUNTINGTON STUDY GROUP REACH, H. D. I. 2015. Safety, tolerability, and efficacy of PBT2 in Huntington's disease: a phase 2, randomised, double-blind, placebo-controlled trial. *Lancet Neurol,* 14**,** 39-47.

IMBERT, J., CULOTTA, V., FURST, P., GEDAMU, L. & HAMER, D. 1990. Regulation of metallothionein gene transcription by metals. *Adv Inorg Biochem,* 8**,** 139-64.

JONES, D. & CANDIDO, E. P. 1999. Feeding is inhibited by sublethal concentrations of toxicants and by heat stress in the nematode Caenorhabditis elegans: relationship to the cellular stress response. *J Exp Zool,* 284**,** 147-57.

KASTRITIS, E. & DIMOPOULOS, M. A. 2016. Recent advances in the management of AL Amyloidosis. *Br J Haematol,* 172**,** 170-86.

KNOWLES, T. P., VENDRUSCOLO, M. & DOBSON, C. M. 2014. The amyloid state and its association with protein misfolding diseases. *Nat Rev Mol Cell Biol,* 15**,** 384-96.

KOZLOWSKI, H., JANICKA-KLOS, A., BRASUN, J., GAGGELLI, E., VALENSIN, D. & VALENSIN, G. 2009. Copper, iron, and zinc ions homeostasis and their role in neurodegenerative disorders (metal uptake, transport, distribution and regulation). *Coordination Chemistry Reviews,* 253**,** 2665-2685.

LANNFELT, L., BLENNOW, K., ZETTERBERG, H., BATSMAN, S., AMES, D., HARRISON, J., MASTERS, C. L., TARGUM, S., BUSH, A. I., MURDOCH, R., WILSON, J., RITCHIE, C. W. & GROUP, P. E. S. 2008. Safety, efficacy, and biomarker findings of PBT2 in targeting Abeta as a modifying therapy for Alzheimer's disease: a phase IIa, double-blind, randomised, placebo-controlled trial. *Lancet Neurol,* 7**,** 779-86.

LAVATELLI, F., IMPERLINI, E., ORRU, S., ROGNONI, P., SARNATARO, D., PALLADINI, G., MALPASSO, G., SORIANO, M. E., DI FONZO, A., VALENTINI, V., GNECCHI, M., PERLINI, S., SALVATORE, F. & MERLINI, G. 2015. Novel mitochondrial protein interactors of immunoglobulin light chains causing heart amyloidosis. *FASEB J,* 29**,** 4614-28.

LEE, S. & DONG, H. H. 2017. FoxO integration of insulin signaling with glucose and lipid metabolism. *J Endocrinol,* 233**,** R67-R79.

LIAO, R., JAIN, M., TELLER, P., CONNORS, L. H., NGOY, S., SKINNER, M., FALK, R. H. & APSTEIN, C. S. 2001. Infusion of light chains from patients with cardiac amyloidosis causes diastolic dysfunction in isolated mouse hearts. *Circulation,* 104**,** 1594-7.

LIBINA, N., BERMAN, J. R. & KENYON, C. 2003. Tissue-specific activities of C. elegans DAF-16 in the regulation of lifespan. *Cell,* 115**,** 489-502.

LIN, K., HSIN, H., LIBINA, N. & KENYON, C. 2001. Regulation of the Caenorhabditis elegans longevity protein DAF-16 by insulin/IGF-1 and germline signaling. *Nat Genet,* 28**,** 139-45.

LINK, C. D., CYPSER, J. R., JOHNSON, C. J. & JOHNSON, T. E. 1999. Direct observation of stress response in Caenorhabditis elegans using a reporter transgene. *Cell Stress Chaperones,* 4**,** 235-42.

LOVELL, M. A., ROBERTSON, J. D., TEESDALE, W. J., CAMPBELL, J. L. & MARKESBERY, W. R. 1998. Copper, iron and zinc in Alzheimer's disease senile plaques. *J Neurol Sci,* 158**,** 47-52.

MACKENZIE, E. L., IWASAKI, K. & TSUJI, Y. 2008. Intracellular iron transport and storage: from molecular mechanisms to health implications. *Antioxid Redox Signal,* 10**,** 997-1030.

MANGO, S. E. 2007. The C. elegans pharynx: a model for organogenesis. *WormBook***,** 1-26.

MARKAKI, M. & TAVERNARAKIS, N. 2010. Modeling human diseases in Caenorhabditis elegans. *Biotechnol J,* 5**,** 1261-76.

MERLINI, G. 2012. CyBorD: stellar response rates in AL amyloidosis. *Blood,* 119**,** 4343-5.

MERLINI, G., SELDIN, D. C. & GERTZ, M. A. 2011. Amyloidosis: pathogenesis and new therapeutic options. *J Clin Oncol,* 29**,** 1924-33.

MERLINI, G. & STONE, M. J. 2006. Dangerous small B-cell clones. *Blood,* 108**,** 2520-30.

MILANI, P., MERLINI, G. & PALLADINI, G. 2018. Light Chain Amyloidosis. *Mediterr J Hematol Infect Dis,* 10**,** e2018022.

MISHRA, S., GUAN, J., PLOVIE, E., SELDIN, D. C., CONNORS, L. H., MERLINI, G., FALK, R. H., MACRAE, C. A. & LIAO, R. 2013. Human amyloidogenic light chain proteins result in cardiac dysfunction, cell death, and early mortality in zebrafish. *Am J Physiol Heart Circ Physiol,* 305**,** H95-103.

MORENO-ARRIOLA, E., CARDENAS-RODRIGUEZ, N., COBALLASE-URRUTIA, E., PEDRAZA-CHAVERRI, J., CARMONA-APARICIO, L. & ORTEGA-CUELLAR, D. 2014. Caenorhabditis elegans: A useful model for studying metabolic disorders in which oxidative stress is a contributing factor. *Oxid Med Cell Longev,* 2014**,** 705253.

MUKHOPADHYAY, A., OH, S. W. & TISSENBAUM, H. A. 2006. Worming pathways to and from DAF-16/FOXO. *Exp Gerontol,* 41**,** 928-34.

NAITO, M. 2014. Amide-adducts in atherosclerosis. *Subcell Biochem,* 77**,** 95-102.

NIENHUIS, H. L., BIJZET, J. & HAZENBERG, B. P. 2016. The Prevalence and Management of Systemic Amyloidosis in Western Countries. *Kidney Dis (Basel),* 2**,** 10-9.

NUVOLONE, M. & MERLINI, G. 2017a. Emerging therapeutic targets currently under investigation for the treatment of systemic amyloidosis. *Expert Opin Ther Targets,* 21**,** 1095-1110.

NUVOLONE, M. & MERLINI, G. 2017b. Systemic amyloidosis: novel therapies and role of biomarkers. *Nephrol Dial Transplant,* 32**,** 770-780.

NUVOLONE, M., PALLADINI, G. & MERLINI, G. 2015. Amyloid Diseases at the Molecular Level: General Overview and Focus on AL Amyloidosis. *In:* PICKEN, M. M., HERRERA, G. A. & DOGAN, A. (eds.) *Amyloid and Related Disorders: Surgical Pathology and Clinical Correlations.* Cham: Springer International Publishing.

OPAZO, C., HUANG, X., CHERNY, R. A., MOIR, R. D., ROHER, A. E., WHITE, A. R., CAPPAI, R., MASTERS, C. L., TANZI, R. E., INESTROSA, N.

C. & BUSH, A. I. 2002. Metalloenzyme-like activity of Alzheimer's disease beta-amyloid. Cu-dependent catalytic conversion of dopamine, cholesterol, and biological reducing agents to neurotoxic H(2)O(2). *J Biol Chem,* 277**,** 40302-8.

OSTREROVA-GOLTS, N., PETRUCELLI, L., HARDY, J., LEE, J. M., FARER, M. & WOLOZIN, B. 2000. The A53T alpha-synuclein mutation increases iron-dependent aggregation and toxicity. *J Neurosci,* 20**,** 6048-54.

PALIKARAS, K. & TAVERNARAKIS, N. 2013. Caenorhabditis elegans (Nematode) A2 - Maloy, Stanley. *In:* HUGHES, K. (ed.) *Brenner's Encyclopedia of Genetics (Second Edition).* San Diego: Academic Press.

PALLADINI, G., DISPENZIERI, A., GERTZ, M. A., KUMAR, S., WECHALEKAR, A., HAWKINS, P. N., SCHONLAND, S., HEGENBART, U., COMENZO, R., KASTRITIS, E., DIMOPOULOS, M. A., JACCARD, A., KLERSY, C. & MERLINI, G. 2012. New criteria for response to treatment in immunoglobulin light chain amyloidosis based on free light chain measurement and cardiac biomarkers: impact on survival outcomes. *J Clin Oncol,* 30**,** 4541-9.

PALLADINI, G. & MERLINI, G. 2009. Current treatment of AL amyloidosis. *Haematologica,* 94**,** 1044-8.

PALLADINI, G., SACHCHITHANANTHAM, S., MILANI, P., GILLMORE, J., FOLI, A., LACHMANN, H., BASSET, M., HAWKINS, P., MERLINI, G. & WECHALEKAR, A. D. 2015. A European collaborative study of cyclophosphamide, bortezomib, and dexamethasone in upfront treatment of systemic AL amyloidosis. *Blood,* 126**,** 612-5.

PATEL, K. S. & HAWKINS, P. N. 2015. Cardiac amyloidosis: where are we today? *J Intern Med,* 278**,** 126-44.

PERFETTI, V., PALLADINI, G., CASARINI, S., NAVAZZA, V., ROGNONI, P., OBICI, L., INVERNIZZI, R., PERLINI, S., KLERSY, C. & MERLINI, G. 2012. The repertoire of lambda light chains causing predominant amyloid heart involvement and identification of a preferentially involved germline gene, IGLV1-44. *Blood,* 119**,** 144-50.

PERFETTI, V., SASSANO, M., UBBIALI, P., VIGNARELLI, M. C., ARBUSTINI, E., CORTI, A. & MERLINI, G. 1996. Inverse polymerase chain reaction for cloning complete human immunoglobulin variable regions and leaders conserving the original sequence. *Anal Biochem,* 239**,** 107-9.

PERFETTI, V., VIGNARELLI, M. C., CASARINI, S., ASCARI, E. & MERLINI, G. 2001. Biological features of the clone involved in primary amyloidosis (AL). *Leukemia,* 15**,** 195-202.

PITHADIA, A. S. & LIM, M. H. 2012. Metal-associated amyloid-beta species in Alzheimer's disease. *Curr Opin Chem Biol,* 16**,** 67-73.

R., N. & L., C. 2008. Caenorhabditis elegans Models of Human Neurodegenerative Diseases. *In:* CONN, P. M. (ed.) *Sourcebook of Models for Biomedical Research.* Humana Press.

RAMIREZ-ALVARADO, M., DE STIGTER, J. K., BADEN, E. M., SIKKINK, L. A., MCLAUGHLIN, R. W. & TABOAS, A. L. 2007. Immunoglobulin Light Chain and Systemic Light-Chain Amyloidosis. *In:* UVERSKY, V. N. & FINK, A. L. (eds.) *Protein Misfolding, Aggregation, and Conformational Diseases: Part B: Molecular Mechanisms of Conformational Diseases.* Boston, MA: Springer US.

REBOLLEDO, D. L., ALDUNATE, R., KOHN, R., NEIRA, I., MINNITI, A. N. & INESTROSA, N. C. 2011. Copper reduces Abeta oligomeric species and ameliorates neuromuscular synaptic defects in a C. elegans model of inclusion body myositis. *J Neurosci,* 31**,** 10149-58.

RITCHIE, C. W., BUSH, A. I., MACKINNON, A., MACFARLANE, S., MASTWYK, M., MACGREGOR, L., KIERS, L., CHERNY, R., LI, Q. X., TAMMER, A., CARRINGTON, D., MAVROS, C., VOLITAKIS, I., XILINAS, M., AMES, D., DAVIS, S., BEYREUTHER, K., TANZI, R. E. & MASTERS, C. L. 2003. Metal-protein attenuation with iodochlorhydroxyquin (clioquinol) targeting Abeta amyloid deposition and toxicity in Alzheimer disease: a pilot phase 2 clinical trial. *Arch Neurol,* 60**,** 1685-91.

ROGNONI, P., LAVATELLI, F., CASARINI, S., PALLADINI, G., VERGA, L., PEDRAZZOLI, P., VALENTINI, G., MERLINI, G. & PERFETTI, V. 2013. A strategy for synthesis of pathogenic human immunoglobulin free light chains in E. coli. *PLoS One,* 8**,** e76022.

ROTH, M., TOMLINSON, B. E. & BLESSED, G. 1966. Correlation between scores for dementia and counts of 'senile plaques' in cerebral grey matter of elderly subjects. *Nature,* 209**,** 109-10.

SANCHORAWALA, V. 2006. Light-chain (AL) amyloidosis: diagnosis and treatment. *Clin J Am Soc Nephrol,* 1**,** 1331-41.

SAYRE, L. M., PERRY, G., HARRIS, P. L., LIU, Y., SCHUBERT, K. A. & SMITH, M. A. 2000. In situ oxidative catalysis by neurofibrillary tangles and senile plaques in Alzheimer's disease: a central role for bound transition metals. *J Neurochem,* 74**,** 270-9.

SCHILLING, S., RAHFELD, J. U., LUES, I. & LEMERE, C. A. 2018. Passive Abeta Immunotherapy: Current Achievements and Future Perspectives. *Molecules,* 23.

SCHIMMER, A. D. 2011. Clioquinol - a novel copper-dependent and independent proteasome inhibitor. *Curr Cancer Drug Targets,* 11**,** 325-31.

SELVARATNAM, R., CAO, J. & KARGER, A. B. 2016. Serum Free Light Chain Analysis. *In:* LINDEN, M. A. & MCKENNA, R. W. (eds.) *Plasma Cell Neoplasms: A Morphologic, Cytogenetic and Immunophenotypic Approach.* Cham: Springer International Publishing.

SENGUPTA, U., NILSON, A. N. & KAYED, R. 2016. The Role of Amyloid-beta Oligomers in Toxicity, Propagation, and Immunotherapy. *EBioMedicine,* 6**,** 42-49.

SEVIGNY, J., CHIAO, P., BUSSIERE, T., WEINREB, P. H., WILLIAMS, L., MAIER, M., DUNSTAN, R., SALLOWAY, S., CHEN, T., LING, Y., O'GORMAN, J., QIAN, F., ARASTU, M., LI, M., CHOLLATE, S., BRENNAN,

M. S., QUINTERO-MONZON, O., SCANNEVIN, R. H., ARNOLD, H. M., ENGBER, T., RHODES, K., FERRERO, J., HANG, Y., MIKULSKIS, A., GRIMM, J., HOCK, C., NITSCH, R. M. & SANDROCK, A. 2016. The antibody aducanumab reduces Abeta plaques in Alzheimer's disease. *Nature,* 537**,** 50-6.

SHEN, P., YUE, Y., ZHENG, J. & PARK, Y. 2018. Caenorhabditis elegans: A Convenient In Vivo Model for Assessing the Impact of Food Bioactive Compounds on Obesity, Aging, and Alzheimer's Disease. *Annu Rev Food Sci Technol,* 9**,** 1-22.

SIDDIQI, M. K., ALAM, P., CHATURVEDI, S. K., SHAHEIN, Y. E. & KHAN, R. H. 2017. Mechanisms of protein aggregation and inhibition. *Front Biosci (Elite Ed),* 9**,** 1-20.

SIRAC, C., BENDER, S., JACCARD, A., BRIDOUX, F., LACOMBE, C., TOUCHARD, G. & COGNE, M. 2011. Strategies to model AL amyloidosis in mice. *Amyloid,* 18 Suppl 1**,** 45-7.

SIRAC, C., HERRERA, G. A., SANDERS, P. W., BATUMAN, V., BENDER, S., AYALA, M. V., JAVAUGUE, V., TENG, J., TURBAT-HERRERA, E. A., COGNE, M., TOUCHARD, G., LEUNG, N. & BRIDOUX, F. 2018. Animal models of monoclonal immunoglobulin-related renal diseases. *Nat Rev Nephrol,* 14**,** 246-264.

SOLLING, K. 1981. Free light chains of immunoglobulins. *Scand J Clin Lab Invest Suppl,* 157**,** 1-83.

SOTO, C. 2003. Unfolding the role of protein misfolding in neurodegenerative diseases. *Nat Rev Neurosci,* 4**,** 49-60.

STOILOVA, T., COLOMBO, L., FORLONI, G., TAGLIAVINI, F. & SALMONA, M. 2013. A new face for old antibiotics: tetracyclines in treatment of amyloidoses. *J Med Chem,* 56**,** 5987-6006.

STRAVALACI, M., BASTONE, A., BEEG, M., CAGNOTTO, A., COLOMBO, L., DI FEDE, G., TAGLIAVINI, F., CANTU, L., DEL FAVERO, E.,

MAZZANTI, M., CHIESA, R., SALMONA, M., DIOMEDE, L. & GOBBI, M. 2012. Specific recognition of biologically active amyloid-beta oligomers by a new surface plasmon resonance-based immunoassay and an in vivo assay in Caenorhabditis elegans. *J Biol Chem,* 287**,** 27796-805.

STROBER, W. & WALDMANN, T. A. 1974. The role of the kidney in the metabolism of plasma proteins. *Nephron,* 13**,** 35-66.

ŠUŠTAR, N. & OSREDKAR, J. 2011. Copper and zinc, biological role and significance of copper/zinc imbalance. *Journal of clinical toxicology,* S3-001**,** 1-19.

TREUSCH, S., CYR, D. M. & LINDQUIST, S. 2009. Amyloid deposits: protection against toxic protein species? *Cell Cycle,* 8**,** 1668-74.

VAN DYCK, C. H. 2018. Anti-Amyloid-beta Monoclonal Antibodies for Alzheimer's Disease: Pitfalls and Promise. *Biol Psychiatry,* 83**,** 311-319.

VERMA, M., VATS, A. & TANEJA, V. 2015. Toxic species in amyloid disorders: Oligomers or mature fibrils. *Ann Indian Acad Neurol,* 18**,** 138-45.

WECHALEKAR, A. D. & WHELAN, C. 2017. Encouraging impact of doxycycline on early mortality in cardiac light chain (AL) amyloidosis. *Blood Cancer J,* 7**,** e546.

WEEKLEY, C. M. & HE, C. 2017. Developing drugs targeting transition metal homeostasis. *Curr Opin Chem Biol,* 37**,** 26-32.

WESTERMARK, P. 2012. Localized AL amyloidosis: a suicidal neoplasm? *Ups J Med Sci,* 117**,** 244-50.

WINTERBOURN, C. C. & CARRELL, R. W. 1977. Oxidation of human haemoglobin by copper. Mechanism and suggested role of the thiol group of residue beta-93. *Biochem J,* 165**,** 141-8.

WONG, B. X. & DUCE, J. A. 2014. The iron regulatory capability of the major protein participants in prevalent neurodegenerative disorders. *Front Pharmacol,* 5**,** 81.

YASSIN, M. S., EKBLOM, J., XILINAS, M., GOTTFRIES, C. G. & ORELAND, L. 2000. Changes in uptake of vitamin B(12) and trace metals in brains of mice treated with clioquinol. *J Neurol Sci,* 173**,** 40-4.

ZARKOWER, D. 2006. Somatic sex determination. *WormBook***,** 1-12.

# Appendixes

***Appendix 1| Clinical and biochemical characteristics of patients at diagnosis of AL amyloidosis or multiple myeloma***

| | | | | | Biochemical source and characteristics | | | | | | | | Cardiac parameters | | | | |
|---|---|---|---|---|---|---|---|---|---|---|---|---|---|---|---|---|---|
| **Code** | **Gender, age** | **Cardiac stage[a]** | **Diagnosis** | **Organ involved[b]** | **Recombinant** | **BJ** | **Germeline gene** | **Deduced MW (kDa/PI)** | **Serum λ FLC (mg/l)** | **κ/λ FLC ratio** | **Proteinuria (g/24 h)** | **Creatinine (mg/dl)** | **NT-proBNP (ng/l)** | **cTnI (ng/ml)** | **IVS (mm)** | **PW (mm)** | **EF (%)** |
| H6 | M, 74 | III | AL | heart | | X | IGLV6-57 | 23.2/5.37 | 683 | 0.009 | 0.45 | 0.73 | 4300 | 0.2 | 15 | 15 | 42 |
| H7 | M, 45 | III | AL | heart | X | X | IGLV1-51 | 22.3/6.15 | 477 | 0.01 | 0.33 | 0.98 | 8882 | 0.16 | 19 | 19 | 45 |
| H18 | M, 69 | III | AL | heart | | X | IGLV3-19 | 22.7/5.88 | 509 | 0.01 | 0.82 | 0.97 | 3839 | 0.34 | 21 | 18 | 61 |
| MM2 | F, 71 | | MM | | – | X | IGLV3-19 | 22.8/5.61 | 6130 | 0.001 | 0.52[c] | 2.07 | 42[d] | 0.007 | 9 | 9 | 65 |
| MM4 | M, 65 | | MM | | – | X | IGLV2-23 | 22.7/7.72 | 1140 | 0.001 | 0.12[c] | 0.89 | 201 | n.a. | 10 | 10 | 64 |
| MM7 | M, 48 | | MM | | – | X | IGLV2-23 | 22.8/8.20 | 573 | 0.01 | 1.87[c] | 0.84 | 14.5 | 0.003 | 10 | 10.5 | 67 |

*Reference ranges: serum λ FLC <26.3 mg/l, κ/λ ratio 0.26–1.65; serum creatinine <1.18 mg/dl in men, <1.02 mg/dl in women; NT-proBNP (Perfetti et al., 1996) <332 ng/l; BNP, <50 ng/l; cTnI <0.04 ng/ml.*

[a]*According to Gertz et al. (Gertz et al., 2005).*

[b]*According to the International Consensus Panel criteria (Gertz et al., 2005).*

[c]*Entirely constituted by BJ proteins.*

[d]*BNP (ng/l).*

***Appendix 2| Effect of hydrogen peroxide on DAF-16 nuclear translocation and HSP-16.2 and SOD-3 pharyngeal expression.***

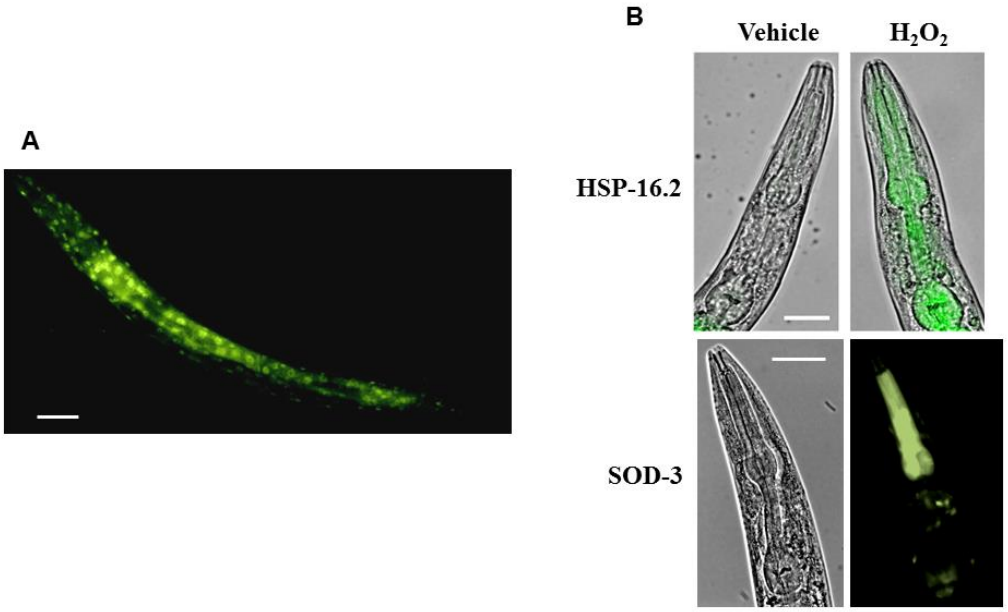


*Transgenic worms were fed with 1 mM $H_2O_2$ for 30 min. Worms were then plated on NGM agar plates seeded with E. coli. (A) Representative image of DAF-16/GFP distribution in transgenic TJ356 C. elegans. Scale bar = 50 nm. (B) HSP-16.2 and SOD-3 expression, as visualized by GFP fluorescence, in transgenic CL2070 and CF1553 worms, respectively. Scale bar =50 µm.*